Johanna Stettner

Self assembled monolayer formation of alkanethiols on gold:

Growth from solution versus physical vapor deposition

DOCTORAL THESIS

for obtaining the academic degree of
Doktorin der technischen Wissenschaften

Doctoral Programme of Technical Sciences
Technical Physics

Graz University of Technology

Supervisor:

Ao. Univ.-Prof. Dipl.-Ing. Dr.techn. tit. Univ.-Prof. Adolf Winkler

Institute of Solid State Physics

Graz, August 2010

EIDESSTATTLICHE ERKLÄRUNG

Ich erkläre an Eides statt, dass ich die vorliegende Arbeit selbstständig verfasst, andere als die angegebenen Quellen/Hilfsmittel nicht benutzt, und die den benutzten Quellen wörtlich und inhaltlich entnommenen Stellen als solche kenntlich gemacht habe.

Graz, am..... .....
(Unterschrift)

STATUTORY DECLARATION

I declare that I have authored this thesis independently, that I have not used other than the declared sources/resources, and that I have explicitly marked all material which has been quoted either literally or by content from the used sources.

…..…….. ……..
(date) (signature)

Danksagung

Das Gelingen einer solchen Arbeit erfordert das Miteinander vieler verschiedener Personen. An erster Stelle möchte ich hier meinen Betreuer Prof. Adolf Winkler nennen. Erst seine Fähigkeit, in jeder Notlage mit Rat und Tat an der Seite zu stehen sowie seine stets aufmunterten Worte haben mir diese Arbeit ermöglicht! Danke!

Meine Kollegen in der Oberflächenphysikgruppe haben mich stets gestützt, es war eine Freude, in einer so kooperativen und hilfsbereiten Gemeinschaft zu arbeiten. Auch die Arbeit mit den Kollegen auf der Chemie unter der Leitung von Prof. Trimmel habe ich sehr genossen. Danke auch für die dort erhaltene Hilfsbereitschaft!

Ganz herzlich möchte ich mich auch bei meinen Eltern bedanken, die immer für mich da sind, wenn ich sie brauche. Und schlussendlich einen ganz besonderen Dank an meinen Freund Christoph für die schöne gemeinsame Zeit, ohne die mir gutes Arbeiten nicht möglich gewesen wäre.

Abstract

This work deals with alkanethiol self assembled monolayer (SAM) formation on gold. The SAMs were prepared using wet chemical preparation methods (ex-situ preparation) as well as physical vapor deposition in an ultrahigh vacuum (UHV) chamber (in-situ preparation). Different gold substrates were used: a Au(111) single crystal, polycrystalline gold foils and Au(111)/mica. In particular the molecules mercaptoundecanoic acid (MUA) and undecanethiol (UDT) were investigated. These molecules only differ in their functional end group and thus provide a suitable pair in order to determine a possible influence of the acid end group on the SAM formation. The MUA and UDT SAMs were investigated with respect to their structure, their formation and their thermal stability. Therefore, many different surface analytical techniques were used. The main aim of this work was to explore the possible application of thermal desorption spectroscopy (TDS) to characterize the SAM, but we additionally performed low energy electron diffraction (LEED), X-ray photoelectron spectroscopy (XPS), Auger electron spectroscopy (AES) as well as infrared reflection absorption spectroscopy (IRRAS) and atomic force microscopy (AFM).

In the case of UDT, the formation of a full-coverage phase of standing molecules could be shown. A crucial step is a sufficiently long residual time in solution (24 h) in the case of ex-situ preparation, while the in-situ preparation demands an equally long residual time in UHV after the deposition of UDT. Standing molecules are stable up to a temperature of 450 K. At low coverage and after the heating at 450 K a ‘striped-phase’ of lying molecules was observed.

A different assembly behaviour was observed in the case of MUA. In this case, only little SAM formation was observed for ex-situ and in-situ prepared layers. A particularly interesting observation was the desorption of gold containing molecules at 700 K. These results indicate thiol induced etching of the gold substrates. It is shown that substrate properties (e.g. the roughness and chemical composition) as well as the residual time in solution influences the formation of gold-thiol complexes.

Kurzfassung

In dieser Arbeit wird die Entstehung selbstordnender Monolagen (SAMs) aus Alkanethiolen auf Goldoberflächen untersucht. Die SAMs wurden einerseits nasschemisch unter Umgebungsbedingungen (ex-situ) hergestellt, andererseits mittels physikalischer Gasphasenabscheidung (in-situ) im Ultrahochvakuum (UHV). Als Substrat dienten unterschiedliche Goldoberflächen: ein Au(111) Einkristall, polykristalline Goldfolien und Au(111)/Glimmer. Im speziellen wurden die Moleküle Mercaptoundecanoic acid (MUA) und Undecanethiol (UDT) untersucht, die sich nur in ihrer funktionellen Endgruppe unterscheiden. Dadurch sind diese zwei Moleküle besonders geeignet, einen möglichen Einfluss der Endgruppe auf die Qualität der SAMs festzustellen. Das Ziel war es, die SAMs bezüglich ihrer Entstehung, ihrer Struktur und ihrer thermischen Stabilität zu charakterisieren. Dazu wurde eine Vielzahl oberflächenanalytischer Methoden angewandt. Das Hauptaugenmerk lag dabei auf der thermischen Desorptionsspektroskopie (TDS), aber auch Beugung niederenergetischer Elektronen (LEED), Röntgen-Photoelektronenspektroskopie (XPS), Auger Elektronenspektroskopie (AES), Infrarot Reflexion - Absorptionsspektroskopie (IRRAS) und Rasterkraftmikroskopie (AFM) wurden durchgeführt.

Die Entstehung einer ‚gesättigten Phase' stehender Moleküle konnte für das UDT Molekül gezeigt werden. Bei ex-situ präparierten Proben ist dafür eine hinreichend lange Verweildauer (24 h) in der Lösung wesentlich. Die in-situ präparierten Proben wiederum benötigen nach dem Bedampfen eine entsprechend lange Zeit im UHV. Stehende Moleküle sind bis zu einer Temperatur von 450 K stabil. Bei höheren Temperaturen und bei niedrigeren

Bedeckungen konnte die Entstehung einer ‚gestreiften Phase' liegender Moleküle gezeigt werden.

Ein anderes Assemblierungsverhalten wurde für das MUA Molekül beobachtet. In diesem Fall konnte mit beiden Präparationsmethoden nur ein geringer Anteil stehender Moleküle erhalten werden. Besonders interessant war die Entdeckung von Golddesorption bei einer Temperatur von 700 K. Anscheinend findet ein Ätzvorgang statt, im Zuge dessen sich Gold-Thiol-Komplexe bilden. Es konnte gezeigt werden, dass die Entstehung dieser Komplexe sowohl von Substrateigenschaften (z.B. der Struktur und der chemischen Zusammensetzung) als auch von der Verweildauer in der Lösung abhängt.

List of abbreviations

α-peak	Desorption peak of standing molecules
AES	Auger electron spectroscopy
AFM	Atomic force microscopy
amu	Atomic mass unit
β-peak	Desorption peak of lying molecules
γ-peak	High-temperature desorption peak
GIXD	Gracing incidence X-ray diffraction
IRRAS	Infrared reflection absorption spectroscopy
LEED	Low energy electron diffraction
MCP	Micro channelplate
MCT	Mercury-cadmium-telluride
MUA	Mercaptoundecanoic acid
NEXAFS	Near edge X-ray absorption fine structure
PVD	Physical vapor deposition
QMS	Quadrupole mass spectrometer
RHEED	Reflection high energy electron diffraction
SAM	Self-assembled monolayer
STM	Scanning tunnelling microscopy
TDS	Thermal desorption spectroscopy
UHV	Ultra-high vacuum
XPS	X-ray photoelectron spectroscopy

Contents

1 Introduction

Self assembled monolayers are ordered molecular assemblies that are formed spontaneously on a surface. The historically most frequently investigated SAM system is that of alkanethiols on gold. The thiol head group acts as an anchor group which is covalently bond to the gold. The carbon chain is referred as the 'backbone' which is assumed to stabilize the SAM due to Van der Waals interactions. The end group (or ‚tail group') in the simplest case consists of a methyl-group. However, a lot of other functionalized end groups have been attached so far and the possibility to chemically modify the end group makes SAMs a powerful system.

The first interest on these molecules came up in 1930 [1-3] due to the amphiphilic properties of long-chain alkanethiols, which were used to control wetting properties [4]. Soon, the power of these molecules in view of surface modification was realized and a vast amount of studies of alkanethiols on various noble metals started. Recent investigations are motivated not only by the possibility to control the wettability [5-10], but also by possible applications of SAMs in the development of (bio)sensors, interfaces and nanofabrications [11-17]. The possibility to perform surface patterning on SAMs [18-24] allows for applications in the semiconductor industry. In particular the introduction of functional end groups that can be addressed chemically, electrochemically or photochemically offers the opportunity of 'writing' and 'reading' information at the molecular level [25].

Up to now, gold has a unique importance as substrate for SAMs, even though silver [26-30] and copper [31-34] substrates have been extensively studied as well. Gold is easy to obtain not only as thin film on a substrate but also as single

crystal. Furthermore, it can be considered as a rather inert material as it does not oxidize at temperatures below its melting point [35]. But in particular the strong bonding of thiols to gold substrates makes this system interesting, and it is the most studied model system.

The common way to produce SAMs is to put the cleaned substrate in ethanolic solution of the corresponding thiols for approximately 24 h [36,37]. Besides the preparation in solution also gas phase deposition of alkanethiols can be performed [37,38]. Even though causing much more experimental effort, physical vapor deposition (PVD) allows not only to investigate the early state of SAM formation but also to characterize the SAM with surface analytical tools. A lot of different characterization techniques have been applied to SAMs. Several methods turned out to be particularly suitable for SAM characterization and therefore a short overview of some of the most important techniques is presented here:

- STM and AFM provide a direct image of the surface structure. However, one has to assure that the image is representative for the whole sample. STM achieves a better spatial resolution, however, reasonable tunnelling currents through standing alkanethiols can only be obtained for $n < 12$ [37].
- LEED and GIXD can be used for diffraction by the SAM structure. The advantage of LEED is that it displays the entire reciprocal lattice at once, while GIXD has a better resolution.
- IRRAS and NEXAFS use the absorption of IR and X–rays, respectively, in order to determine e.g. the orientation of the molecules.
- XPS directly provides the chemical composition of the surface and furthermore allows the characterization of the bond states of the atomic species.

- TDS is particularly suitable to determine the thermal stability and the desorption states of the SAM.

The present work describes fundamental aspects of alkanethiol SAM formation on gold. We therefore investigated the alkanethiols undecanethiol (UDT) and 11-mercaptoundecanoic acid (MUA) on gold. These molecules differ only in their functional end group (-CH_3 and -COOH) and thus provide a suitable pair in order to investigate its influence on the SAM formation. Furthermore, we compared the ex-situ (from solution) with the in-situ (by PVD) preparation methods with respect to the SAM formation. Finally, the influence of substrate properties (e.g. structure and chemistry) on the SAM formation was investigated.

2 Fundamentals

2.1 Adsorption kinetics and thermodynamics

Adsorption is a process where molecules from the gas phase or from solution bind in a condensed layer on a solid or liquid surface [39]. *Multilayer adsorption* takes place when several layers of adsorbate exists on the surface. This typically occurs when one works at sufficiently low temperatures. In contrast, if only one layer is present on the surface the adsorption process is referred as *monolayer adsorption*. It can be achieved at temperatures hundreds of degrees above the boiling point [39] and it is usually dominated by interactions between the adsorbate and the surface.

Concerning the nature of the bonding between adsorbate and substrate surface, one typically distinguishes two different types of adsorption:

- Physisorption: In this case the molecule is held by weak polarization (Van der Waals) interactions. There is no significant change in the electronic structure of the molecule. Typical physisorption energies are 2 – 10 kcal/mol.

- Chemisorption: The electronic structure of the adsorbate is significantly perturbed, as electrons are shared between the adsorbate and the surface. Typical chemisorption energies are 15 – 100 kcal/mol.

Usually, a molecule can physisorb and chemisorb on the same surface. It typically happens that the molecule is first physisorbed and then converted into a chemisorbed state.

Furthermore, it is convenient to distinguish between nondissociative (molecular) adsorption when the adsorbing molecules stay intact during adsorption, and dissociative adsorption where bonds break during the adsorption process. The non-dissociatively adsorbed molecules are physisorbed, while dissociatively adsorbed molecules are chemisorbed. A simple model concerning these two adsorption processes has been proposed by Lennard-Jones [40].

2.1.1 The Lennard-Jones potential

When a species (either a molecule or an atom) approaches a surface, mainly two forces occur. In the Lennard – Jones model, they are both assumed to be only dependant on the distance from the surface. There is an attractive van der Waals interaction, which accelerates the molecules towards the surface. On the other hand, at closer approximation to the surface, the Pauli repulsion dominates. This leads to a potential of the form as shown in Figure 1.

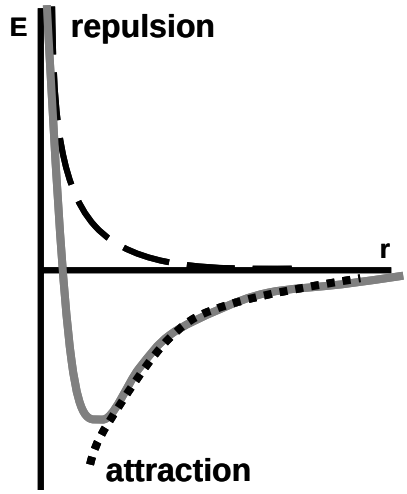

Figure 1. The Lennard-Jones potential for adsorption. At a high distance from the surface, the molecule is attracted by Van der Waals interaction. At lower distances, the Pauli repulsion dominates.

In order to distinguish between dissociative and nondissociative adsorption, the respective Lennard-Jones potentials are considered in Figure 2a-c. In Figure 2a, the case of pure molecular adsorption is depicted. In this case, the molecular state is more strongly bound (as it has a lower energy) than the dissociated state. In the second case (Figure 2b), the dissociated state has a lower energy than the molecular state, but there is an activation barrier to get from the molecular state into the chemisorbed state. In the third case (Figure 2c), there is an activation barrier between the physisorbed and chemisorbed state, but it lies below the energy of the free molecule AB. The incoming molecule always has the energy to surmount the activation barrier if it does not lose energy before dissociation.

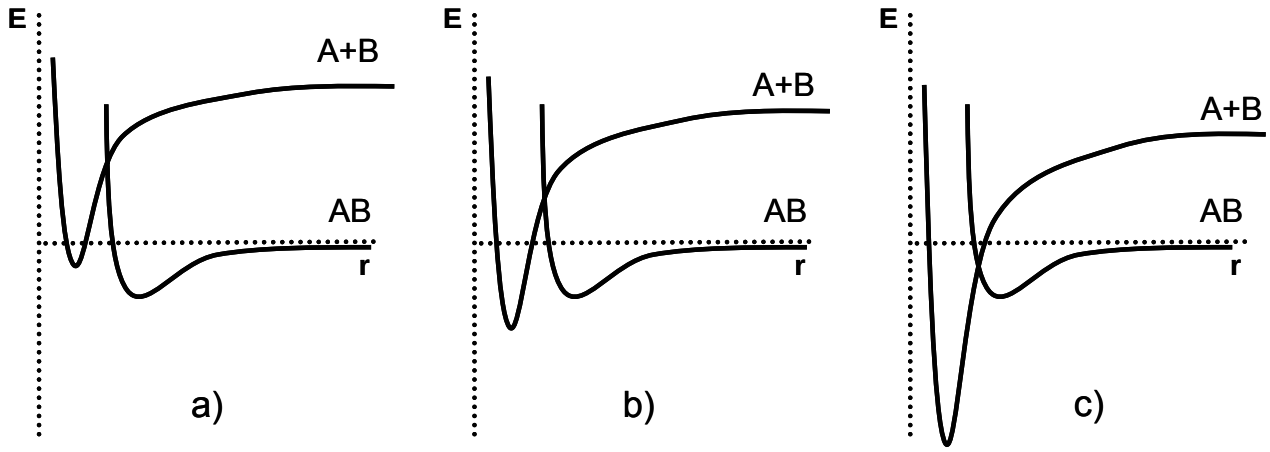

Figure 2. The Lennard-Jones model of adsorption for pure molecular adsorption (a), activated dissociative adsorption (b) and inactivated dissociative adsorption (c).

2.1.2 The Langmuir adsorption model

The Langmuir adsorption model is a particularly simple model to describe the adsorption kinetics. It is based on several assumptions:

- The sticking coefficient s = 1 on an empty side and s = 0 on a filled side. Therefore the sticking probability is given by

$$f(\Theta) = (1-\Theta)^n, \tag{1}$$

  wherein n denotes the number of dissociation products of the adsorbate (e.g. n=1 for non-dissociative adsorption, n=2 when the molecule dissociates in two species upon adsorption).
- The adsorption is limited by monolayer coverage.
- All adsorption sites are equivalent.
- The adsorbates are non-interacting.

In the case of mobile dissociation products, the adsorption rate is then given by

$$r_{ads} = I \cdot (1-\Theta)^n \tag{2}$$

with the impingement rate

$$I = \frac{p}{\sqrt{2\pi m k_B T}}, \tag{3}$$

wherein m corresponds to the mass of the particles, p is the pressure and T is the temperature.

Several extensions of this simple model can be useful [41]. The initial sticking coefficient usually is not exactly unity, but rather has a value $s = s_0$. Furthermore, the adsorption can be activated.

The generalized form to describe the adsorption rate is then given by:

$$r_{ads} = I \cdot s_0 \cdot (1-\Theta)^n \cdot e^{\left(\frac{-E_{ads}}{RT}\right)} \quad (4)$$

wherein E_{ads} is the activation energy for adsorption.

2.2 The growth of alkanethiols on gold

2.2.1 SAM formation in solution

The most common protocol for SAM formation is to immerse the clean substrate into dilute ethanolic solution of the thiols for approximately 18 h. This procedure is widely used as it is easy to perform and does not require any expensive technical equipment. In a first approximation, it is assumed that a simple Langmuir growth takes place [37], which is characterized by the growth rate being proportional to the number of available sites. However, different groups [42-47] reported a first adsorption step with ~ 80% coverage after several minutes and then a much slower growth which is related to the straightening of the hydrocarbon chains and the reorientation of the terminal groups. The adsorption of a monolayer thus happens very fast, however, the reorganization of this layer in order to obtain a densely packed monolayer of standing molecules requires several hours [36]. There are a lot of different factors which influence the final adsorption state of the SAM. The most important parameters are the solvent, the cleanliness of the substrate as well as the concentration of the solution and the immersion time.

Ethanol is the most commonly used *solvent* for alkanethiols. It solvates a variety of alkanethiols and it is available in high purity. Furthermore it is rather inexpensive and not toxic. However, the effect of a solvent on the self assembling process is complex and poorly understood. It is assumed that the solvent – substrate interactions can hinder the adsorption rate of thiols as the solvent molecules have to be replaced from the surface prior to thiol adsorption. This is corroborated by the finding that the initial adsorption rate is significantly lower for longer-chain solvents than for shorter-chain solvents [36]. The tendency to interact with the surface is more pronounced for large molecules and this leads to

some delay in the SAM formation. Several studies suggest that the SAM formation occurs faster in certain non-polar solvents, e.g. heptane or hexane, than in ethanol [43,48]. However, it seems that these SAMs are less organized than that formed in ethanol [36]. In summary the studies have shown that the choice of the solvent is of importance with respect to the SAM formation without being able to fully describe the complex interactions between solvent, surface and adsorbate during SAM formation.

A further important parameter is the *cleanliness* of the substrate. When the SAM is prepared under ambient conditions, the cleanliness of the substrate is not easy to control and it seems that this can have a strong influence on the growth behaviour [37]. A certain delay of the onset of the adsorption process due to surface contaminations has been observed, but it has been shown that these contaminations typically are displaced by the SAM during time [44].

However, the influence of the substrate cleanliness on the SAM formation is an interesting parameter and not so frequently investigated, even though hardly any paper renounces to emphasise its importance. We refer to Section 5.3.5, where this issue is treated in more detail for UDT SAMs on gold.

A further influencing parameter is the *concentration of the solution*, which is strongly related with the *immersion time*. Many groups found that the initial growth rate increases with the concentration [42,44,49,50]. A lower concentration of thiols in the solution thus requires a longer immersion time in solution in order to obtain a well ordered SAM. Typically, the substrate is immersed in 1mM solution of the corresponding thiols for ~ 18 h. As the surface density of molecules is ~ 4.5 x 10^{14} molecules/cm^2, the minimum concentration to form a densely packed monolayer can in principle be estimated to be ~ 6 x 10^{14} molecules/cm^3, which corresponds to a 1μM solution [36]. However, Bain et al. [44] found that from strongly diluted solutions in the μM range only imperfect monolayers are formed. Therefore typically solutions in the mM range are used.

Most studies suggest that the properties of a SAM do not change significantly when it is exposed to 1mM solutions of thiols for more than 18 h [36]. STM and RAIRS studies rather suggest a decrease of the defects of a SAM upon immersion times longer than 7 days [51]. However, there are only a few studies that investigate immersion times longer than one week and therefore this issue will be treated in Section 5.3.6 in more detail.

2.2.2 SAM formation by gas phase deposition

The second commonly used method for SAM preparation is the deposition from the gas phase. In this context, frequently the term *physical vapor deposition* (PVD) is in use, which describes a variety of methods to deposit thin films by the condensation of a vaporized form of the material. The gas phase deposition of alkanethiols on gold requires considerably more experimental effort than growth from solution. Long chain alkanethiols (n > 11) lack adequate vapor pressures, which makes the deposition more difficult. However, gas phase deposition also provides several advantages in comparison to the SAM preparation under ambient conditions. The substrate cleanliness can be better controlled and a wide range of experimental techniques can be used in UHV. Adsorption from the gas phase is particularly useful for studying the early stage of SAM formation and it provides the opportunity to prepare sub-monolayer coverages rather easily. Indeed, the current understanding of the self-assembly mechanism and the phase diagram principally stems from *in situ* experiments.

In a first approach, the SAM growth can be described by a simple Langmuir adsorption model, as derived from ex-situ and in-situ experiments. It presupposes that the adsorption is limited by monolayer coverage and that all adsorption sites are equivalent. This implicates that no lateral interactions between the molecules occur, which obviously is not valid. Indeed, several studies [42-44,52] indicate that this simple model is an inaccurate description. Extensive studies have shown that the adsorption mechanism is more complicated including different phases which exhibit different time scales.

A rather comprehensive picture of the mechanism of the self-assembly process is given in [53]. It has been shown that the monolayer assembles by nucleation and growth of islands. At low coverages, a so-called ‘striped phase’ of lying molecules evolves. This phase has already been extensively studied and will be discussed in more detail in the next section. Increasing coverage lead to the evolution of so-called ‘intermediate-phases’, which in contrast to the striped- and the terminal structure are not so well established. A variety of intermediate phases has been observed so far [54-58]. The final phase is a densely packed monolayer of standing molecules. It is obvious that this adsorption mechanism can not accurately be described by one simple model, in particular as the different phases are characterized by different time scales. Schreiber et al. found that the standing up phase grows by a factor of ~ 500 slower than the lying down phase [59]. A scheme of a phase diagram for decanethiol on Au(111) as shown in [60] is depicted in Figure 3. The phase boundaries separate the different phases such as the low-coverage striped phase and the full-coverage phase of standing molecules. At higher temperatures, a phase transition to a liquid phase occurs. For the fully covered monolayer it is at approximately 100 °C, thus significantly higher than in the bulk, which is explained by stabilization through the chemical bond to the substrate.

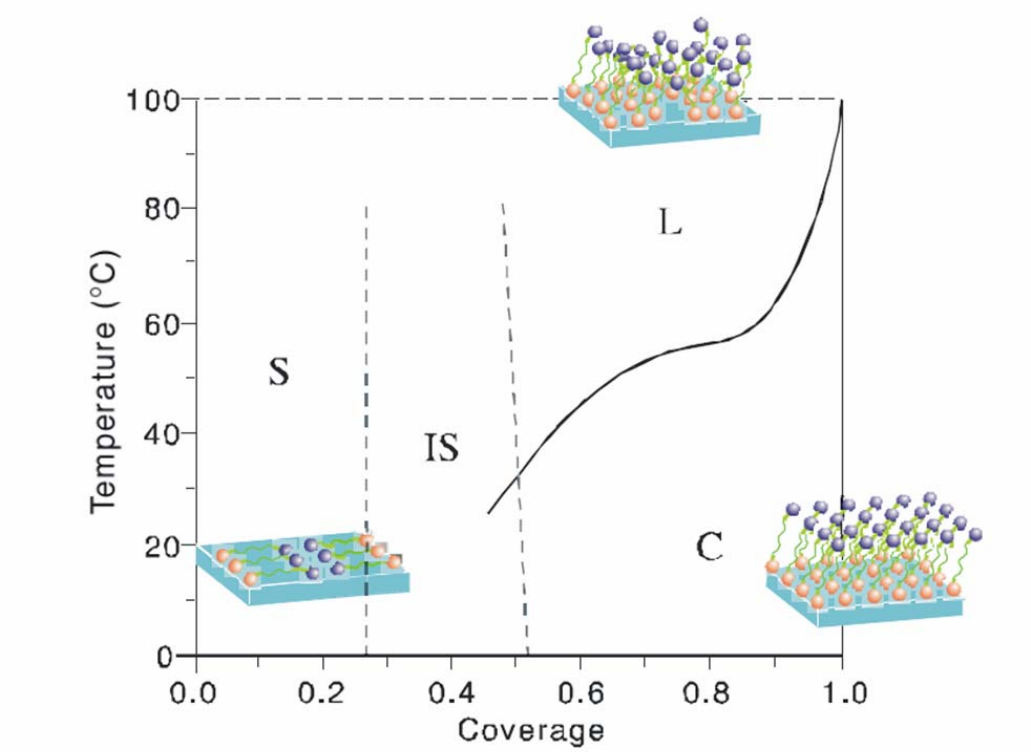

Figure 3. A scheme of the phase diagram as shown in [60] for decanethiol on Au(111). S: striped phase, IS: intermediate phase, C: c(4x2) – phase, L: liquid phase. The broken lines indicate phase boundaries which are not yet fully established.

2.2.3 Carboxylic acid-terminated alkanethiols on gold

In order to tune the chemical properties of SAMs, various functional groups have been attached at the end of the alkane chain [4,61-65]. In view of applications, acid-terminated alkanethiols are of special interest [66-73]. In particular, they also provide the opportunity to be further modified [74-76]. However, it is not certain whether replacing the terminal CH_3-group results in the formation of a well ordered layer or whether possible interactions between the acid end groups lead to a different ordering pattern or even to disorder.

Regarding the structural ordering of such films, there are a lot of unsolved problems and discrepancies in the literature. In the first paper describing SAMs made from mercaptohexadecanoic acid (MHDA), Nuzzo et al. [62] reported that these films exhibit a high degree of orientational order. But the formation of a well ordered monolayer of acid-terminated alkanethiols on gold was cast into doubt repeatedly in the last decades. Several groups [64,77] observed rather disordered structures. It is assumed that the presence of hydrogen bonds between neighbouring carboxylic acid groups prohibits the SAM formation.

In addition, also strong interactions of the acid with the gold substrate are proposed [64,78], leading to a rather complex disordered structure as shown in Figure 4.

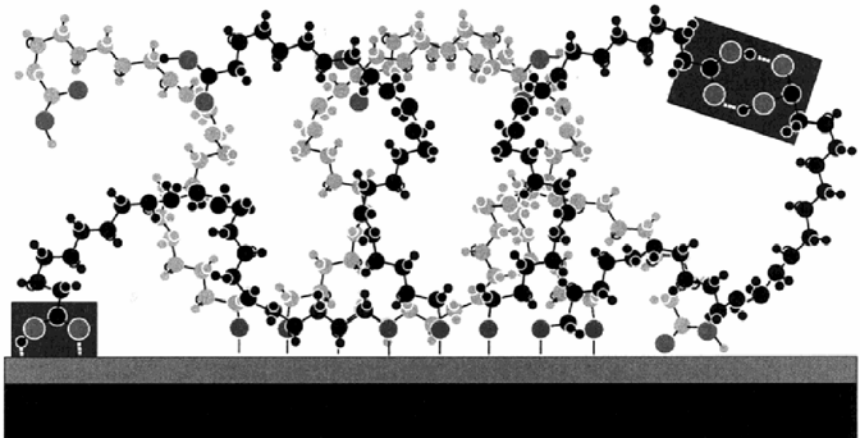

Figure 4. Scheme of complex disordered structure for carboxylic acid-terminated alkanethiols on gold as depicted in [78].

A lot of preparation recommendations can be found in the literature in order to obtain well ordered acid-terminated SAMs. They range from the use of a highly diluted (in the range of µm) solution [78] to the addition of acid in the incubation solution [79-81]. On the other hand, several studies suggest that well ordered acid-terminated SAMs can be obtained using simple ethanol solution [82-84]. In fact, there are still a lot of contradictory studies demanding further research on this area.

2.3 Structure investigations of alkanethiols on Au(111)

2.3.1 General remarks on the notation

For describing the superstructure of adsorbates, frequently the notation of Wood [85] is applied. With $\mathbf{a}_1$ and $\mathbf{a}_2$ the lengths of the basic translation vectors of the superlattice of the adsorbate and $\mathbf{s}_1$, $\mathbf{s}_2$ those of the substrate plane, this notation reads:

$$S(hkl)-\left(\frac{\mathbf{a}_1}{\mathbf{s}_1}\mathbf{x}\frac{\mathbf{a}_2}{\mathbf{s}_2}\right)R\alpha\,. \tag{5}$$

S is the chemical symbol of the substrate and (hkl) are the Miller indices describing the crystallographic orientation of the substrate surface. The quantity $\left(\frac{\mathbf{a}_1}{\mathbf{s}_1}\mathbf{x}\frac{\mathbf{a}_2}{\mathbf{s}_2}\right)$ describes the ratio of magnitudes between the unit vectors of the adsorbate and the substrate, while $R\alpha$ specifies the rotational angle between these two unit cells. A possible centering of the unit cell is described by the character *c.*

Another method to describe superstructures is the notation proposed by Park and Madden [86]. This method can more generally be applied to all sorts of ordered superstructures. The adsorbate vectors $\mathbf{a_1}$, $\mathbf{a_2}$ and the substrate vectors $\mathbf{s_1}$, $\mathbf{s_2}$ can be linked by the equations:

$$\mathbf{a_1} = M_{11}\mathbf{s_1} + M_{12}\mathbf{s_2}$$
$$\mathbf{a_2} = M_{21}\mathbf{s_1} + M_{22}\mathbf{s_2}$$

and the superstructure is specified by the matrix $\mathbf{M}$:

$$\mathbf{M} = \begin{pmatrix} M_{11} & M_{12} \\ M_{21} & M_{22} \end{pmatrix} \tag{6}$$

Different types of superstructures can be distinguished according to the elements of the matrix $\mathbf{M}$ [41]: If all of the elements of the matrix are integers, the structure is commensurate with the substrate and all of the adsorbates occupy identical adsorption sites. If the elements are rational numbers, the overlayer forms a coincidence lattice, which is an incommensurate structure. If the elements of the matrix are irrational, no common periodicity between the layer and the substrate exists. In this case, the structure is called an incoherent structure, which is also an incommensurate structure.

2.3.2 The Au(111) surface

The most frequently investigated substrate for SAM formation of alkanethiols is the Au(111) plane, which has the lowest surface energy and which is thus preferred in the growth of thin gold films. Several important properties of the gold bulk are listed in Table 1. The gold bulk arranges in a fcc crystal-structure. The outmost layer of the Au(111) plane exhibits a hexagonal rotational symmetry. When the second layer is considered as well, the symmetry reduces to a threefold rotational symmetry. A scheme of the ideal Au(111) plane is shown in Figure 5a. However, gold is the only element with a fcc crystalline structure

whose (111) face reconstructs [87]. The surface layer is contracted along the $\langle 1\bar{1}0\rangle$ direction and its packing density is 4% higher than that of the underlying layers [88]. This reconstruction can be described by a (22 x √3)-structure, as 23 atoms sit on 22 bulk atoms. As the fcc- and hcp- sites are energetically favoured, this contraction does not occur homogeneously. This can be described by a rather complex stacking fault model [87]. The atomic rows are periodically translated in the $\langle 11\bar{2}\rangle$ direction and additionally exhibit an out of plane corrugation normal to the surface with a maximum value of 0.03 nm [89,90].

STM images of the Au(111) surface clearly show this corrugation in terms of darker and brighter areas within the unit cell (Figure 5b, inset). The large-scale STM image reveals a zigzag pattern (named 'herringbone-reconstruction') which stems from joining of 120° rotated domains. In fact, three different 120° rotated domains could virtually exist due to the three-fold symmetry of the Au(111) plane [91]. The permanent absence of the third rotational domain is explained by surface stress arguments.

Au	Atomic weight……196.97
	Melting point……1064 °C
	Boiling point…… 2856 °C
	Stable isotope…….No
	Crystal structure…….fcc

Table 1. Several important properties of gold according to ref. [92].

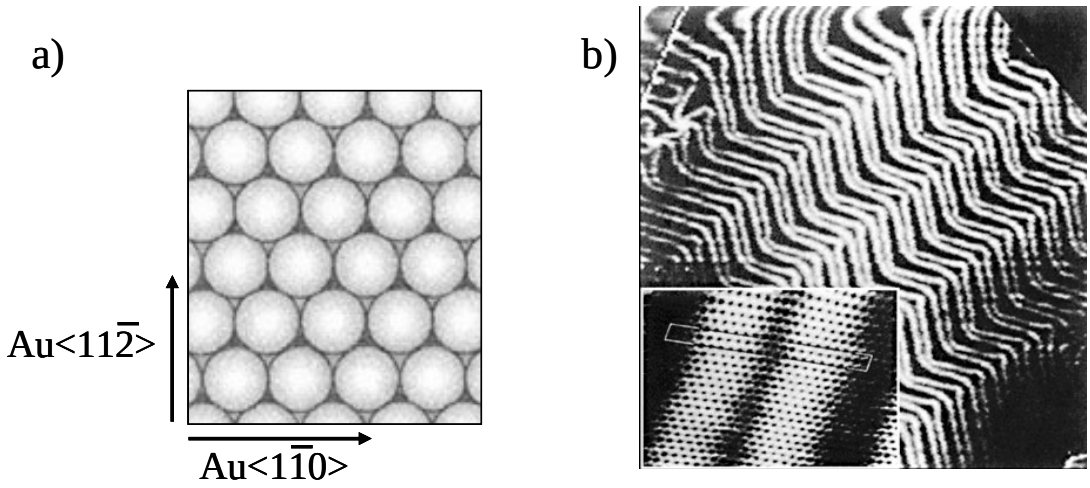

Figure 5. Scheme of the ideal Au(111) plane (a) and its reconstruction (b) as detected by STM (size: 120 x 120 nm²) showing the typical zig-zag pattern. The inset shows an atomic resolution STM image (8 x 6 nm²) indicating a pair of corrugation lines [91].

2.3.3 The striped phase and the full-coverage structure of alkanethiols on Au(111)

At low coverage of alkanethiols on gold, frequently a so-called 'striped-phase' has been observed. It is characterized by the molecular backbones lying flat on the surface. This structure has also been observed after partial desorption of the full-coverage phase [93]. This phase can in general be described by a (m x √3) structure, wherein m depends on the length of the alkane chain (Figure 6). For decanethiol, Camillone et al. [94] as well as Balzer et al. [95] reported a value of m = 11. This corresponds to 31.7 Å and is close to twice the length of one molecule. It has been found that m increases about (0.84 ± 0.04) Å per methylene group [56]. The head to head arrangement is assumed to stem from sulfur-sulfur interactions.

In fact two slightly different types of unit cells have been reported. Besides the primitive unit cell also a centered unit cell was observed several times [37,54,57].

This structure is obtained after a small displacement of every second row. In the case of decanethiol it is labelled c(23 x √3). However, these two phases have been found within one set of experiments and it is assumed that the c(23 x √3) structure converts to a p(11 x √3) at a little higher coverage [37].

The second well established phase of alkanethiols on Au(111) is the full coverage phase which corresponds to a densely packed monolayer. Early studies revealed that this phase exhibits a (√3 x √3) R30° structure with respect to Au(111) surface. This structure corresponds to a molecule-molecule spacing of ~ 5 Å. However, additionally a second phase has been observed corresponding to a (2√3 x 3)rect. structure. This phase is frequently reported as c(4 x 2) structure, meaning c(4 x 2) relative to the (√3 x √3)R30° unit mesh, not relative to the (1 x 1) substrate mesh [96]. This superlattice is four times larger in area and contains four molecules per unit mesh with at least two different local geometries. A scheme of the superstructure is shown in Figure 7a, a STM image of the c(4 x 2) structure of octanethiol on gold is shown in Figure 7b.

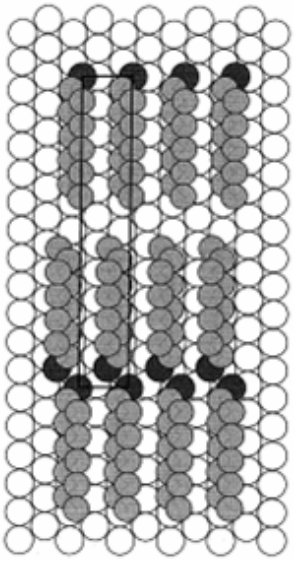

Figure 6. Scheme of the striped phase of alkanethiols on Au(111) as shown in [37]. For decanethiol, the unit cell can be described by a (11 x √3) structure.

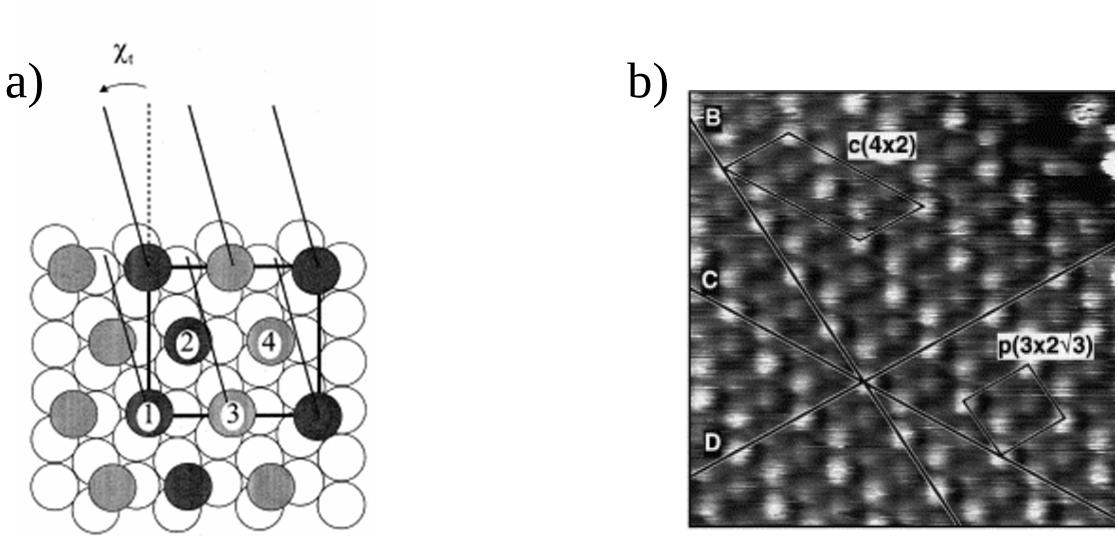

Figure 7. Scheme of the c(4x2) superstructure as shown in [37]. The molecules labelled 1 and 2, as well as 3 and 4, are symmetry-equivalent (a). STM image (60 x 60 Å) of octanethiol on Au(111) as shown in [4]. The p(3 x 2√3) unit mash and the c(4 x 2) superlattice are outlined.

GIXD measurements have revealed that this superstructure cannot fully be explained by different molecular orientations and twist angles, but that also the sulfur positions deviate from the hexagonal (√3 x √3) R30° symmetry [37]. Fenter et al. [97] proposed a strong deviation of the sulfur atoms, leading to a S-S spacing of only ~ 2.2 Å instead of 5 Å, which can be interpreted as 'sulfur – pairing' on the surface. However, there are still a lot of discussions on this topic, in particular concerning the local adsorption geometry of the sulfurs. Different adsorption sites have been proposed by different groups [98,99]. Recent studies, however, reveal that this discrepancies stem from the fact that gold adatoms are involved in the SAM formation process [96].

2.3.4 The generation of gold adatoms during SAM formation

Over the past years indications for the involvement of gold adatoms in the SAM formation have increased in quantity [96,100-102]. There is experimental [103-

107] and theoretical [108-111] evidence that the herringbone reconstruction of the Au(111) plane lifts as the thiolate coverage increases. As explained in Section 2.3.2, the outermost atomic layer of the Au(111) plane is compressed leading to an Au-Au atomic spacing which is smaller than that of the underlying bulk. As this reconstruction is lifted during SAM growth, a noticeable amount of gold adatoms is released. It is assumed that movement of these gold-adatom-thiolate moieties produces the SAM structure. A further indication of the involvement of gold-adatoms in the SAM growth procedure is the existence of pit-like defects, ~2.5 Å in depth, which have frequently been observed by STM [112-116]. These defects are assigned to gold vacancies. It is assumed that the vacancy islands form by ejection of excess gold atoms which are released as the surface reconstruction is removed [4].

3 Analytical methods

A comprehensive study on SAMs requires the use of different surface-sensitive methods. In this work, the focus was put on thermal desorption spectroscopy (TDS). Low energy electron diffraction (LEED), X-ray photoelectron spectroscopy (XPS) and Auger electron spectroscopy (AES) facilitated the interpretation of the TD spectra and provided interesting results allowing a deeper insight into the SAM formation. In addition, atomic force microscopy (AFM) and infrared reflection absorption spectroscopy (IRRAS) were successfully performed. In this chapter, the basic principles of these methods are described. It is not the scope of this chapter to describe the methods in detail, but to explain the basics as far as it concerns the interpretation of the experimental results.

3.1 Thermal desorption spectroscopy

Thermal desorption spectroscopy (TDS) is a frequently used method in order to investigate the energetic and the desorption behaviour of lightweight molecules and atoms on surfaces. However, in the context of large organic molecules it is not so commonly used. After having introduced the basics of the method, several peculiarities which arise from the investigation of large organic molecules will be discussed.

TDS is performed in UHV. The sample is installed in the UHV chamber and heated up linearly during the experiment leading to thermally induced desorption of the adsorbates. The desorption rate r_{des} of the particles is detected with a mass spectrometer. The mass-signal, which is correlated to the pressure increase, is plotted versus the temperature and called the TD-spectrum. In order to obtain a proportionality of the pressure p to the time-dependent decrease of the coverage

$\frac{d\Theta}{dt}$, a sufficiently high pumping speed is required. This becomes evident considering the pumping equation [117]:

$$-A\frac{d\Theta}{dt} = \frac{V}{kT}\left(\frac{dp}{dt} + \frac{S}{V}p\right) \tag{7}$$

A is the area of the sample and Θ is its coverage in molecules/area, V the volume of the chamber, p the pressure and S the pumping speed. In order to obtain a proportionality $p \sim \frac{d\Theta}{dt}$, the pumping speed S needs to be sufficiently high.

The rate of desorbing particles R_{des} is usually given in molecules/(area·time) and can be described by the **Polanyi-Wigner equation** [39]. This equation relates the desorption rate to the activation energy for desorption E_{des} and the frequency factor ν:

$$r_{des} = -\frac{d\Theta}{dt} = \nu \cdot \Theta^{(x)} \cdot e^{\left(-\frac{E_{des}}{kT}\right)} \tag{8}$$

x corresponds to the desorption order and describes the coverage dependence of the desorption rate. The coverage Θ is defined as adsorbate species per surface area, e.g. molecules/cm². Alternatively, the coverage can be defined as the ratio of the number of adsorbate species to the number of surface atoms of the substrate per unit area, which is designed Θ_A [39]. In this case, the desorption rate is given by

$$R_{des} = \frac{d\Theta_A}{dt} \cdot N_s, \tag{9}$$

where N_s is the concentration of surface sites per cm².

One distinguishes the following three scenarios [117], according to the coverage dependence of the desorption rate:

- Zero order (x = 0) desorption: In this case, the desorption rate does not depend on Θ and thus is constant at a given temperature. This is e.g. the

case for multilayer desorption. The peak maximum typically shifts to higher temperatures with increasing coverage.

- First order (x = 1) desorption: This corresponds to a desorption rate which is proportional to Θ, e.g. to particles which directly desorb from their sites. First-order desorption peaks have a characteristic asymmetric shape and their peak maximum remains constant with increasing coverage.
- Second order (x = 2) desorption: The desorption rate is proportional to Θ^2. This corresponds to associative desorption of two atoms stemming from different sites. In this case, the peaks are of nearly symmetric shape and they move to lower temperatures with increasing coverage.

In general, the determination of the desorption energy E_{des} and the frequency factor ν is rather difficult, as both parameters can be dependant on the coverage. A comprehensive analysis can be performed after the method of King [118]. However, if one assumes that E_{des} and ν are independent on the coverage, a rather simple approach is given by Redhead [119]. It is assumed that the sample temperature is linearly increased with a heating rate β, therefore:

$$T = T_0 + \beta \cdot t \,, \tag{10}$$

where T_0 is the initial temperature. Inserting Equation 6 in the Polanyi – Wigner equation yields for the temperature-dependent rate of desorbing particles:

$$-\frac{d\Theta}{dT} = \frac{\nu}{\beta} \cdot \Theta^{(x)} \cdot e^{\left(-\frac{E_{des}}{kT}\right)}. \tag{11}$$

The maximum in the desorption rate will occur when

$$\left.\frac{dR_{des}}{dT}\right|_{T_m} = 0$$

For the case of first-order desorption, Redheat established a relationship between E_{des} and the peak temperature T_m:

$$E_{des} \approx k_B T_m \left(\ln \frac{\nu T_m}{\beta} - 3.64 \right) \tag{12}$$

This gives a simple method to estimate E_{des} from TD data to ~20% [39], as for atoms and small molecules the frequency factor ν is typically in the order of 10^{13} s^{-1}. However, this result depends on a guess of ν, and it turned out that in particular large organic molecules can exhibit frequency factors which are significantly higher (see below). In this case, one rather uses

$$-\ln\left(\frac{d\Theta}{dT}\right) = \ln\left(\frac{\nu}{\beta} \cdot \Theta^{(x)}\right) - \frac{E_{des}}{kT} \tag{13}$$

and makes an Arrhenius type plot of $\ln(d\Theta/dT)$ vs $1/(T)$, presuming that $\Theta^{(x)}$ is known. This plot yields the desorption energy E_{des} from the slope of the straight line and ν from the y–axis intercept.

TDS on large organic molecules

Several peculiarities have to be considered when performing TDS on large organic molecules. It has already been noted before that the assumption of a frequency factor in the range of 10^{13} s^{-1} is only valid for atoms and small molecules. There is now ample of experimental evidence that for large organic molecules the frequency factor is frequently much higher [120-123]. This fact can be explained by the transition state theory (TST). According to TST, the pre-exponential factor can be expressed by the partition functions of the adsorbed phase q_a and the partition function of the desorbed state $q_\otimes$ [120, 124]:

$$\nu = \frac{kT}{h} \cdot \frac{q_\otimes}{q_a} \tag{14}$$

Values in the range of 10^{13} s^{-1} can only be expected if the adsorbates do not interact and if no change in the vibrational, rotational and translational degrees of freedom occur. Values of $\nu > 10^{13}$ s^{-1} indicate that $\frac{q_\otimes}{q_a} > 1$. This means that the

desorbed state has degrees of freedom which are more easily excited by thermal energy than the adsorbed state. In the case of large molecules it is obvious that the partition function of the free molecule is larger than that of the adsorbed molecule due to many rotational and vibrational degrees of freedom.

The analysis of TD spectra of large molecules can be more complicated than that of small molecules. Large molecules typically crack in the QMS upon ionisation leading to the detection of a complex cracking pattern rather than the mass of the intact molecule. In order to distinguish between the decomposition of the molecules on the surface and the cracking of the molecules in the QMS, a detailed knowledge of the cracking pattern of the molecules is indispensable. The cracking pattern of a lot of molecules can be found in different databases. However, one should bear in mind that the cracking pattern typically is characteristic for a special type of QMS, and it also depends on the ionization energy of the QMS. High ionization energies promote the cracking process while exceedingly small ionization energies can decrease the sensitivity. In Figure 8 the multilayer desorption of mercaptoundecanoic acid (MUA) is shown for different ionization energies. The reduction of the ionization energy from 70 V to 30 V leads to an increase of the mass signal 199 while the mass signal 41 significantly decreases.

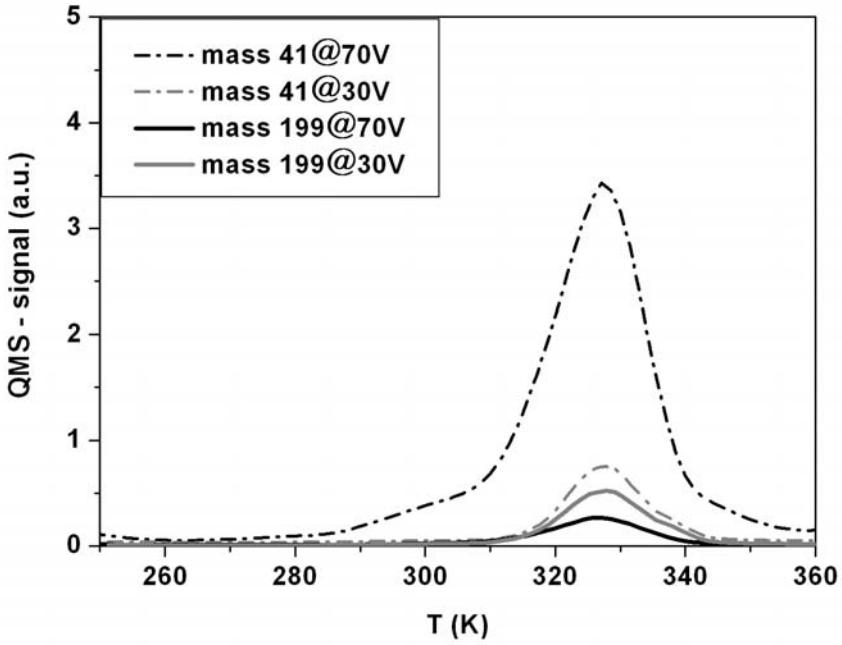

Figure 8. TDS of the multilayer of MUA. The cracking products 199 amu and 41 amu are shown for different ionization energies in the QMS.

3.2 Low energy electron diffraction

3.2.1 The method

Low energy electron diffraction is a commonly used method in order to determine the structure of surface adsorbates. It is a suitable method to probe the structure of regular organic monolayers such as SAMs. The initial observation of low energy electron diffraction was made by Davisson and Germer in 1927 [125]. However, it took nearly 50 years until it could be used to determine atomic positions [126] because of the lack of an adequate UHV setup and a proper scattering theory. The basic principle of this method relies on the wavelike behavior of the electrons. Low energy electrons (between 20 – 500 eV) have a deBroglie wave length of several Å, according to

$$\lambda = \frac{h}{m_e v} \tag{15}$$

These electrons are suitable to probe crystalline structures as their wavelengths are in the same order of magnitude as the inter-atomic distances in a solid. Due to their low energy and their strong interaction with the atomic potentials the electrons are backscattered within the first few layers. Alternatively, also high energy electrons can provide surface diffraction when the incident beam is directed at grazing incident (RHEED).

A scheme of a typical experimental setup for LEED is shown in Figure 9. Electrons are accelerated from a cathode filament towards the sample, where some of them are backscattered elastically. The scattered electrons typically reach a hemispherical grid arrangement. The first and third grids are on earth potential in order to guarantee a field free space. On the second grid, a negative bias is applied which is several volts below the acceleration voltage. Thereby only elastically scattered electrons go through the second grid and finally are accelerated towards the fluorescent screen where they produce a diffraction pattern.

A complete description of the positions and intensities of diffraction spots requires a dynamic theory that accounts for multiple scattering from all the layers that contribute to the scattering. The description of this sophisticated theory is out of scope in this thesis and can be found in literature [127]. An adequate description of the observed diffraction pattern can frequently be obtained by the simpler kinematic theory.

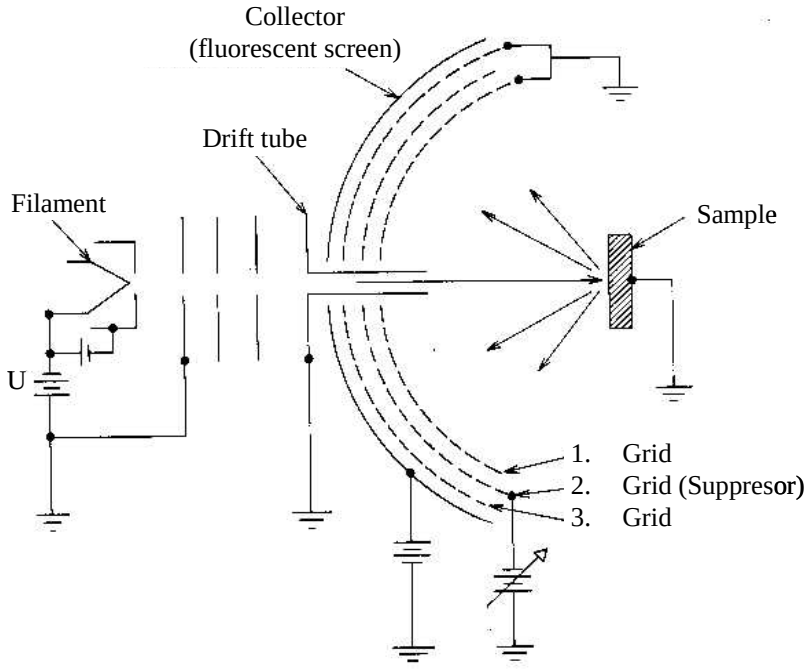

Figure 9. Scheme of the experimental setup for LEED as shown in [128]

3.2.2 The kinematic theory and the Laue-conditions

The kinematic theory only accounts for single scattering processes of the primary electrons with the periodic surface structure [128]. The basic equations can be obtained by several geometrical considerations: The diffraction condition for a lattice of periodicity a is

$$a \cdot (\sin\varphi - \sin\varphi_0) = n \cdot \lambda \tag{16}$$

where φ and φ_0 are the angles of the scattered and of the incident beam, respectively, and n denotes the diffraction order. Typically normal incident is used and as $\lambda[\text{Å}] \approx \sqrt{\frac{150}{U[V]}}$, one obtains:

$$\sin\varphi = \frac{n}{a} \cdot \sqrt{\frac{150}{U}} \,. \tag{17}$$

This equation forms the basis of kinematic LEED analysis.

In analogy to the geometrical consideration, the condition for constructive scattering can be expressed by the *Laue–condition* and visualized by the *Ewald-sphere* [88]. It can be shown that constructive interference occurs when the change of the incident wave vector $\Delta\mathbf{k}$ during the scattering process corresponds to a reciprocal lattice vector $\mathbf{a}^* = h\mathbf{a}_1^* + k\mathbf{a}_2^*$**.** This yields the Laue-equations:

$$\begin{aligned} \mathbf{a}_1^* \cdot \Delta\mathbf{k} &= 2\pi h \\ \mathbf{a}_2^* \cdot \Delta\mathbf{k} &= 2\pi k \end{aligned} \tag{18}$$

In order to visualize the Laue condition for constructive scattering, one can use the Ewald construction as shown in Figure 10. The reciprocal lattice is infinitively expanded in the direction orthogonal to the surface, one therefore typically draws rods. The wave vector of the incident wave $\mathbf{k_0}$ is drawn in such a way that it ends up with the (0,0) point. A sphere with radius **k** of the scattered vector is designed around the origin of $\mathbf{k_0}$. Diffracted beams produce spots where the Ewald sphere intersects with the reciprocal lattice rods.

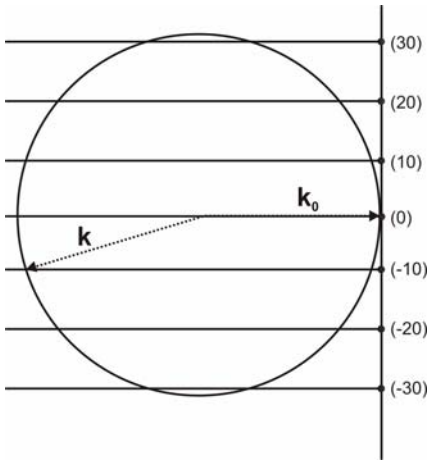

Figure 10. The Ewald construction for electron scattering on a surface.

3.2.3 Analysis of LEED patterns

The correct analysis of a LEED pattern can be rather complicated, in particular when an adsorbate is present on the surface. If the LEED pattern of the underlying substrate is known, spots due to the superstructure can be identified as extra spots. When an adsorbate structure has a lower symmetry than the substrate, differently oriented domains may occur. In this case, the diffraction pattern is a composition of the differently oriented domains. It thus can happen that one observes a higher symmetry in the diffraction pattern than is in reality present.

On the other hand, the domains have to reach a certain area in order to yield a diffraction pattern. The minimal area is determined by the coherence length of the incident electrons, which is limited by the energy spread of the incident beam and its angular divergence [129]. Only structures which are ordered within lengths comparable to the coherence length can contribute to the LEED pattern. Nowadays, a variety of LEED simulation programs are available, which facilitate the LEED pattern analysis enormously.

3.3 Auger electron spectroscopy

Auger electron spectroscopy (AES) is a frequently used technique in order to investigate the surface composition. For a detailed description of the method the reader is referred to the literature [117,130-133]. This method is based on the Auger effect, its principle is depicted in Figure 11. The surface is irradiated with an electron beam of an energy in the range of 2-10 keV. These primary electrons create core holes in the surface atoms, and the atom can relax back by one of two processes: it either ejects an X-ray photon or it transfers its energy to an

Auger electron. In particular for light elements, the X-ray fluorescent becomes negligible and Auger emission becomes favourable. The Auger transition is primarily characterized by the location of the initial hole and the final two holes. The kinetic energy of an Auger electron is given by [117]:

$$E_{kin}(KL_1L_{23}) = E_k - E_{L_1} - E_{L_{23}} - E_{inter}(L_1L_{23}) + E_R - \Phi \qquad (19)$$

wherein E_{inter} (L_1L_{23}) is the interaction energy between the holes in the L_1 and L_{23} shell and E_R is the sum of the intra-atomic and extra-atomic relaxation energies. Φ is the work function of the material. The energy range of the Auger electrons is typically between 20-1000 eV, which corresponds to an inelastic mean free path between 2-6 ML.

This explains the remarkable surface sensitivity of the method. The kinetic energy of the electrons is characteristic for a special atom and therefore elemental identification is provided. In analogy to XPS the Auger peak position reflects the chemical environment of the atoms which leads to the observation of so-called chemical shifts (see next section). However, the quantitative interpretation of these shifts is much more difficult in this case by the fact that three electrons are involved in the Auger process.

The most commonly used energy analyzer for AES is the cylindrical mirror analyzer (CMA), a scheme of the CMA is shown in Figure 12. The electrons enter the region between the two concentric cylinders. While on the outer cylinder a negative voltage is applied, the inner cylinder is grounded. Thereby only electrons with a certain energy E_0 pass through the output aperture and then are detected by the electron multiplier.

AES is usually considered as a non-destructive method but in the case of organic molecules the incident electron beam may destroy the layer and AES therefore has to be performed with care.

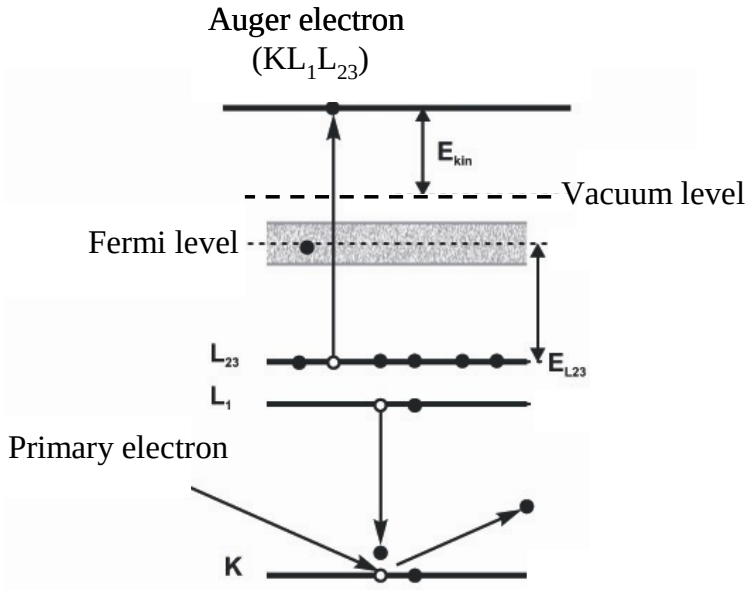

Figure 11. Scheme of the Auger process.

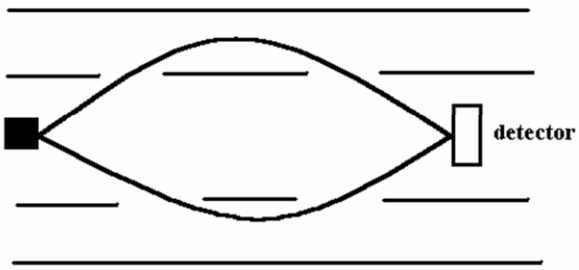

Figure 12. A scheme of a cylindrical mirror analyser (CMA).

3.4 X-ray photoelectron spectroscopy

X-ray photoelectron spectroscopy (XPS) is one of the most currently used surface-analytical techniques. A detailed description of this method can be found in the literature [131-133]. XPS is based on the photoelectric effect. When a surface is irradiated with soft X-rays, photoelectrons with the following kinetic energy are ejected:

$$E_{kin} = h\nu - E_B - \Phi . \tag{20}$$

E_B is the binding energy of the electron and Φ is the work function of the material. As no two elements share the same set of electron binding energies, the measurement of the kinetic energy of the ejected electrons enables elemental analysis. The typical energy range of the photoelectrons is between 200-1500 eV. This corresponds to an inelastic mean free path between 4-8 ML, which explains the surface sensitivity of the method.

The experimental setup includes a monochromatic source of photons and an electron energy analyser [117]. The typical laboratory sources for XPS are X-ray tubes wherein the X-ray flux is created by bombarding a target with high energy electrons. In practice Mg and K are the most commonly used target materials. The X-radiation from these materials is quite complex. Besides the principles $K_{\alpha 1,2}$ lines at 1253.6 eV (Mg) and 1486.6 eV (Al), a series of further lines, so called satellites lines, also exist, but with a much smaller intensity.

The universally employed analyser is a concentric hemispherical analyser (CHA), which is a deflection type analyser. The main elements are two metallic concentric hemispheres. The outer hemisphere is biased negatively with respect to the inner hemisphere to produce an electrostatic field which balances the centrifugal force of the electrons on their trajectory.

XPS can not only be used to identify the composition of the surface but it also allows to determine the composition quantitatively through the peaks heights.

Furthermore, any changes in the binding energies of the electrons are reflected in their kinetic energy. Thus changes in the chemical environment can be followed by monitoring changes in the photoelectron energies, so-called *chemical shifts*.

3.5 Fourier–transform infrared spectroscopy

Infrared (IR) spectroscopy is widely used in order to analyse molecules in a bulk or on a surface. It can be used to identify compounds as well as to investigate specific properties of a sample of known composition. IR-spectroscopy is based on the fact that a sample can absorb electromagnetic radiation in the near and middle infrared region (1.5-10 µm), if the incident light interacts with the dipole moment of the molecules. A typical modern setup for IR-spectroscopy is shown in Figure 13. A frequently used IR-light source is the glowbar. It consists of SiC and is typically heated up to 1500 K, providing an emission spectrum similar to a black body emitter. In order to obtain a wavelength-selective spectrum, one needs a dispersive element. In modern devices therefore typically a Michelson Interferometer (MI) is used due to its high resolution. The maximal displacement x of the mirror in the MI is related to the resolution of the spectrometer. After passing the MI, a signal $I(x)$ is detected. In order to obtain a wavelength-dependent signal $\tilde{I}(\nu)$ a Fourier-transformation is performed:

$$\tilde{I}(\nu) = \int_{-\infty}^{+\infty} dx \, I(x) \cdot e^{i 4\pi x \nu} . \tag{21}$$

In general, the Fourier transformation is automatically calculated by the software of the spectrometer.

In order to detect the IR – radiation, frequently DTGS (deuterated triglycinsulfat) or MCT (mercury-cadmium-tellur) detectors are used due to their good sensitivity.

The DTGS detector is a pyroelectric detector which reacts on the heat of the impinging radiation, while the MCT detector is a semiconductor detector. It relies on the excitation of electrons from the valence in the conduction band due to the incident electromagnetic radiation.

IR-measurements can be performed *in-transmission*, thus the IR-light transmits the sample, or *in-reflection*, which means that the IR-light is reflected on the sample surface. The latter method is also reported as infrared reflection absorption spectroscopy (IRRAS) and is particularly suitable to investigate SAMs on gold, as the gold surface provides a highly reflecting substrate. However, the analysis of the spectra can be rather difficult, therefore a lot of databases are available. For further information about this method the reader is referred to the literature [134-140].

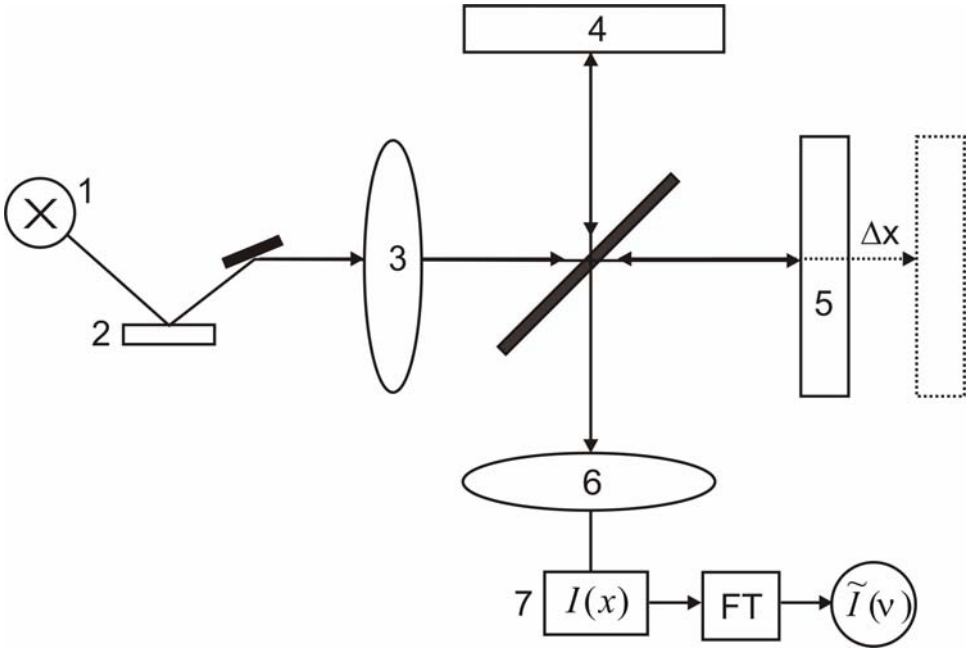

Figure 13. Scheme of an FTIR-apparatus.1: IR light source, 2: sample, 3: lens, 4: fixed mirror, 5: movable mirror, 6: lens, 7: detector.

3.6 Atomic force microscopy

AFM belongs to the group of scanning force microscopes which are based on the measurement of various forces which occur between a sharp tip and a sample surface, e.g. electrostatic, magnetic or Van der Waals forces [117,141]. The basic components of an AFM are a sharp tip which is mounted on a soft cantilever, a detection system which measures the deflection of the cantilever, a piezoelectric translator to move the tip relative to the sample and an imaging system. In order to measure the deflection of the cantilever, typically a laser beam is used which is focused on the rear of the cantilever. The reflected laser beam is directed towards a photodiode. As soon as the position of the cantilever changes, the laser beam is deflected and its position on the photodiode changes.

In particular the tip and the cantilever have to fulfil a number of requirements. The tip should be very sharp with a small radius of curvature in order to trace fine details on the surface. The cantilever should be softer than the bonds between the atoms on the sample in order to achieve a deflection of the cantilever without displacement of surface atoms. AFM is essentially based on the interatomic, short-range repulsive forces between tip and sample surface which causes the cantilever to deflect. Also long-range forces (e.g. Coulomb forces) and dipole-dipole interactions are encountered. A simple approach for a force versus distance curve is shown in Figure 14. At the right side of the curve, when the tip-to-sample separation is rather large, the tip is weakly attracted to the surface. The attraction increases with decreasing distance until at a certain distance (several Å) the repulsion dominates. Depending on the distance between tip und sample surface, one can distinguish different operation regimes:

- Contact mode: In the contact mode, the distance between tip and sample is in the range of a few Å. In this case, the tip is in soft physical contact with the sample and short-ranging, repulsive forces occur. This

regime enables high-resolution images due to the extreme short-range nature of the force.

- Non-contact mode: In this mode the tip-sample separation is in the order of tens to hundreds of Å and the tip is subjected to weak attractive forces. A piezoelectric drive is used to shake the cantilever at a resonant frequency. The amplitude, frequency and phase of the oscillations are then measured. Due to interactions with the surface, the frequency f changes according to $f \propto \sqrt{c - F'}$, with c the spring constant of the cantilever and F' the force gradient.

- Tapping mode: Again the cantilever is driven into resonant oscillations. The tip is brought close enough to the surface that it touches the surface at the bottom of each oscillation. Again one measures variations in the oscillation frequency, amplitude or phase. This mode is favoured in order to image rough surfaces with topographical corrugations.

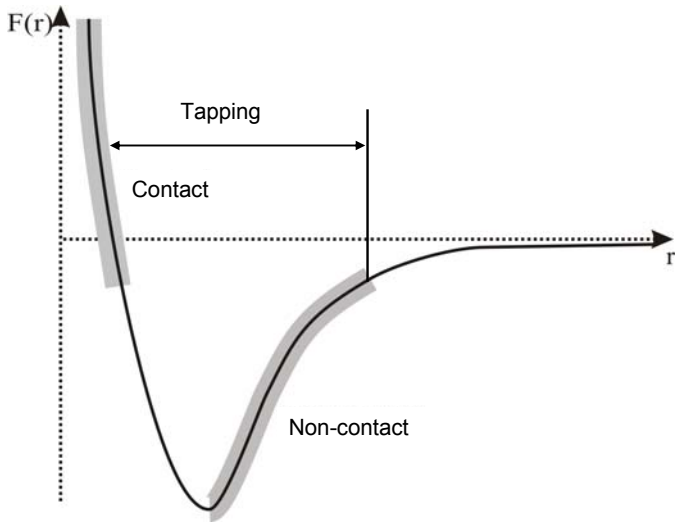

Figure 14. A simple approach for a force-versus-distance curve. The regions of the AFM contact and non-contact mode are indicated.

4 Preparation of UDT/MUA layers

4.1 The substrates

The influence of the substrate on the SAM formation was of special interest in this work. Therefore, three different substrates were investigated: Au(111)/mica, gold foils and a Au(111) single crystal. The Au(111)/mica samples with a nominal gold film thickness of 300 nm were purchased from Georg Albert PVD [142]. The 99,99% high purity polycrystalline gold foils (0.1 mm thick, 10 mm x 10 mm) were purchased from Ögussa Inc. [143] and the Au(111) single crystal (2 mm thick, Ø 10 mm) was obtained from MaTecK Inc. [144]. These substrates could be shown to differ in their morphology and structure, which was investigated by means of AFM and LEED, as well as in their chemical composition as observed by XPS and AES. Two different cleaning methods were used in order to obtain preferably clean and smooth substrates: The substrates either were cleaned under ambient conditions in Piranha solution[1] or by Ar^+ sputtering and annealing up to 900 K in UHV.

4.1.1 The chemical composition

In order to characterize the substrates regarding to their chemical composition, AES and XPS measurements were performed. While XPS is particularly sensitive for heavy atoms like gold, AES is favoured for the detection of the typically 'light' impurities as carbon and sulfur. In Figure 15 XP spectra of differently prepared *gold foils* are shown. The untreated sample is highly contaminated by carbon and oxygen, leading to a strong attenuation of the gold peaks.

[1] Caution: Piranha solution (70% H_2SO_4, 30% H_2O_2) reacts violently with most organic materials and must be handled with extreme care.

After 20 min cleaning in Piranha solution still carbon and oxygen contaminations are present on the surface. In contrast, after 15 min Ar^+-sputtering and annealing no more contaminations can be detected in the XP spectrum. Therefore the gold foils usually were cleaned by Ar^+ - sputtering and annealing in UHV, even though this causes more experimental effort if the SAM preparation is performed under ambient condition. In this case, the substrates were cleaned *in situ* in the UHV chamber and then removed and put in solution *ex situ*.

In this context the chemical inertness of the gold foils under ambient condition was of interest. Therefore the UHV chamber was vented for several hours after the cleaning procedure and then was evacuated again. The corresponding XPS spectrum is shown in Figure 16a, for comparison the spectrum of the freshly cleaned gold foil is added. A rather low carbon contamination is observed and no significantly increase of oxygen contaminations was detected. We therefore assume that the gold surface remains rather clean during exposure to air for several hours.

Further characterization of surface contaminations was performed by AES. This method reveals the presence not only of carbon and oxygen, but also of chloride contaminations on the untreated gold foils (Figure 16b). Furthermore it was found that the carbon contaminations are not fully removed after 15 min sputtering, differently than suggested by XPS. The AES carbon-peak did not vanish until 60 min Ar^+ - sputtering was performed.

In the case of *Au(111)/mica*, the cleaning in Piranha solution was not possible as the gold layer flaked off from the mica surface. But also Ar^+ - sputtering and annealing had to be performed with care: Long sputtering (>10 min) as well as annealing up to temperatures higher than 800 K damaged the gold layer. Fortunately, rather low contaminations were found on these substrates (Figure 16c) and therefore short sputtering times could be applied, not longer than 5 min

in order to protect the gold layer. In contrast, the *Au(111) single crystal* was sputtered and annealed up to 900 K for several hours in order to get a clean and smooth surface.

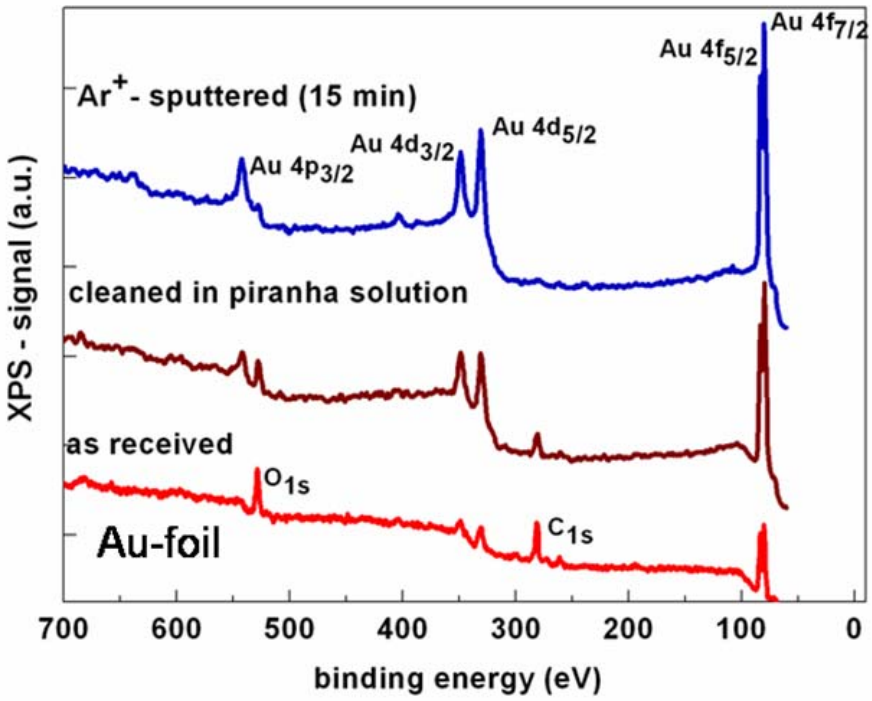

Figure 15. The cleaning of the gold foils as characterized by XPS. The cleaning in Piranha solution is compared to the Ar^+ sputtering in UHV.

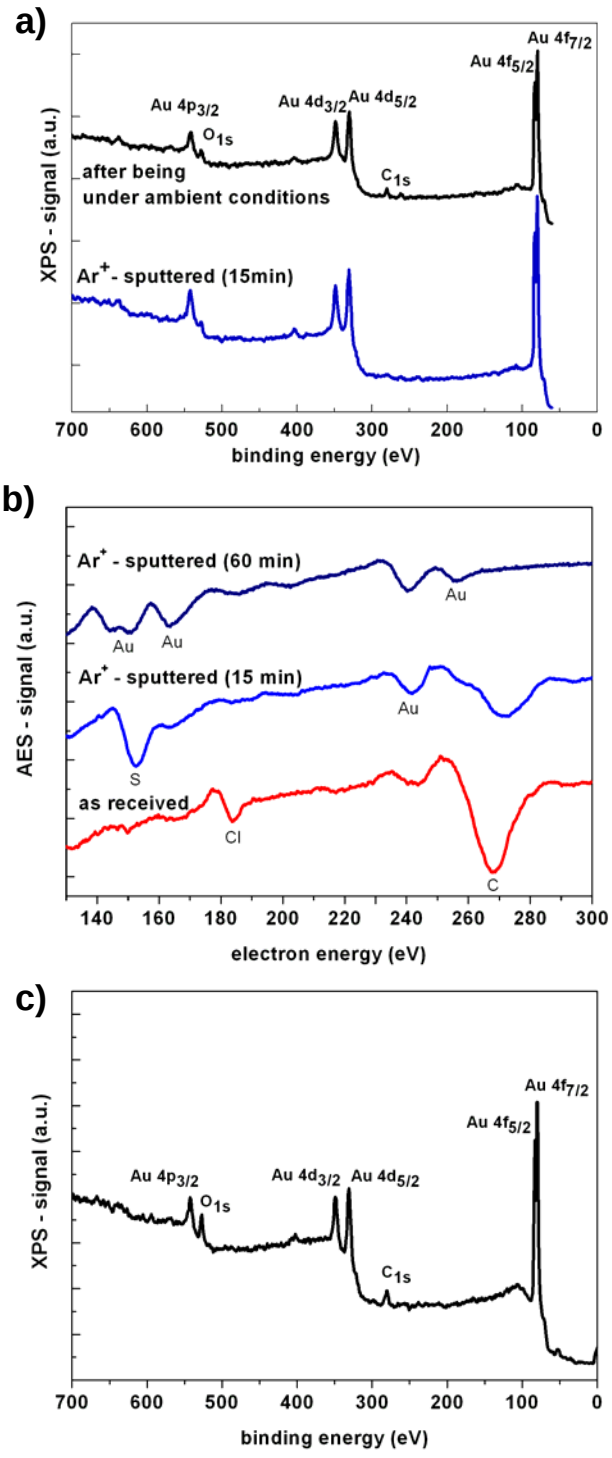

Figure 16. The gold substrates as characterized by XPS and AES. Small carbon contaminations after exposure of the clean substrate to air (a). Auger spectra of differently long Ar^+-sputtered gold foils (b) and the XPS spectrum (c) of an untreated Au(111)/mica.

4.1.2 The morphology and structure

A prerequisite for the formation of SAMs is an atomically flat gold film [145]. This strongly suggests the use of an **Au(111) single crystal** as substrate, which provides a smooth and densely packed surface. The LEED pattern of the gold single crystal showing the six spots of the (111) plane is depicted in Figure 17a. Each of them is surrounded by six additional spots (see inset) stemming from the well-known herringbone reconstruction of the Au(111) plane [146,147].

However, gold single crystals are rather expensive and must be handled with care. For repeatedly performed *ex-situ* experiments, typically other substrates are favoured. In fact, gold was found to grow epitaxially on the mica surface with a strong preference of the (111) orientation. The LEED pattern of a **Au(111)/mica** sample is shown in Figure 17b. In comparison to the single crystal, the spots are more expanded which indicates smaller crystallites. After 5 min sputtering and annealing up to 800 K the LEED spots become even cloudier (Figure 17c). This is explained by a roughening of the surface during Ar^+ – sputtering that can not be annealed within short times.

In Figure 18a,b AFM images of Au(111)/mica samples are shown. One can observe a facet like structure, which has frequently been described in the literature [145,148,149]. However, the origin of these facets is not unambiguously clarified. In [148] it is stated that they are a consequence of the (111) orientation of the film. They also could stem from the release of stress originated in the gold/mica interface caused by cooling down from elevated temperatures to room temperatures and slightly different coefficient of thermal expansion of gold and mica [145]. This stress is assumed to effect the deep trenches which can consistently be observed (e.g. in the left upper corner of Figure 18a). The surface roughening due to Ar^+ - sputtering is shown in Figure 18c,d. Due to the tendency of the gold layer to flake off during sputtering and annealing, these samples are not appropriate for repeated use. An experimentally far more convenient substrate is provided by the **gold foils**.

The gold foils consist of various, differently oriented crystallites. Long term sputtering and annealing yields grains up to several 100 µm in diameter [150], as shown in Figure 19a,b using light-microscopy. The LEED pattern of the polycrystalline gold foil is shown in Figure 17d. It consists of various sharp diffraction spots in a wide range of energy, which stem from the differently oriented domains. AFM images of a sputtered and annealed gold foil are shown in Figure 18e,f.

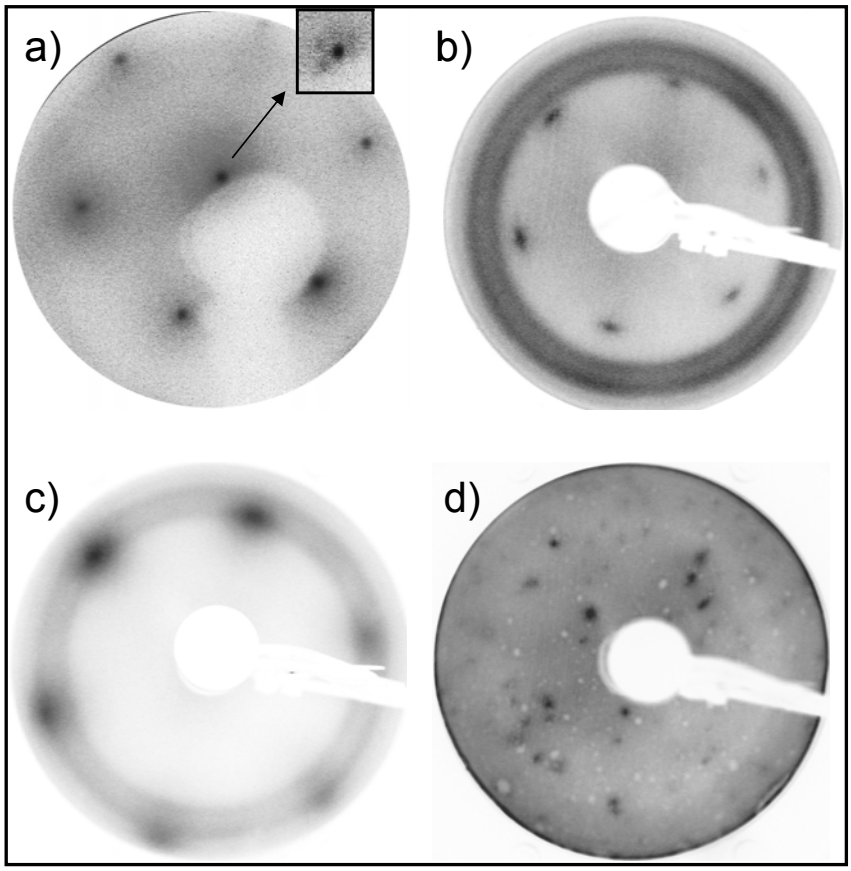

Figure 17. The LEED patterns of the different gold substrates. The six spots of the Au(111) single crystal (a, 205 V), of Au(111)/mica (b, 206 V) and of sputtered Au(111)/mica (c, 122 V). In the case of the polycrystalline gold foils, various sharp diffraction spots are observed at a wide range of energy (d, 26 V).

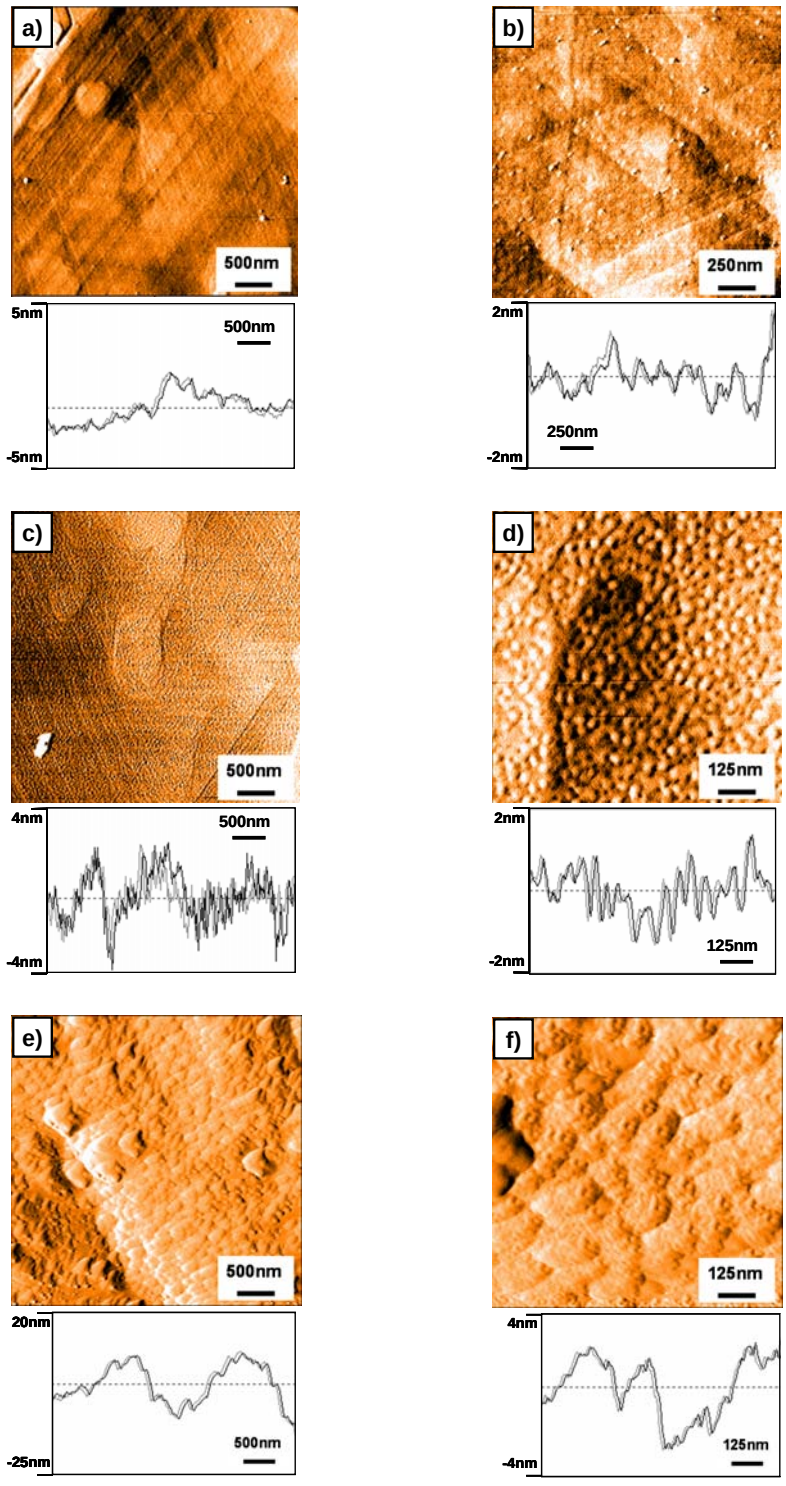

Figure 18. AFM images of different gold substrates. Au(111)/mica (a,b), sputtered Au(111)/mica (c,d), and sputtered and annealed gold foils (e,f).

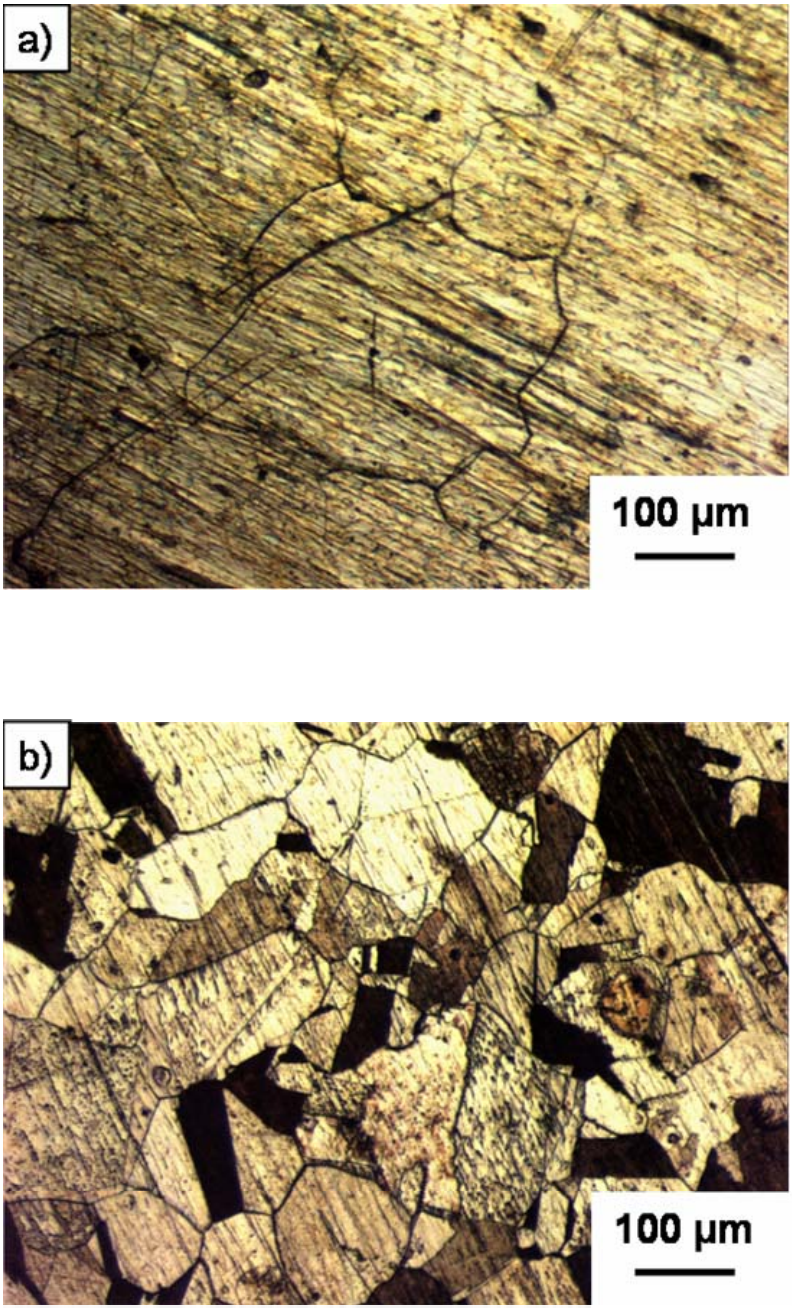

Figure 19. Light microscopy pictures of the gold foil after 24h annealing at 900 K (a) and after subsequent etching in aqua regia (nitric acid and hydrochloric acid (b)).

4.2 In situ preparation

There are basically two methods to prepare a SAM. One can either put the substrate in a solution of the corresponding molecule or one can deposit the molecules by evaporation of the material in a UHV chamber. Even though the latter method demands significantly more experimental effort, it provides a lot of advantages:

- The surface composition is better known, as the SAM can be prepared after the cleaning without exposure to air.

- It is possible to deposit a well defined amount of material, including sub-monolayer and multilayer coverages at low temperatures.

- No solvent is necessary, whose influence on the SAM formation frequently is little known.

- One can recycle the sample easily by Ar^+ - sputtering.

- The SAM can be analyzed directly after the preparation, without being under ambient conditions and without installing it into the sample holder, which can cause damage of the SAM.

4.2.1 The UHV – chamber

A scheme of the UHV setup is shown in Figure 20. A turbo molecular pump (T1, S = 500 l/s) and a rotary vane pump as booster pump are installed in the main chamber. The sample is mounted on a rotatable sample holder which is differentially pumped with a small T2. The UHV chamber has a base pressure of

$1x10^{-10}$ mbar, but most of the experiments were performed without baking the system, leading to a background pressure in the low 10^{-8} mbar range.

For the TD measurements, an elaborated sample mounting is necessary in order to assure that only particles desorbing from the sample surface are detected (see below). The gold foils and the Au(111)/mica samples were fixed to a stainless steel plate via thin tantalum wires, as shown in Figure 21a. Additional tantalum wires were spot welded on the backside of the plate in order to connect it to the sample holder. The stainless steel plate could be heated by resistive heating via the tantalum wires up to 1000 K and cooled by liquid nitrogen down to 100 K. The temperature was measured by a Ni/NiCr thermocouple attached to the backside of the samples. The temperature was controlled by a *LabView* program which allowed to maintain a constant sample temperature as well as a linear heating rate.

The Au(111) single crystal was suspended on thin, 0.2 mm diameter Ta wires which were inserted in a thin groove at the rim of the sample and clamped to the sample holder (Figure 21b). The thermocouple was spot welded to the backside of the crystal.

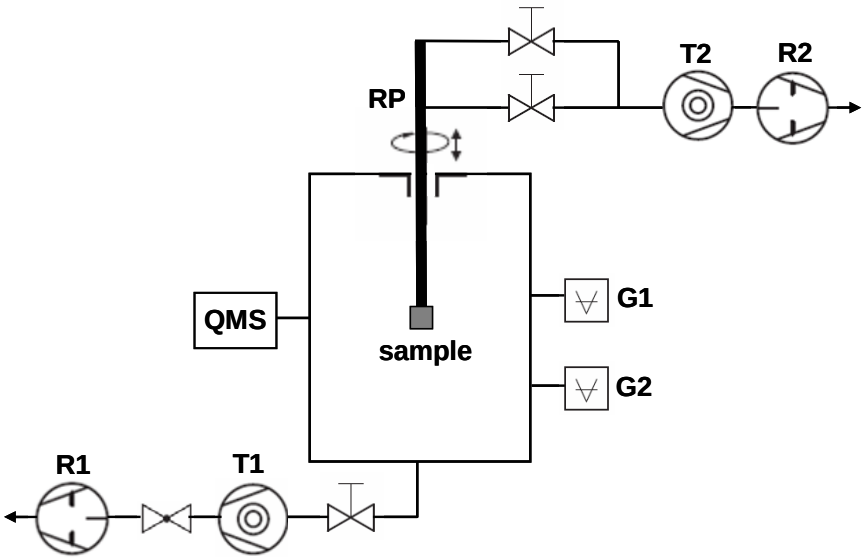

Figure 20. A schematic side view of the UHV chamber. G: ionization gauge, R: rotary vane pump, RP: rotational platform, T: turbo molecular pump, QMS: quadrupole mass spectrometer.

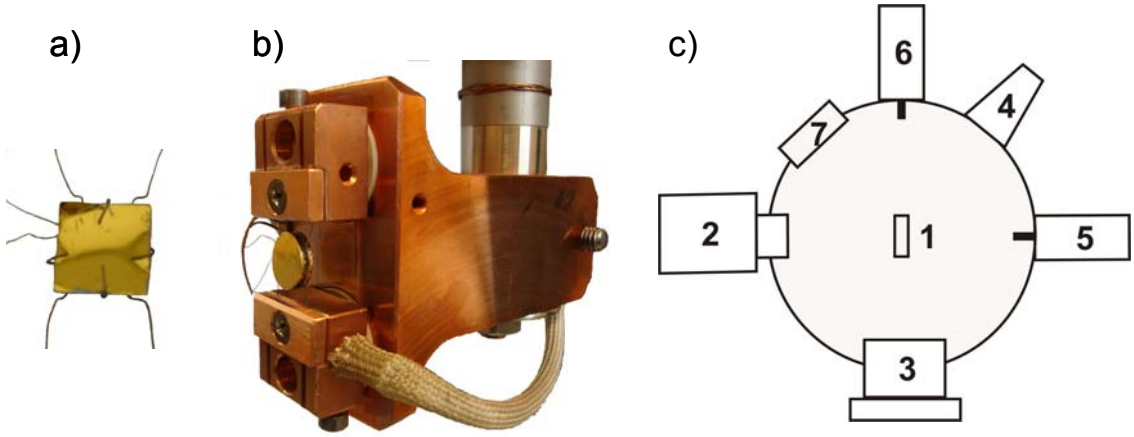

Figure 21. The stainless steel plate whereon a gold sample is mounted (a). The installation of the single crystal onto the coppery sample holder (b). A scheme of the analytical setup (c) 1: the sample, 2: QMS, 3: LEED, 4: Ar^+-sputter gun, 5: MUA evaporation source, 6: UDT evaporation source, 7: window.

The analytical equipment is placed circular around the sample, a scheme is shown in Figure 21c. A quadrupole mass spectrometer (QMS, Pfeiffer Inc.) with a magnetic field enhanced cross-beam ion source was used to control the residual gas phase as well as to perform TDS. For this purpose, the desorption flux was monitored by the multiplexed mass spectrometer in in-line position. The detectable mass range was 1 to 500 amu. Some of the measurements were performed with a Prisma 200 QMS (Pfeiffer Inc.), with a smaller detectable mass range from 1 to 200 amu. The cleaning of the substrates was performed by an Ar^+-sputter gun. The LEED experiments were performed with a micro-channelplate-enhanced series 855 MCP-LEED instrument (Omicron Inc.). This LEED optics can be operated at very low emission currents to reduce damaging of the SAM. For some of the experiments, instead of the LEED optics an Auger spectrometer was installed (Staib instruments ES100) in order to determine the surface cleanliness and the chemical composition of the SAM. However, when performing AES on organic molecules, one should bear in mind that the impinging electrons can destroy the organic layer. In order to avoid significant damage, the electron emission currents were kept below 0.4 µA.

The XPS measurements were performed in a separate UHV chamber (again the base pressure was 10^{-8} mbar without baking the system). This apparatus was equipped with an X-ray photoelectron spectrometer (Leybold Heraeus, EA 10/100). The X-ray source could be switched between Mg $K_{\alpha 1,2}$ (1253.6 eV) and Al $K_{\alpha 1,2}$ (1486.6 eV) radiation. The source voltage was set to 10 kV and the emission current was 30 mA. Electron energy analysis was performed with a concentric mirror analyzer and the electrons were detected by a secondary electron multiplier.

Atomic force microscopy was performed under ambient conditions using a Nanosurf Easyscan 2 scanning probe microscope in tapping mode.

Infrared reflection absorption spectroscopy (IRRAS) was performed with a Bruker IFS 66 v/s spectrometer using p-polarized light incident at 82° with respect to the surface normal. A nitrogen cooled MCT detector was used. The measurement chamber was continuously purged with gaseous N_2.

The importance of the sample suspension for TDS

The correct dimensioning of the sample suspension is of utmost importance for TDS. As an example, a UDT desorption feature at an unreasonably high desorption temperature of 720 K is shown in Figure 22. This desorption peak was detected repeatedly after UDT deposition, even without installing a sample onto the sample holder. Due to the increase of this feature with altering sample holder position in front of the QMS, it was concluded that it concerns UDT multilayer desorption from the copper brackets used to clamp the stainless steel plate onto the coppery sample holder (see Figure 21b). In order to reduce the heating of these brackets, they were designed two times as thick as before. This indeed eliminated the desorption feature.

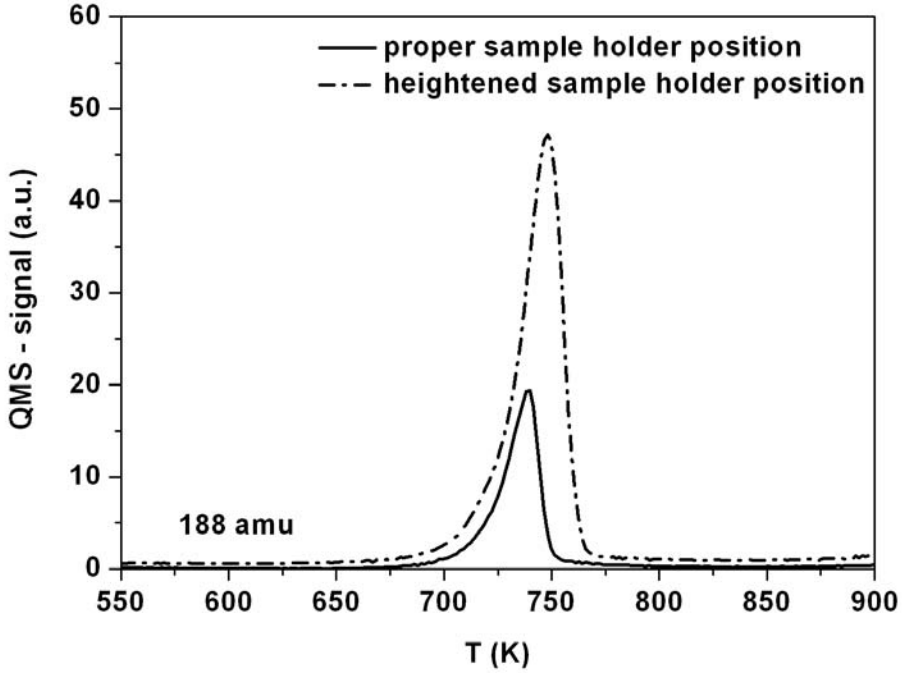

Figure 22. Influence of desorption from the sample holder. A desorption feature at an unreasonably high desorption temperature of 730 K was detected. This peak was observed irrespective of whether a sample was installed on the sample holder or not. Furthermore, it increased with altering sample holder position. This feature was attributed to UDT multilayer desorption from the copper brackets used to clamp the sample (see text).

4.2.2 The deposition of MUA and UDT

In order to perform deposition of UDT (Figure 23a) on the sample in UHV, the liquid material was stored in a glass container and the vapor, according to the vapor pressure at room temperature, was supplied via a leak valve and a 2 mm ID tube directly onto the sample (tube exit-sample distance: 20 mm). The actual exposure is a combination of the direct impingement of the molecules and the isotropic impingement due to the partial pressure increase of UDT in the vacuum chamber. Strictly speaking, the description of the exposure in terms of Langmuir

(1 L = 10^{-6} Torr sec = 1.33 x 10^{-6} mbar sec) is therefore not appropriate. However, in order to obtain a good measure of the actual exposure, the following procedure was applied: In a first experiment, UDT was fed directly onto the cooled sample (in-line dosing) for a certain time, followed by thermal desorption of the layer. In a second experiment, UDT was led into the chamber for an equally long time while the sample was turned away from the inlet tube (isotropic dosing) and again the desorption peak was detected. The ratio between the amounts of desorbing particles yields the so called enhancement factor for direct dosing, which turned out to be ≈ 40 in our case. As the isotropic partial pressure increase was typically in the range of $2x10^{-8}$ mbar, one can assume the actual pressure at the sample surface in front of the inlet tube to be 40 times higher, leading to a pressure of $8x10^{-7}$ mbar. The values of exposure given in this thesis are thus calculated by the pressure increase, corrected with the enhancement factor, and multiplied with the time of evaporation.

The MUA (Figure 23b) is a solid at room temperature and therefore had to be heated up to approximately 50 °C to get a liquid with an appropriate vapor pressure. A picture of this evaporation source is shown in Figure 24. Again the vapor was fed onto the sample via a leak valve and a 2 mm ID stainless steel tube. The whole gas inlet system was permanently held at 150 °C in order to avoid re-condensation on the inner wall of the gas inlet tube (tube exit-sample distance: 20 mm). In this case, no significant isotropic pressure increase in the chamber could be observed, due to the much smaller vapor pressure. Thus, the actual exposure is just given by the exposure time and the vapor pressure according to the temperature of the substance in the container. The vapor phase was purified by several freeze/thaw cycles and differential pumping of the gas line.

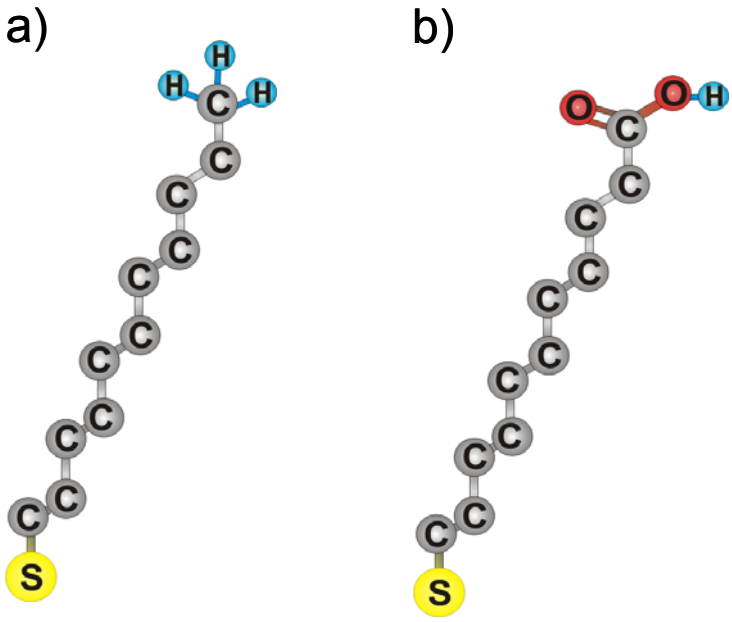

Figure 23. Scheme of the UDT (a) and of the MUA (b) molecule. For simplicity, the hydrogens of the carbon chain and next to the sulfur are skipped.

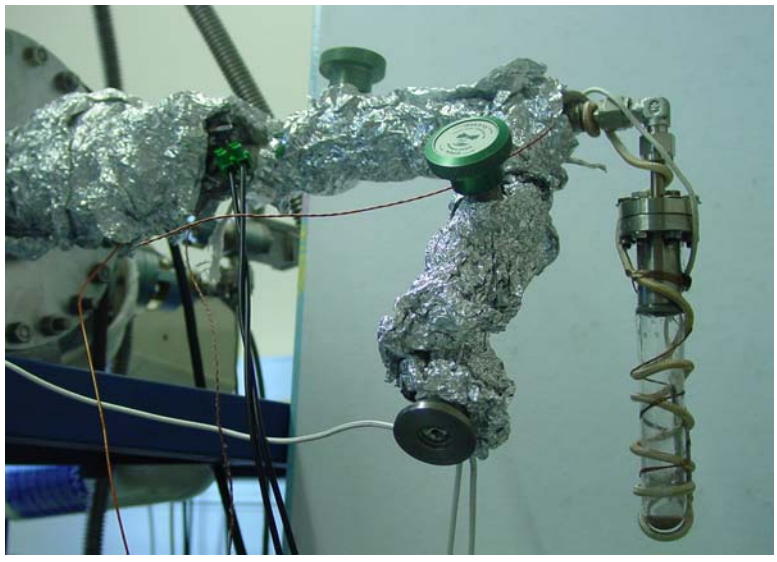

Figure 24. The MUA evaporation source.

Peculiarities of UDT/MUA deposition

One of the following two scenarios is convenient for gas phase deposition in UHV: the evaporated material should either be gaseous at room temperature, so that it can be pumped, or solid, so that it condenses on the walls of the chamber and does not contribute to the residual gas. MUA is a solid at room temperature and therefore does not pose a challenge in this connection. However, UDT is a fluid at room temperature and ranks among a third group of material, which is experimentally difficult to be handled. The molecules tend to stick on the walls and then desorb slowly again which makes them very difficult to be pumped. 18 hours after the UDT deposition still a significant part of UDT molecules in the residual gas could be detected. Storage of the sample in the UHV chamber was therefore not possible without further adsorption of UDT.

4.3 Ex situ preparation

The substrates were either cleaned by Ar^+ - sputtering or in Piranha solution. Subsequently, the substrates were put in 1 mM ethanolic solution of the corresponding molecule for 24 h. Thereafter, the samples were dried with CO_2 - spray and installed immediately into the UHV chamber for further characterization.

5 Experimental results

5.1 The multilayer regime of UDT and MUA

5.1.1 Characterization of the multilayer by TDS

An important prerequisite for the analysis of desorption spectra is the knowledge of the cracking pattern of the molecules under investigation. The cracking products are generated in the QMS upon ionization and depend on the ionisation energy (as described in Section 3.1). In order to determine the cracking pattern, two methods were applied:

1) The material was evaporated directly into the QMS. Thereby, a rather large amount of material is provided. In this case, the QMS was operated in a multiplexed mode detecting *all* masses of its mass range. This method is particularly suitable to determine the different cracking products of the cracking pattern.

2) The material was deposited in form of a multilayer on the sample. Thereafter, multilayer desorption was performed and the desorbing masses were detected in the QMS. In this case, smaller amounts of material are detected. Multiplexing *all* possible masses therefore is not advisable; in order to enhance the sensitivity typically ~10 masses were recorded simultaneously. This method is suitable to determine the exact ratio between the different cracking products, as contributions from the residual gas can be more or less neglected.

The cracking pattern of UDT and MUA as determined via direct evaporation into the QMS are shown in Figure 25a,b. A quite complex cracking pattern is observed for both molecules. In addition to the intact molecules at 188 amu

(UDT) and 218 amu (MUA), bunches of C_xH_y are observed. In the case of UDT, intense lines are observed at 43 amu (C_3H_7) and 55 amu (C_4H_7). Furthermore, a rather discrete line is observed at 155 amu (e.g. $C_{11}H_{23}$). In the case of MUA, bunches of C_xH_y are observed at m = 27, 28, 39, 41 and 55 amu. In addition, several discrete lines are detected at 149 amu (e.g. $C_{11}H_{17}$), 167 amu (e.g. $C_{11}H_{19}O$), 182 amu (e.g. $C_{11}H_{18}O_2$) and 200 amu (e.g. $SC_{10}H_{20}CO$).

A more detailed characterization of the cracking pattern was performed by multilayer desorption. The multilayer of UDT and MUA was prepared in the UHV chamber. For this purpose the sample was cooled to 200 K and a sufficient amount of molecules was deposited. As the deposition of a specific amount of material was difficult (see Section 4.2.2), the actual coverage was determined afterwards from the area under the desorption peak. The multilayer desorption spectra of UDT and MUA from a gold foil are shown in Figure 26a,b respectively. The multilayer of UDT desorbs at a significantly lower temperature (at 275 K) than the multilayer of MUA (at 325 K). This rather large discrepancy of the multilayer desorption temperature is attributed to hydrogen bonds ($OH^{\cdots}OH$) which are present between the carboxylic acid end groups of the MUA molecules. For UDT, besides the mass of the intact molecule (188 amu), two prominent cracking products are shown: 55 amu and 43 amu, which can be attributed to C_xH_y fragments of the alkyl chain. They are thus representative for the intactly desorbing UDT molecules in the TD spectra. The most important cracking products of MUA are 200 amu, 55 amu and 43 amu. The intensity of the intact MUA molecule in the mass spectrum is very weak and is therefore not shown here. The highest mass which is detectable with a sufficient sensitivity is mass 200. This mass stems most likely from the separation of the -OH group, in addition to the S-H bond splitting during ionization.

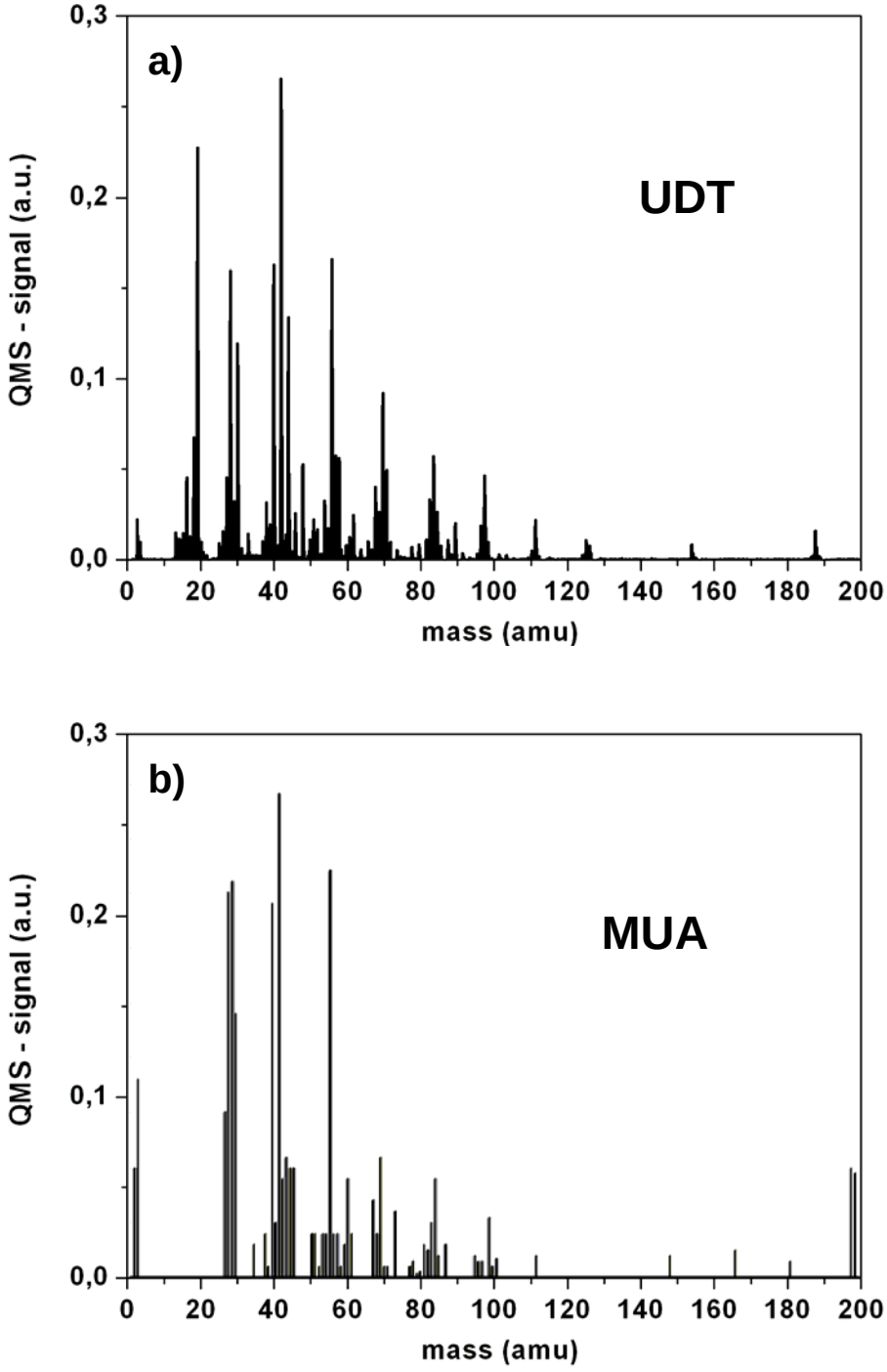

Figure 25. The cracking pattern of UDT (a) and of MUA (b) as determined via direct evaporation in the QMS.

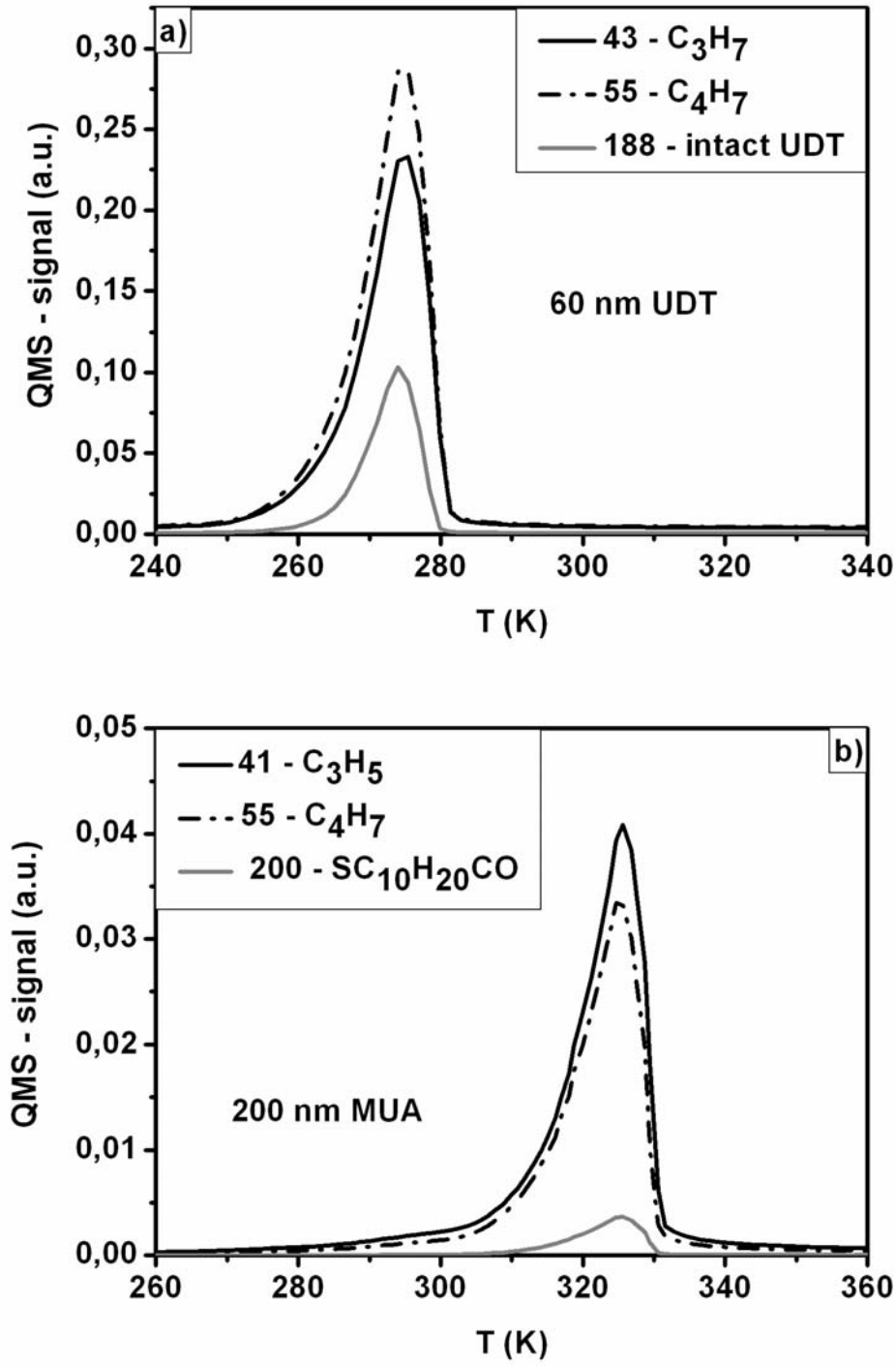

Figure 26. Thermal desorption spectrum of a multilayer of UDT (a) and MUA (b). The most important cracking products are shown.

For the quantitative evaluation of the multilayer TD spectra, the QMS signal (m=43 amu (UDT), m=41 amu (MUA)) has to be calibrated. For this purpose, it was assumed that the area under the desorption peak of lying molecules (β-peak, see Section 5.2.2) contains 1.3 x 10^{14} molecules/cm^2 for both UDT and MUA, as deduced from LEED experiments (see Section 5.2.3). This corresponds to a coverage of 9% of the Au(111) surface which is providing 1.4x10^{15} surface atoms/cm^2. By comparing the TD spectra, the multilayer of UDT is attributed to an amount of approximately 1x10^{16} molecules, while the multilayer of MUA contains 5x10^{16} molecules. Taking into account the density of UDT and MUA (0.8 g/cm^3 and 1 g/cm^3, respectively) one can determine the mean thickness *d* of the investigated multilayers. For the films presented in Figure 26a,b the calculation yields *d* = 60 nm in the case of UDT and *d* = 200 nm in the case of MUA.

From the determination of the adsorbed amount, and hence the absolute desorption rate, the desorption energy E_{des} and the frequency factor ν can be calculated from the multilayer peak using the Polanyi-Wigner equation for zero order desorption. E_{des} and the frequency factor ν can be obtained by an Arrhenius type plot of $\ln(r_{des}/\Theta)$ vs 1/(kT), as explained in Section 3.1. Θ is the coverage of the actual outmost layer. As this value is not known, the outmost layer is assumed to consist of a mixture of lying and standing molecules. This leads to a rough guess of approximately 3 x 10^{14} molecules/cm^2. The Arrhenius type plots are shown in Figure 27a,b, respectively. In the case of UDT, we obtain for the slope k =-1.33 x 10^{-19} and for the y-axis intercept d = 38.7. This leads to:

$$E_{des} = (0.8 \pm 0.1)\ \text{eV}$$
$$\nu = 6 \times 10^{(16\pm1)}\ \text{Hz}$$

In the case of MUA, we obtain for the slope k = -1.62 x 10^{-19} and for the y-axis intercept d = 41, which leads to:

$$E_{des} = (1.0 \pm 0.1)\ \text{eV}$$
$$\nu = 6 \times 10^{(17\pm1)}\ \text{Hz}.$$

The values for ν are significantly higher than the usually reported values of ν = 1 x 10^{13} Hz. However, it has already been discussed in Section 3.1 that this value only holds for atoms and small molecules, and that for larger organic molecules sometimes very high frequency factors are observed [120].

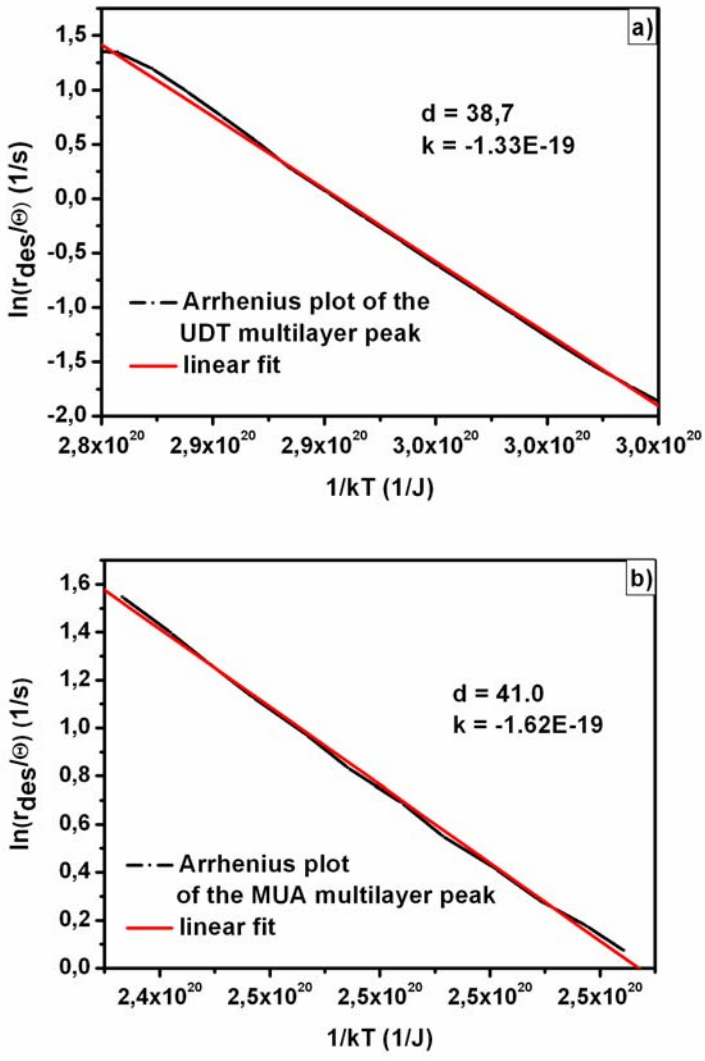

Figure 27. Arrhenius type plot of the multilayer of UDT (a) and MUA (b), respectively. The desorption energy E_{des} can be obtained from the slope of the straight line, the y-axis intercept yields the frequency factor ν.

5.1.2 AFM of the multilayer

The verification of a SAM with AFM is a delicate endeavour, as it is difficult to demonstrate the presence of a well ordered monolayer on a smooth surface. AFM was used therefore mainly to observe large-scale defects and multilayer agglomeration. Figure 28 shows a series of AFM images of MUA on Au(111)/mica.

Figure 28a was taken immediately after removing the sample out of solution. One can see a large island (labelled with “A”) with a height of about 9 nm, according to the cross section. The following images Figure 28b,c,d ere taken after 3, 4 and 6 hours under ambient conditions, respectively. The disappearance of the island is referred to the multilayer desorption of MUA. We have made sure that the island features do not stem from the ethanolic solvent, by applying AFM under comparable conditions to samples which have just been immersed in pure ethanol. The AFM measurements were performed at a temperature of approximately 300 K. In the last section it was shown that the multilayer of MUA desorbs under vacuum conditions at a slightly higher temperature with a peak maximum at 325 K. However, the desorption process of MUA already starts at lower temperatures and therefore it is obvious that small multilayer agglomerations will desorb within time already at 300 K. The relatively high desorption probability of the multilayer at room temperature can be seen as an advantage in comparison to other SAM/substrate systems, where long and careful ethanol rinsing is necessary to get rid of the multilayer [151]. The SAM, which is located underneath the multilayer, can not be distinguished from the clean substrate by AFM in this range of resolution.

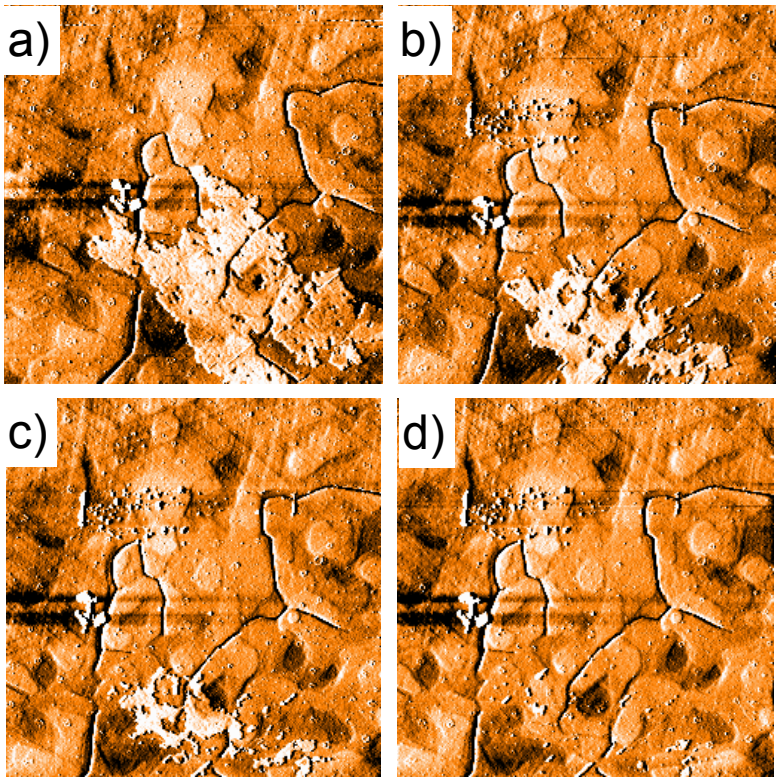

Figure 28. Series of AFM images (8μm x 8μm) of MUA on Au(111)/mica immediately after removing the sample out of solution (a), 3h under ambient conditions (b), 4h under ambient conditions (c) and 6h under ambient conditions (d). The island labelled “A” stems from a multilayer which disappears under ambient conditions.

5.2 UDT/MUA SAM formation by gas phase deposition

So far, the multilayer regime of UDT and MUA has been investigated. The monolayer, which is located underneath the multilayer, has not been considered. It has been shown that the multilayer desorbs around 300 K for both molecules. In order to investigate the monolayer regime, the sample is heated to 300 K which results in desorption of the multilayer. However, in order to obtain well ordered monolayers of standing molecules, further aspects had to be taken into account, in particular the waiting time after the deposition turned out to play a crucial role.

5.2.1 The uptake curve

In order to characterize the monolayer formation of the MUA molecules, the **uptake curve** was determined. This was done by depositing the material for various time slots. After each deposition, a TDS measurement was performed, as shown in Figure 29 for MUA. For this experiment, the evaporation source was heated to 55 °C, the sample temperature was 250 K. The mass 41 is shown as a representative for the whole molecule according to the cracking pattern of MUA. After 2 min deposition, one desorption feature is observed at 510 K, which is denoted β-peak. This peak could be attributed to lying molecules according to the LEED measurements (see Section 5.2.3). The longer the applied deposition time, the higher this peak becomes. After 10 min deposition, the formation of a multilayer peak is additionally observed. The area under these peaks yields a quantity which is related to the amount of material on the surface. As we investigate the monolayer formation, only the area under the β-peak was considered.

In order to obtain the uptake curve, this quantity is plotted versus the deposition time (Figure 30). The saturation of the monolayer is observed after 20 min deposition. Assuming that $\Theta = 1$ at full coverage, we obtain a straight line when plotting $\ln(1-\Theta)$ versus the time (Figure 31). This indicates that first order Langmuir adsorption is present (see Section 2.1.2). The evolution of the full-coverage phase of standing molecules is more complicated, as described in Section 2.2.2.

The uptake curve was not determined for the UDT molecules, as exact dosing of UDT was not possible due to its difficult pumping properties (see Section 4.2.2).

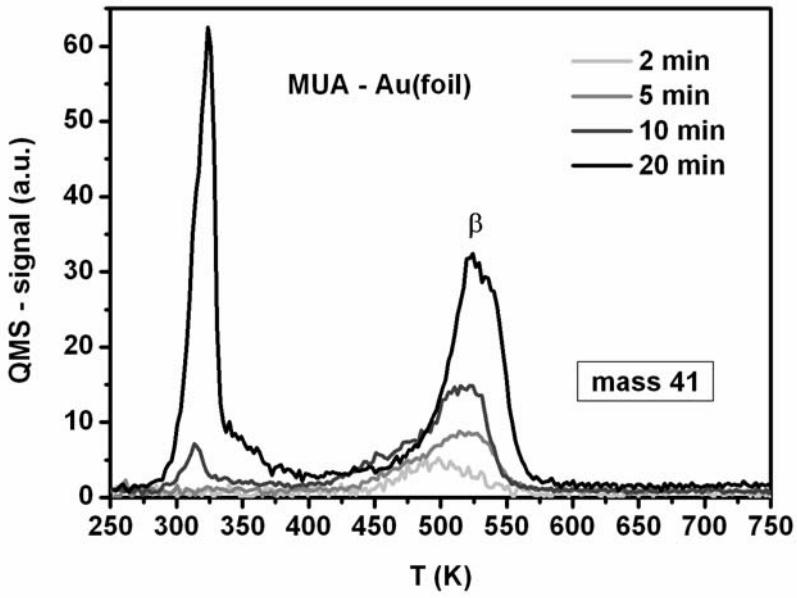

Figure 29. Desorption spectra of MUA on a gold foil for differently long time slots of deposition. In addition to the monolayer peak (β) of lying molecules at 510 K, multilayer formation starts after 10 min deposition.

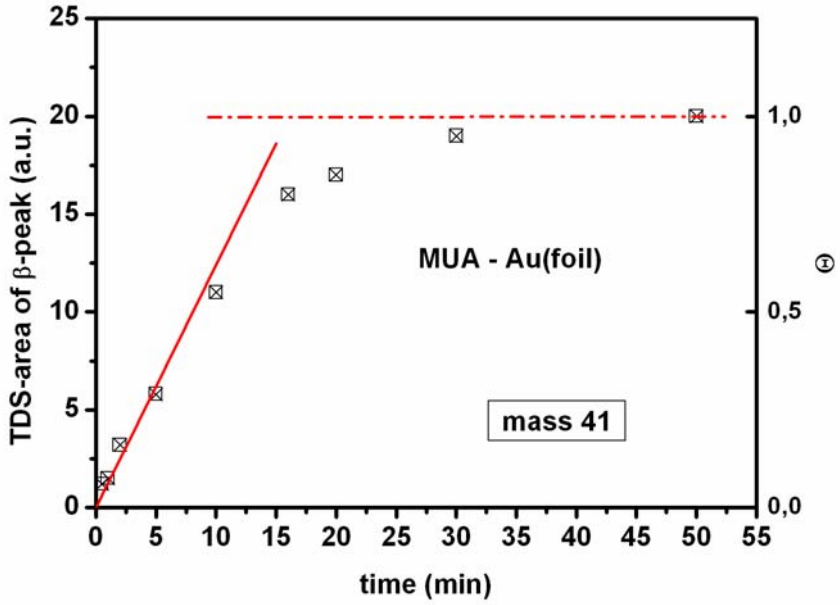

Figure 30. The uptake curve of MUA on a gold foil as obtained from the areas of the β-desorption peaks for differently long deposition times.

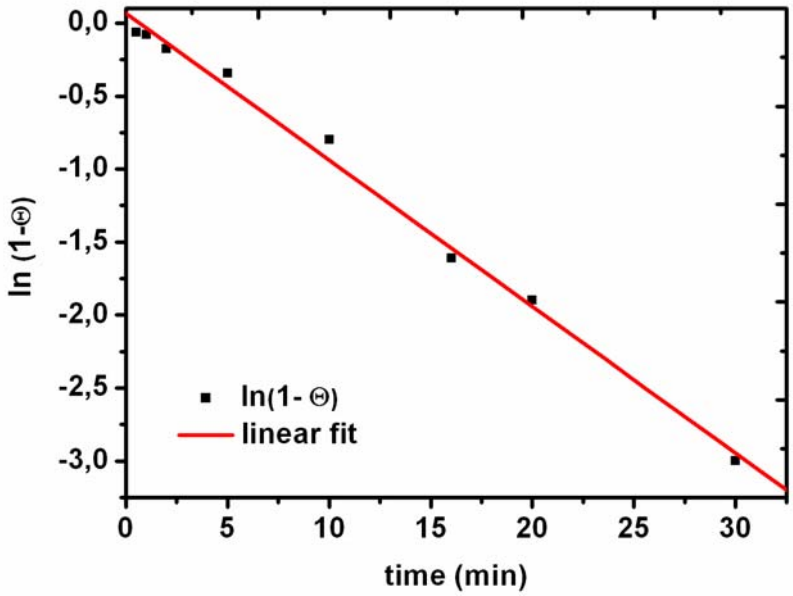

Figure 31. The ln(1-Θ) is plotted versus the time. The Θ-values are obtained from the uptake curve, assuming that Θ=1 at saturation coverage. A straight line is obtained, indicating that first-order Langmuir adsorption is present.

5.2.2 TDS on in-situ prepared monolayers

For UDT SAM formation, rather high exposures were applied to the sample in order to assure saturation of the monolayer. In Figure 33a the desorption spectra of UDT on the Au(111) single crystal are shown for different preparation procedures. The mass of the cracking product (mass 43) is shown. The spectra were obtained after an exposure of 500 L of UDT at room temperature and different waiting times: a) a few seconds, b) one day and c) three days after the deposition, respectively. While the first one is characterized by a single desorption peak at approximately 500 K (β-peak), the evolution of a second peak at 400 K (α-peak) can be seen in the latter two spectra. These two peaks could be attributed to standing (α-peak) and lying (β-peak) molecules, respectively, using LEED (Section 5.2.3).

The area under the desorption curve can be correlated with the amount of desorbing particles. Remarkably, this area is significantly increased after one day waiting time. This is explained by postadsorption of UDT due to the fact that UDT is quite difficult to be pumped. As mentioned in Section 4.2.2, this leads to a background pressure of UDT over a period of several hours after the deposition. While the SAM (of standing molecules) is formed, bare substrate areas are generated on which the UDT molecules from the residual gas can further adsorb. Thus, while the lying molecules of the saturated monolayer slowly form patches of well aligned standing molecules (SAM) via a thermally activated process, bare substrate areas are generated on which subsequently molecules from the still relatively high partial pressure adsorb and are incorporated in the SAM. A scheme of the adsorption process is shown in Figure 32.

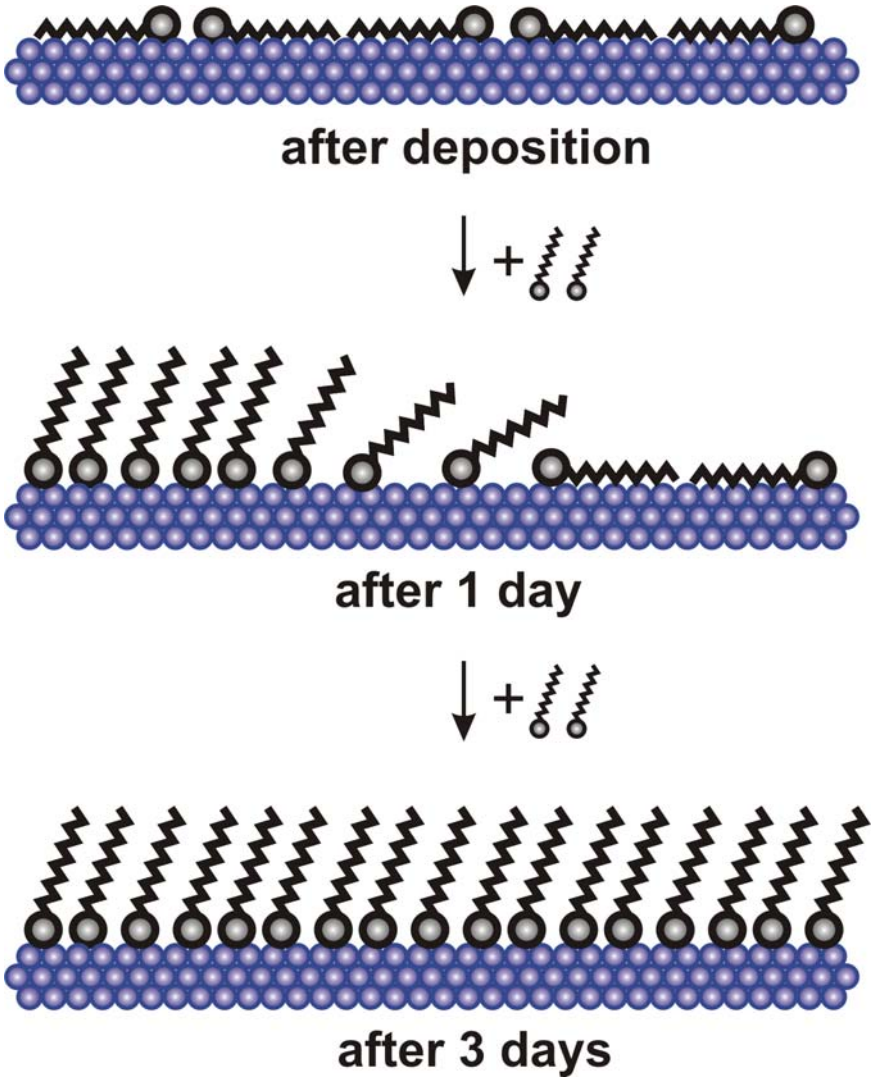

Figure 32. Scheme of in-situ UDT SAM formation. Molecules are flat lying on the surface immediately after the deposition (b-peak). The evolution of standing molecules is observed within time.

Along with the α-peak, a desorption peak of mass 374 emerges with increasing waiting time, as shown in Figure 33b. This gives clear evidence that the standing molecules desorb as disulfides. In fact, the cracking pattern of the α-peak differs

slightly from that of the β-peak, indicating that not the same molecular species desorb from the surface in both cases. This implicates that mass 43 is the cracking of a single UDT molecule in case of the β-peak, but the cracking of a disulfide in case of the α-peak. Apparently, for a densely packed monolayer of standing molecules a rather strong sulfur-sulfur interaction exists, leading to the desorption of disulfide molecules. As a consequence, this leads to a weakening of the S-Au bond and therefore to a lower desorption temperature of the disulfide than for the single molecules. The tendency of alkanethiols to form disulfides has already been reported previously in the literature [152-155], it has even been proposed that a sulfur-pairing exists on the surface (see Section 2.3.3). However, the observation of disulfides in the TD spectrum does not confirm this theory, as it can happen that molecules recombine during desorption (‘recombinative desorption’).

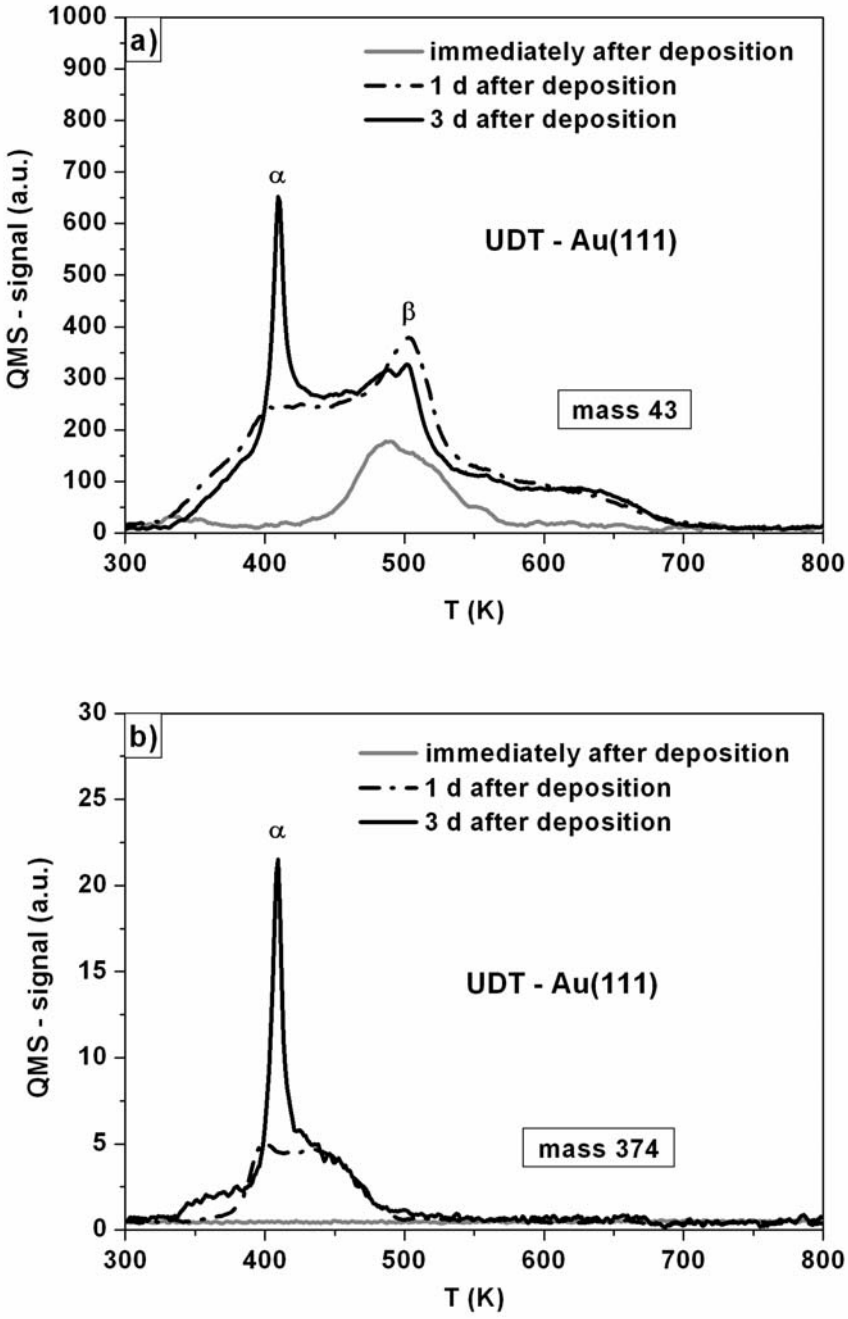

Figure 33. The evolution of the desorption spectrum of UDT on Au(111) as a function of the waiting time (a: mass 43, b: mass 374) in the monolayer regime (exposure: 500 L; adsorption temperature: 300 K, heating rate: 1 K/s). The β-peak can be attributed to lying molecules, the α-peak stems from standing molecules. The latter are shown to preferably desorb as disulfides.

A further detail on these peaks is shown in Figure 34a,b, where the mass ratio 187/188 is considered in the monolayer and the multilayer regime of UDT on a Au(111) surface. The monolayer was prepared by an exposure of 500 L of UDT at room temperature and a waiting time of 3 days, the multilayer was prepared by applying an exposure of 1000 L of UDT at a sample temperature of 200 K. The mass 187 corresponds to the thiolate. There is a significantly different 187/188 mass ratio in the multilayer peak as compared to the α- and β- peaks. This is not surprising, as the α-peak is known to stem from desorption of disulfides. One would rather assume that in this case hardly any cracking mass 188 should be observed. The fact that mass 188 is detected, nevertheless, is attributed to some cross-talking of the QMS. Interestingly, the 188/187 ratio is similar for the β-peak, which indicates that almost all lying molecules desorb as thiolates. This has already been argued for the similar system octanethiol on Au(111) [153].

Comparing these results of UDT to the desorption behaviour of MUA (Figure 35a,b), one can find similarities as well as differences. The desorption of lying molecules again takes place at approximately 500 K. However, even after a waiting time of 14 days only a small α-peak could be observed. Seemingly the formation of standing molecules is much less pronounced in this case. One interesting feature is the desorption of mass 34 (H_2S) which takes place at a somewhat higher temperature than the β-peak (designed β'-peak). At the same temperature, desorption of mass 185 could be observed, which can be attributed to the sulfur-free MUA molecule. The β'-peak therefore is attributed to dissociative desorption upon cracking of the sulfur-carbon bond. Two similar desorption peaks were observed for the related molecules decanethiol by Lavrich et al. [156] and for anthracene-2-thiol on Au(111) by Käfer et al. [151]. In the latter paper the authors also attributed the second peak to the sulfur-free molecule.

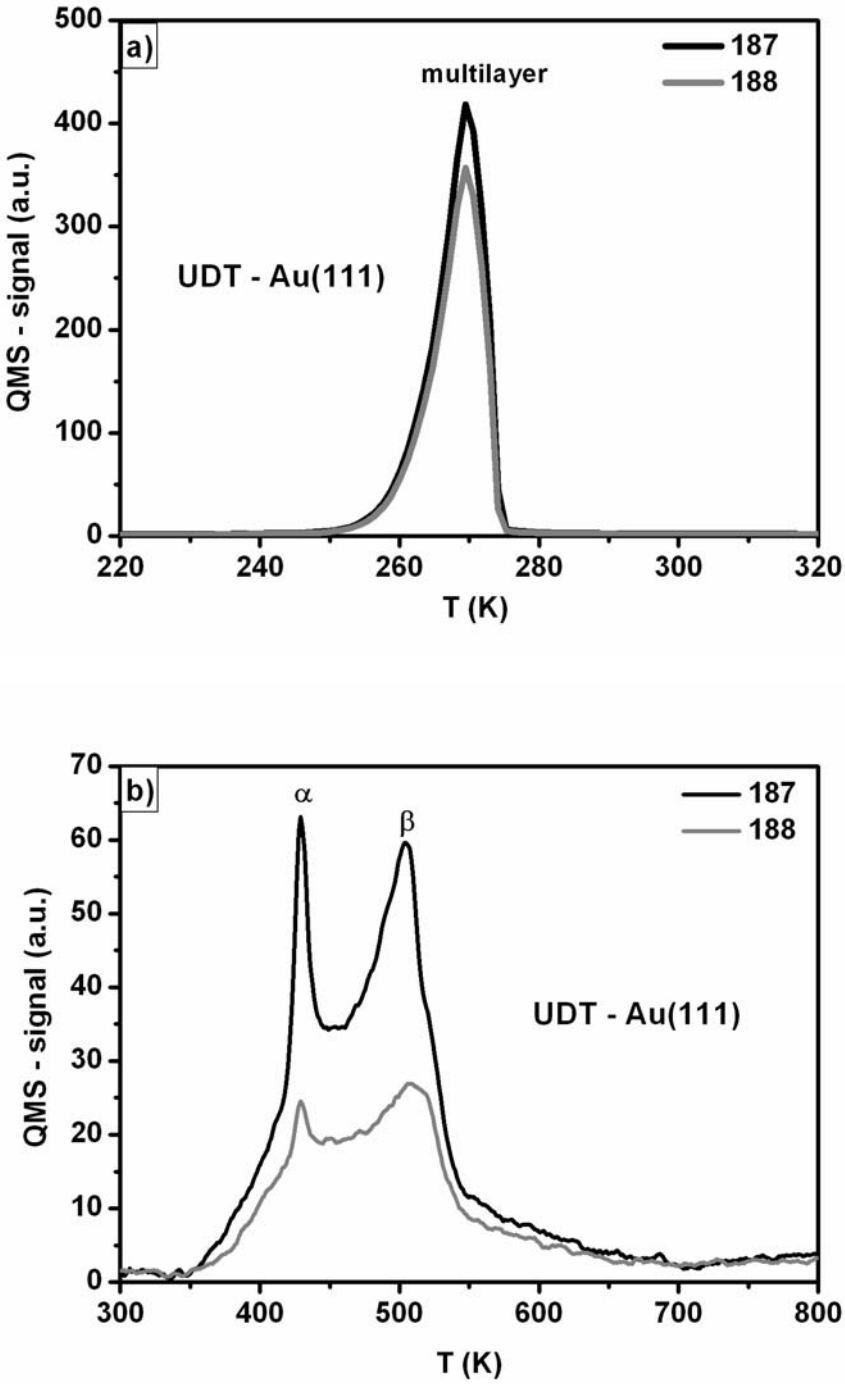

Figure 34. Comparison of the mass 188 (intact UDT) and mass 187 (corresponding thiolate) in the desorption spectrum of UDT from Au(111) from the multilayer (a) and from the monolayer (b) regime. The multilayer can be assumed to stem from intact molecules. This demonstrates that monolayer desorption of UDT mainly proceeds in form of thiolates.

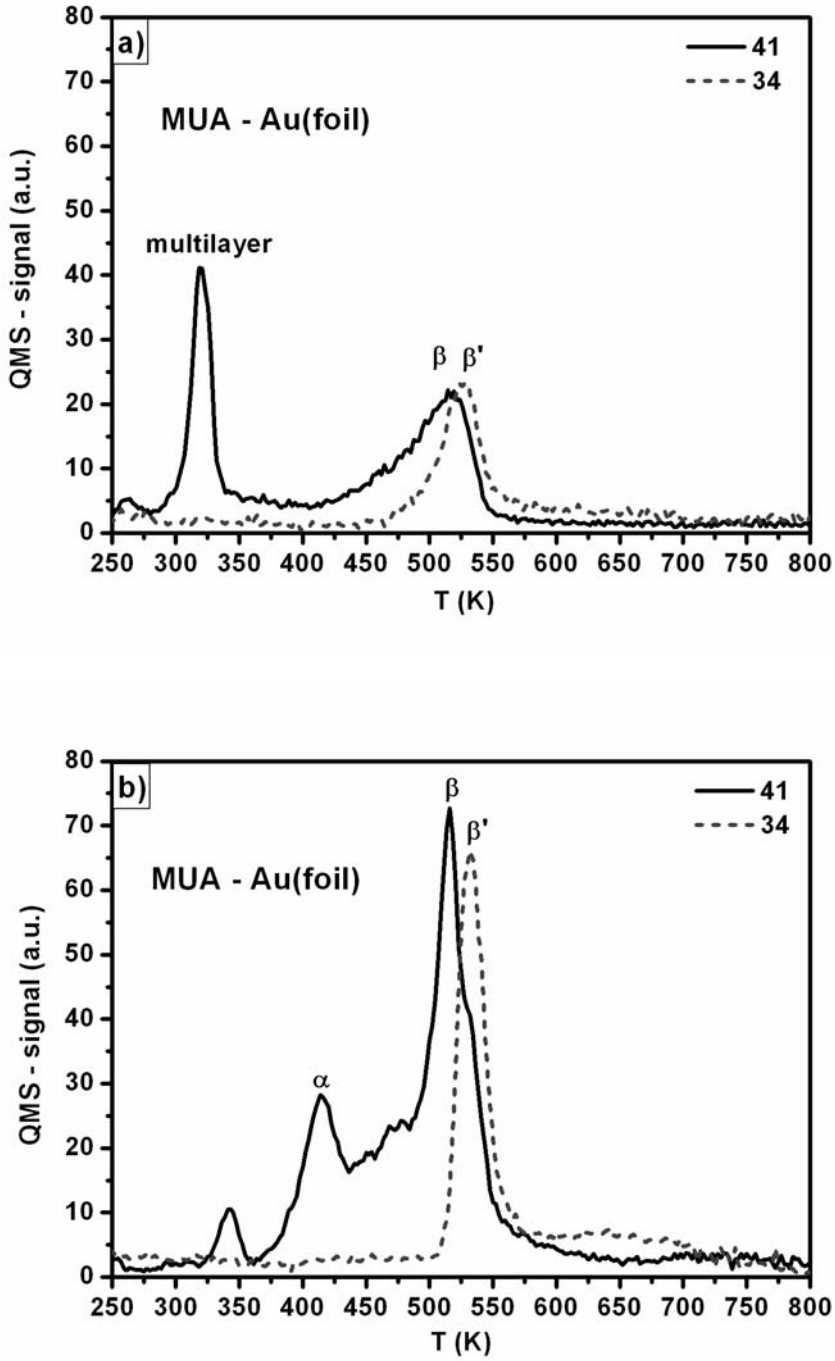

Figure 35. Desorption spectra of MUA on a gold foil immediately after deposition at 200 K (a) and after a waiting time of 14 days (b). Only little SAM formation takes place within time (α-peak). Desorption of mass 34 (H_2S) at a slightly higher temperature than the β-peak (designated β'-peak) indicates the cracking of the sulfur-carbon bond.

5.2.3 LEED on in-situ prepared SAMs

It is a rather delicate task to get LEED patterns from organic monolayers. An important prerequisite is a well prepared, single crystalline substrate. In fact, UDT/MUA SAMs on Au(111)/mica did not deliver any diffraction pattern which is explained by the low crystalline quality of these substrates (Section 4.1.2). The Au(111) single crystal was Ar^+-sputtered and contemporaneously annealed up to 900 K for several hours before SAM preparation. Figure 36a shows the LEED pattern which was observed immediately after an exposure of 50 L of UDT to the Au(111) single crystal at room temperature. The LEED observation was performed at liquid nitrogen temperature, in order to increase the signal/noise ratio. A similar pattern was observed for MUA. The pattern can be best described by a (12 x √3) rect. structure (Figure 36b, the unit cell is marked in red), as obtained by an appropriate simulation. The simulation was performed using LEEDSIM[2], the input parameters were the Au-Au interatomic distance a = 0.288 nm and the length of the UDT molecule, which is l = 1.7 nm [157]. According to the literature [96], the unit cell is assumed to contain two lying molecules, oriented with their carbon chains parallel to the surface along the $\langle 1\bar{1}0 \rangle$ direction and with their sulfur groups at the opposite ends (Section 2.3.3). A scheme of this structure is shown in Figure 36c. The corresponding coverage is 0.09 ML with respect to the Au(111) surface. Further deposition of UDT leads to a weakening of the LEED pattern, and finally it vanishes after an exposure of about 500 L, indicating the disappearance of the low-coverage phase.

However, waiting overnight and repeated exposure resulted in a new diffraction pattern in case of UDT, as depicted in Figure 36d. This pattern can be attributed to a (2√3 x 3) rect. structure, which is well known to be formed by alkanethiols on Au(111) (Section 2.3.3). The simulated pattern is shown in Figure 36e, the red

[2] (http://www.sim4tec.com/?Products:LEEDsim_-_LEED_simulation_software)

rectangle indicates the unit cell. This structure is assumed to stem from 0.33 ML standing molecules with the carbon chain tilted ~ 30° from the surface normal, which implies 4 molecules per unit cell [96]. A scheme of this structure is shown in Figure 36f. The Wood description of this structure would be a c(4√3 x 2√3)30° structure, with 8 molecules in the unit cell [96]. These LEED results reveal that the ratio between the coverages of standing and lying molecules is 0.33 : 0.09, which implicates that the full-coverage phase contains ~ 3.5-times as many molecules as the low-coverage phase. This is in good agreement with our results of TDS (see Figure 33), wherein the area of the spectrum of standing molecules is approximately 3-times as large as that of lying molecules. Heating the SAM up to 450 K resulted again in the pattern of the lying molecules. Basically, these LEED patterns are in good agreement with the results obtained by Gerlach et al. [57] for decanethiol on Au(111). As to the MUA molecule, such a pattern could not be observed under equivalent preparation conditions.

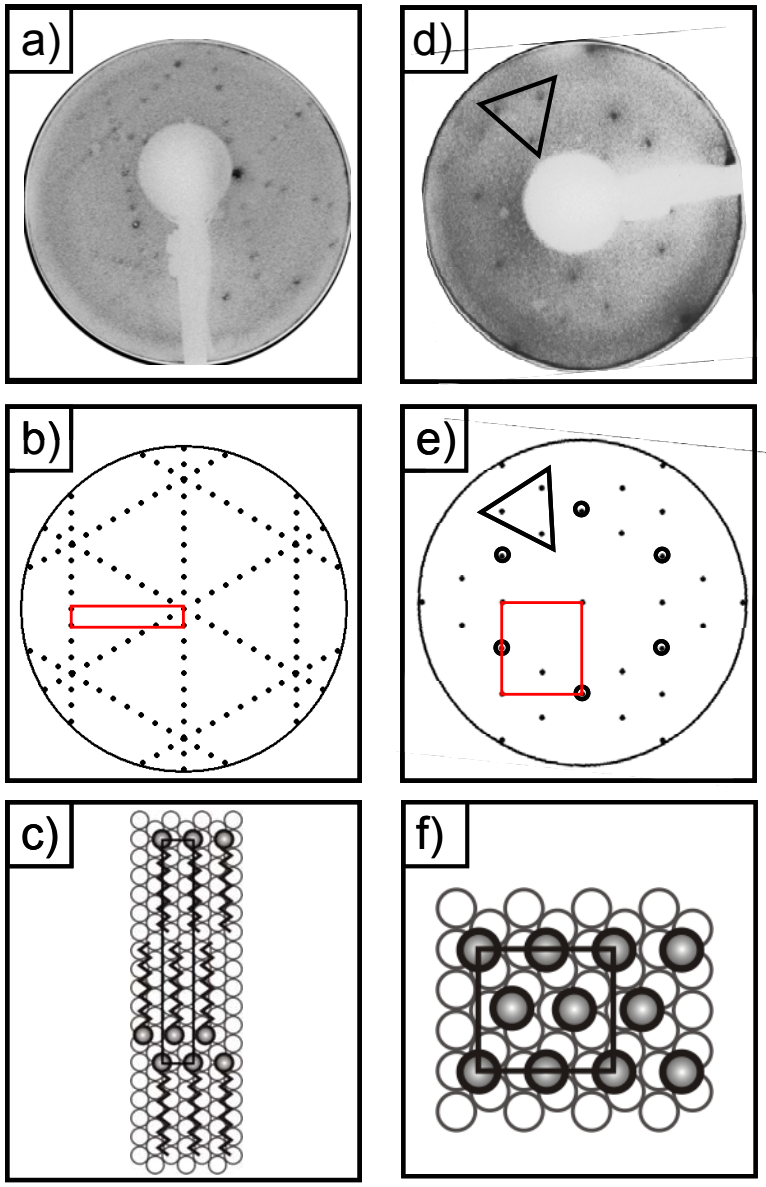

Figure 36. Measured LEED pattern immediately after an exposure of 50 L of UDT on Au(111); beam energy: U = 41 V (a). In addition, the calculated pattern of a (12 x √3)rect. structure is shown, the simulation was performed with LEEDSIM (b). This pattern can be attributed to molecules lying on the surface, as shown in the scheme (c). LEED pattern of UDT on Au(111), two days after the deposition, beam energy U = 28 V (d). The calculated pattern is shown in (e), revealing a (2√3 x 3)rect. structure. The encircled spots are not visible in the measured LEED pattern due to the existence of glide planes, as described in the literature [95]. This pattern can be attributed to a SAM of standing molecules, as shown in the scheme, where the arrangement of the head groups are shown (f).

5.2.4 AES of the in situ prepared SAMs

For further characterization of the SAM formation, AES has been performed. In comparison to XPS, AES on alkanethiols has the advantage of a high sensitivity for the sulfur. Therefore, useful fingerprints can be expected, although one has to keep in mind a possible influence of the impinging electrons on the SAM arrangement (Section 4.2.1). To check the reliability of the spectra, repeated measurements on the same sample position up to ten times were performed. Thereby no change of the peak positions or heights was found.

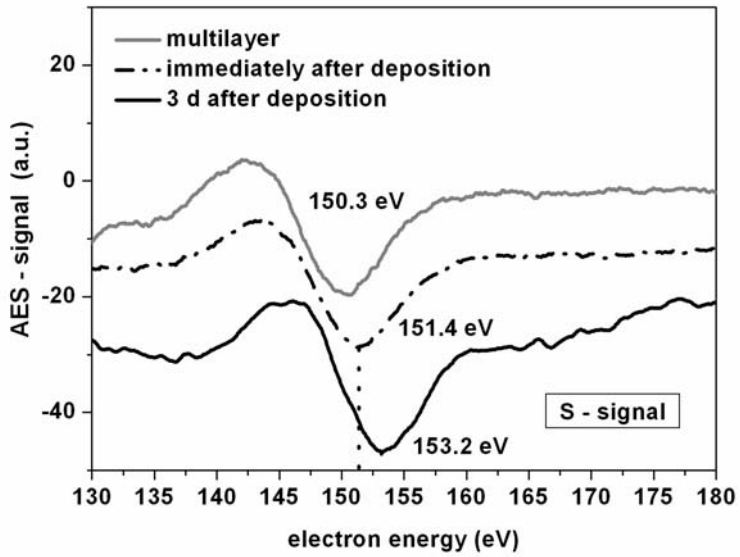

Figure 37. The AES sulfur signal of three differently prepared UDT layers on a gold foil by PVD. A clear shift of the Auger signal towards higher energies, starting from the multilayer (intact molecules), via the monolayer of lying molecules to the monolayer of standing molecules (SAM) can be observed. This can be used as a fingerprint for SAM formation.

The interesting finding is that one can observe a clear shift of the sulfur peak dependent on the layer preparation: In Figure 37, the Auger spectra in the sulfur region for a monolayer immediately after the UDT deposition at room temperature and three days after the deposition are shown. For comparison, the sulfur signal of a multilayer of UDT is added. There is an energy shift of 1.1 eV between the

multilayer and a monolayer of lying molecules and a further shift of 1.8 eV between a lying monolayer and a standing monolayer. Thus, the AES S-signal can be used as a fingerprint to characterize the quality of a SAM.

5.2.5 The substrate quality and the in-situ SAM formation

5.2.5.1 The influence of the crystalline structure of the substrate

In the last sections, our results of UDT/MUA SAM formation on the Au(111) single crystal were shown. In order to determine a possible influence of the substrate structure, also SAMs on sputtered and annealed gold foils were investigated. These gold foils consist of many, differently oriented crystallites (Section 4.1.2). A set of TD spectra for in-situ prepared UDT SAMs on sputtered and annealed gold foils is depicted in Figure 38a. A similar experiment as described in Section 5.2.2 for the Au(111) single crystal was performed. The spectra were recorded after an exposure of 500 L and different waiting times: immediately after the deposition, 1 day after the deposition and three days after the deposition. As representative for the whole UDT molecule again the mass 43 is shown. One can observe a similar trend as for UDT SAM formation on Au(111): The α-peak, which is attributed to standing molecules, is formed within time. It is again characterized by desorption of disulfides (Figure 38b).

In Figure 39a,b the TD spectrum of UDT on the gold foil after three days waiting time is compared to that of the Au(111) single crystal. In the case of the single crystalline substrate, the α-peak is notably narrower. But even more noticeably, the ratio between the α- and the β-peak differs for the two substrates. The α-peak is significantly higher in the case of the Au(111) single crystal. This is explained by the polycrystallinity of the gold foil which exposes surfaces with different packing densities. Obviously, the formation of a densely packed monolayer of standing molecules is favoured on the (111) plane.

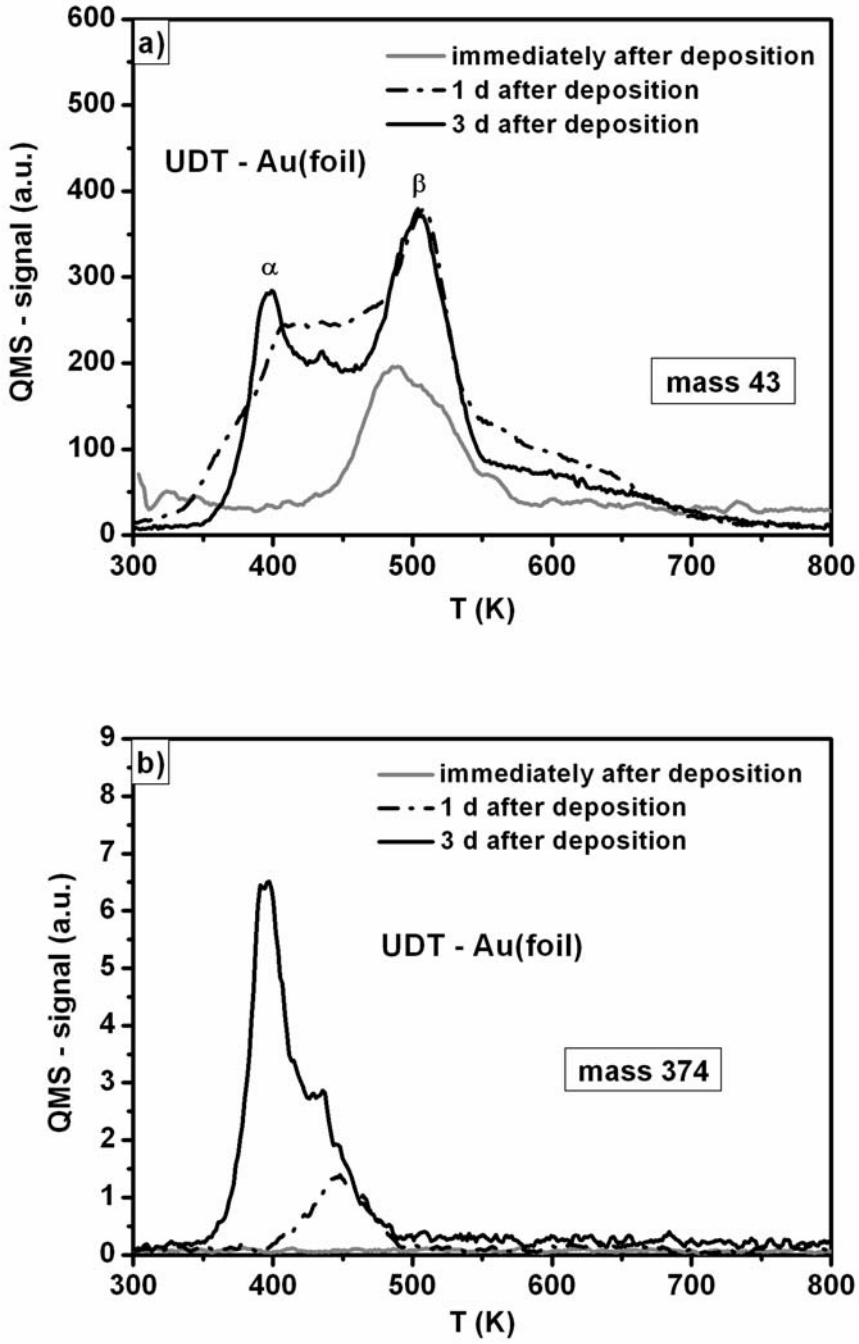

Figure 38. TD spectra of in-situ SAM formation of UDT on a gold foil. The desorption spectrum of mass 43 again shows the evolution of the α-peak of the standing molecules within time, in addition to the β-peak of lying molecules (a). Desorption of the mass 374 indicates that standing molecules desorb as disulfides.

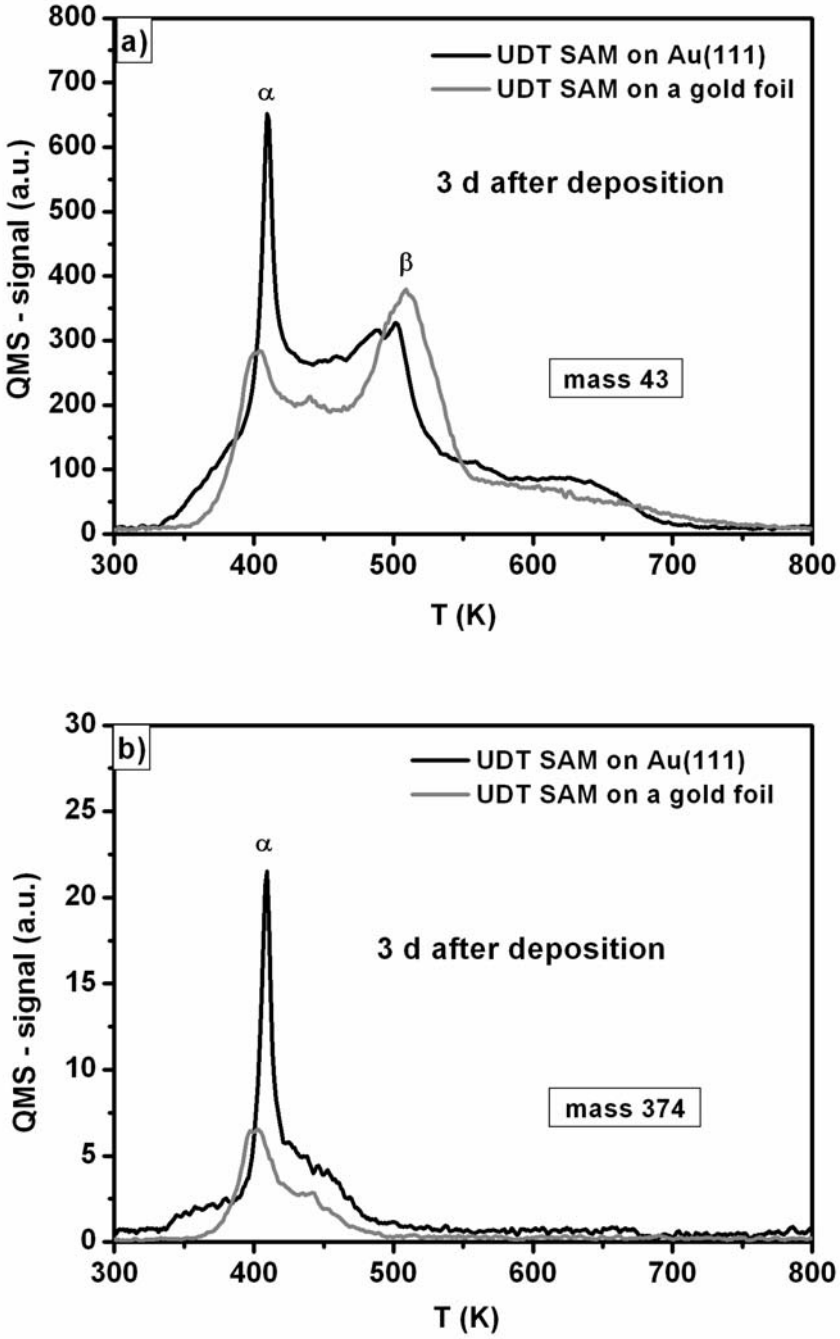

Figure 39. TD spectra of in-situ prepared UDT SAMs on different gold substrates. The SAM formation on a polycrystalline gold foil (a,b). Desorption spectrum of a UDT SAM on a Au(111) single crystal in comparison to a UDT SAM on a polycrystalline gold foil (c,d).

5.2.5.2 The influence of surface impurities

The influence of impurities of the substrate surface on the SAM formation was investigated for two different scenarios: At first, an initially clean gold foil was intentionally contaminated. This was performed by several adsorption and desorption cycles of MUA, without sputtering the sample in between. Repeatedly, MUA was deposited on the sample surface and then the sample was heated up to 800 K. AES reveals that after the heating still carbon and sulfur contaminations are present on the surface. After approximately ten cycles, these signals did not further increase. An Auger-spectrum of such an intentionally contaminated gold foil is shown in Figure 40. In Figure 41a, the TD spectrum after 10 min deposition of MUA on the contaminated substrate is shown. As representative for the whole MUA molecules, the cracking product mass 41 is shown. For comparison, the TD spectrum of MUA on a clean substrate is added. The β-peak of lying molecules is observed for both substrates and the shape of the peak is remarkably similar. However, the peak heights differ significantly, revealing that the amount of adsorbed material decreases on the contaminated substrate. In Figure 41b, the uptake curve of MUA on the contaminated substrate is shown. For comparison, the uptake curve on the clean substrate is added. Not only the initial sticking coefficient decreases in the case of the contaminated substrate (as deduced from the lower slope at the beginning of the curve), but also the saturation occurs at a smaller amount of adsorbed material.

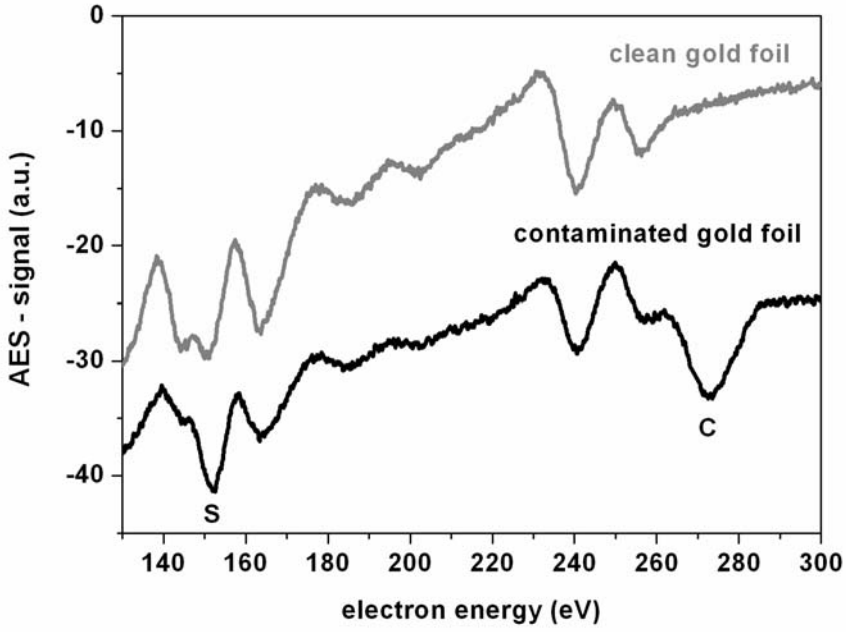

Figure 40. The Auger spectrum of an intentionally contaminated gold foil (see text) in comparison to a clean gold foil. The spectra reveal carbon and sulfur impurities on the contaminated gold foil.

In addition to this 'slightly contaminated' gold foil, also a more heavily contaminated gold foil was investigated as substrate for SAM formation. It is shown in Section 4.1.1, that the gold foils were heavily contaminated when received from Ögussa Inc. The Auger spectrum of such a gold foil is shown in Section 4.1.1, revealing a huge amount of carbon contaminations. UDT-exposures up to 2000 L did not result in the adsorption of any material in this case. The corresponding desorption spectrum is shown in Figure 42d. Neither the whole molecule nor one of its cracking products can be detected

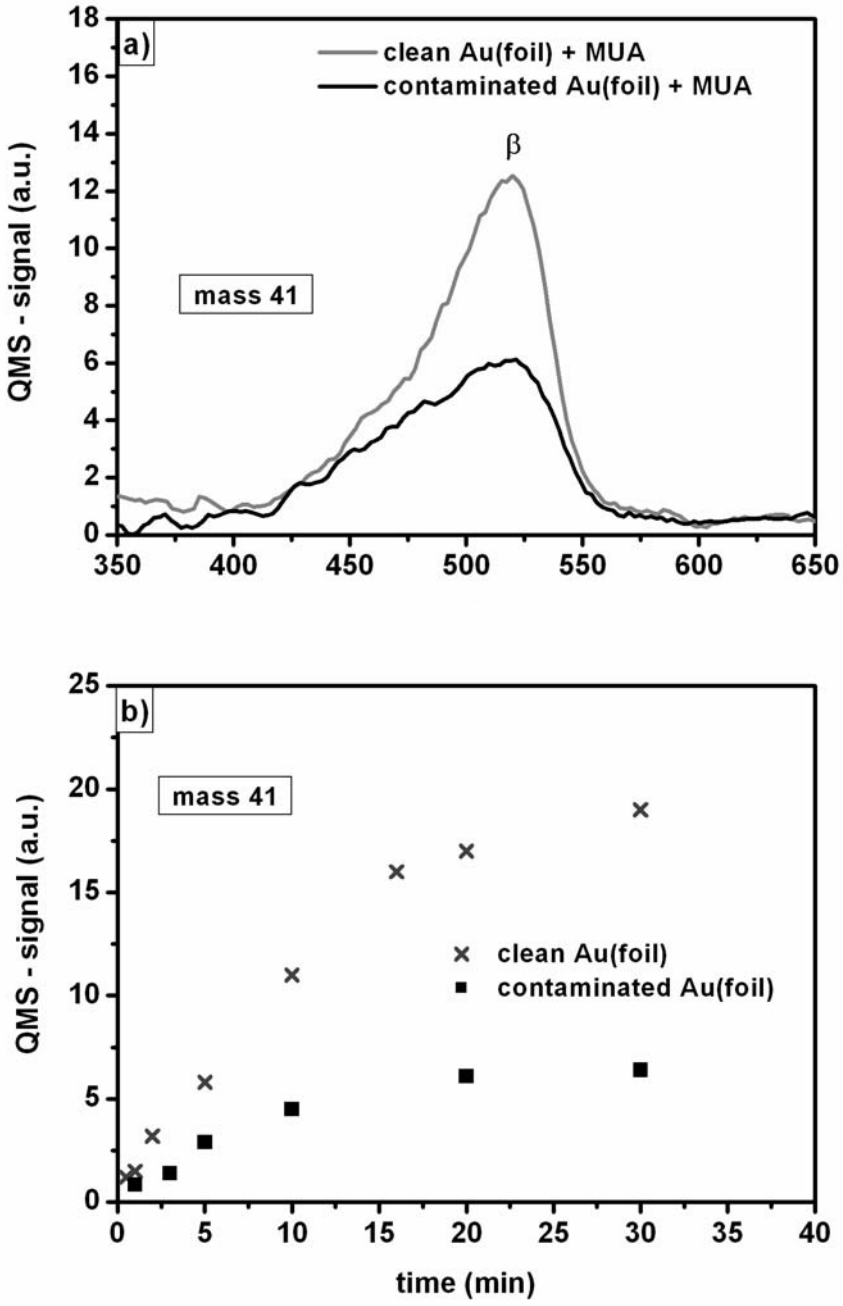

Figure 41. The influence of surface contaminations on the SAM formation. The desorption spectrum of MUA from a clean and from an intentionally contaminated gold foil (exposure time: 10 min) (a). The uptake curve of MUA on the contaminated and on the clean gold foil is shown in (b).

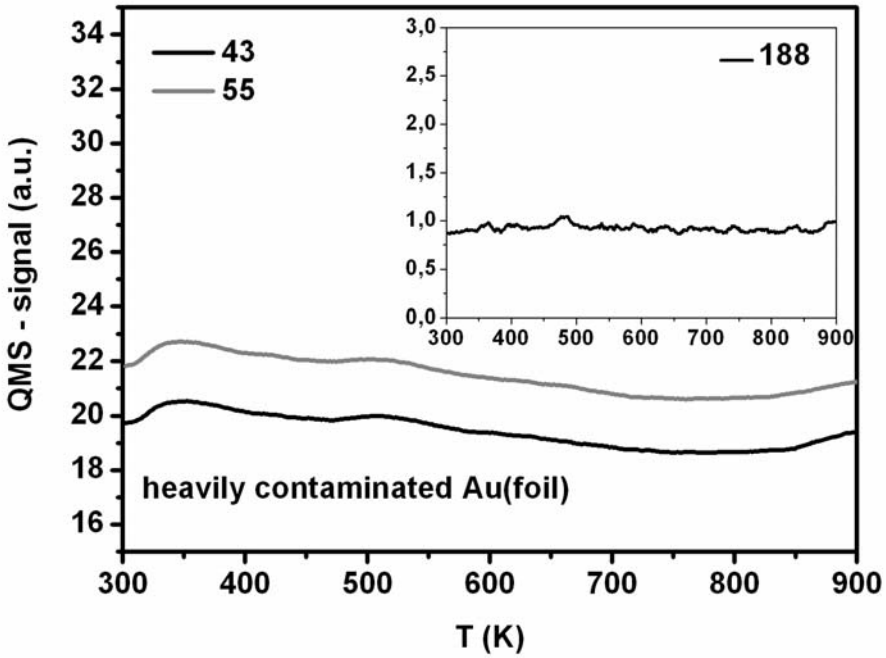

Figure 42. TDS after an exposure of 2000 L of UDT on a heavily contaminated gold foil. No desorption peak is observed.

5.3 UDT/MUA SAM formation in solution

The preparation of SAMs in solution can easily be performed, as mentioned already in the experimental section. Nevertheless, the sample has to be installed in the UHV chamber for in-situ analysis. This was particularly intricate for the TDS measurements, as the ex-situ prepared samples could only be used for one TD experiment. The reproducibility of the spectra was moderate in comparison to the in-situ prepared SAMs. However, the large set of TD experiments allowed us to deduce several very interesting conclusions. In addition to TDS, also XPS, IRRAS and AES measurements were performed on the ex-situ prepared SAMs.

5.3.1 XPS of the ex-situ prepared SAMs

Figure 43 shows an overview XP-spectrum of an ex-situ prepared MUA SAM on Au(111)/mica. The C1s and O1s peaks can clearly be seen in addition to the gold peaks, whereas the sulfur S2p peak is barely visible. In Figure 44a,b detailed spectra of the S2p and C1s peaks are shown, respectively, as obtained by using a higher data acquisition time and a narrower energy range. For the least squares fit Gauss distributions were used with a full width at half maximum (FWHM) of 2.1 eV and a spin-orbit splitting separation of 1.2 eV for the S2p peak. [83]. The observation of the S2p peak maximum at 162.7 eV is characteristic for sulfur bonded to the gold substrate, the strong attenuation is often referred as an indication that the sulfur is indeed at the bottom of the SAM [82]. Considering the C1s signal, the observed binding energy of 284.7 eV is characteristic for the alkane chain. In addition, using the Gaussian fit procedure, one can denote a second peak at around 289 eV, which is referred to the carboxylic carbon [158,159]. A third peak might exist around 286 eV, which can be attributed to emission from the C atoms next to the sulfur atoms and the C atoms next to the carboxylic carbon, respectively [82]. The XPS results are compatible with the

features which one would expect for a well defined MUA SAM. However, more detailed information was obtained performing IRRAS and TDS measurements.

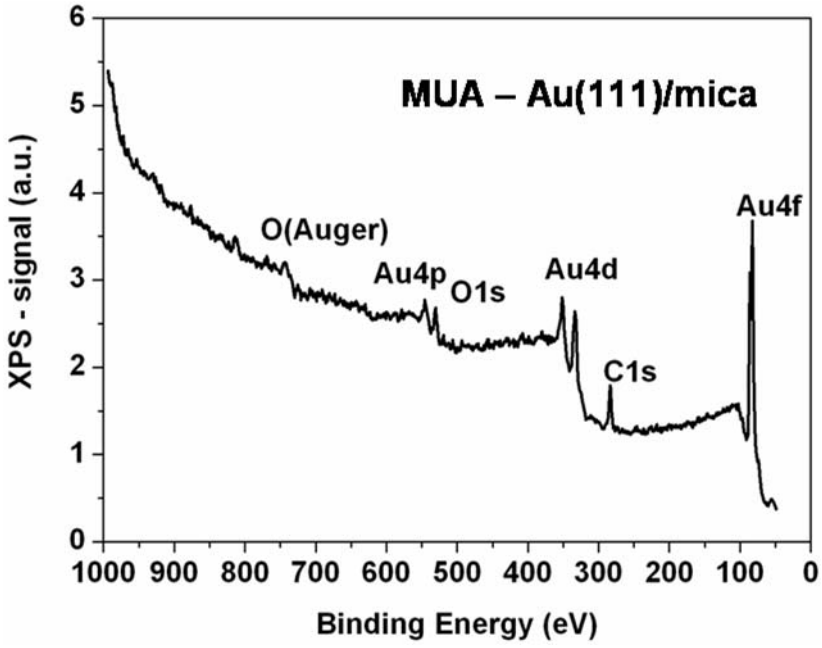

Figure 43. Overview XPS spectrum for an ex-situ prepared MUA SAM on Au(111)/mica. The sulfur signal is too small to be seen in this spectrum.

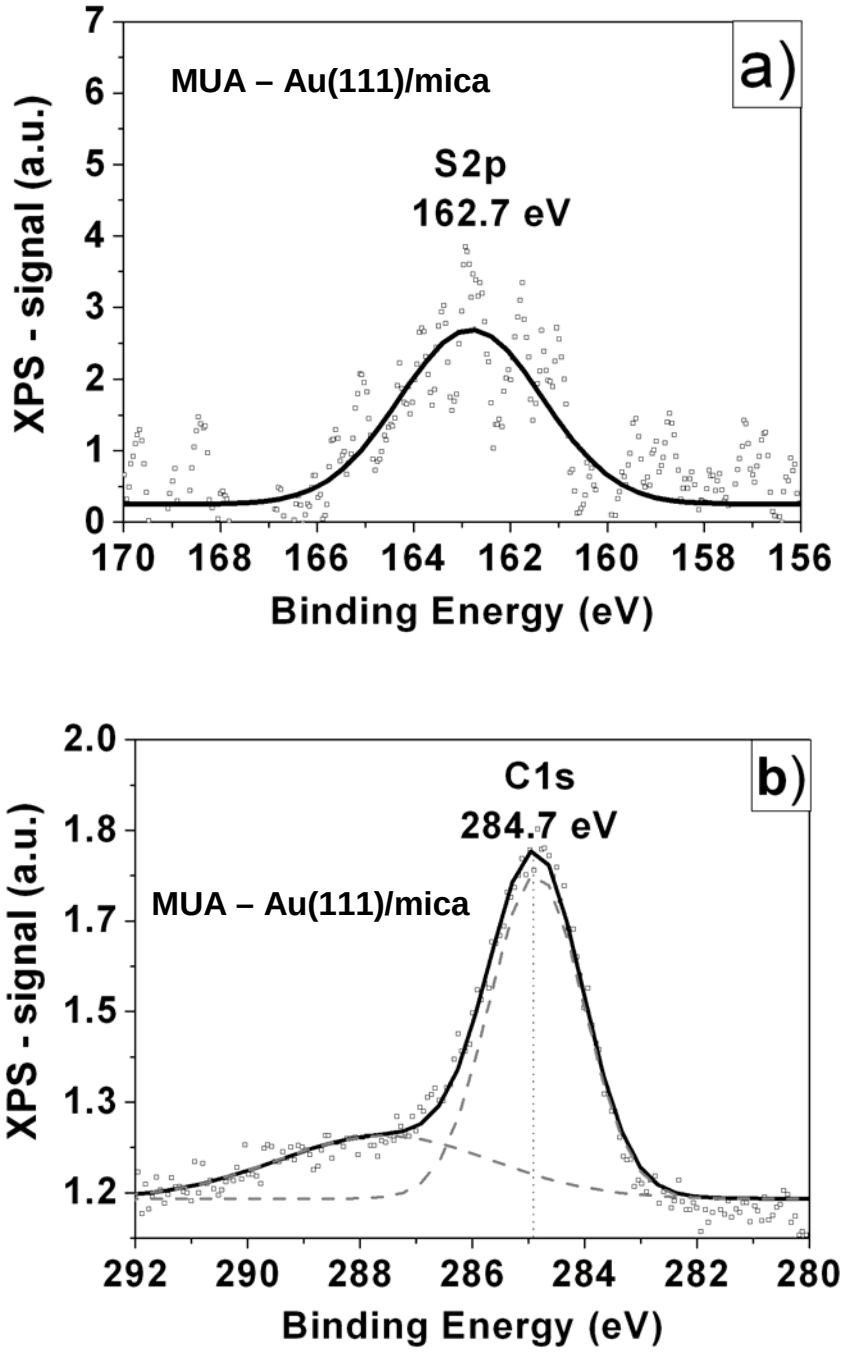

Figure 44. Detailed XPS spectra for an ex-situ MUA SAM on Au(111)/mica. The S2p peak at 162.7 eV indicates sulfur bonded to the substrate (a). The C1s peak at 284.7 eV stems from aliphatic carbon, the broad shoulder at 289 eV is an indication of carboxylic carbon (b).

5.3.2 IRRAS of ex-situ prepared SAMs

Further information of the SAM quality was obtained by IRRAS. Figure 45 shows the FTIR spectrum of an ex-situ prepared MUA SAM on Au(111)/mica. In Table 2 the respective band positions are specified. Asymmetric and symmetric stretch vibrations of the CH_2 groups of the alkane chain yield the absorption bands at 2919 cm^{-1} and 2850 cm^{-1}, respectively (Figure 45a). As reported in [160], the location of the CH_2 stretch vibrations gives information about lateral interactions between the n-alkyl chains. A so called 'liquid-like state' is characterized by peak positions at 2928 cm^{-1} and 2856 cm^{-1} for the $\nu_a(CH_2)$ and $\nu_s(CH_2)$ mode, respectively, while the peak positions of 2920 cm^{-1} ($\nu_a(CH_2)$) and 2850 cm^{-1} ($\nu_s(CH_2)$) correspond to the 'solid-like state'. Since for these measurements the resolution of the FTIR spectrometer was set to 4 cm^{-1}, our observed peak positions at 2919 cm^{-1} and 2850 cm^{-1} clearly correspond better with the 'solid-like state' (Figure 45a).

Freq, cm^{-1}	Mode assignment
2919	CH_2 stretch, asymm.
2850	CH_2 stretch, symm.
1710	C=O stretch
~1450	COO^- stretch, symm.
1435	C-O-H deformation

Table 2. Spectral mode assignments for MUA SAMs on Au(111)/mica.

The most important feature, however, is the C=O stretching band of the acid end group which occurs at 1710 cm^{-1} (Figure 45b). A similar value is described in several papers [75,161] and is usually referred to an acid group which is participating in hydrogen bonding processes [78,81,161]. The absorption band at 1435 cm^{-1} is attributed to the C-O-H deformation vibration [78]. In addition, a

band at ~1450 cm^{-1} (COO^-, symm.) reveals that part of the MUA molecules is transformed into the corresponding carboxylates [78], that means they are deprotonated.

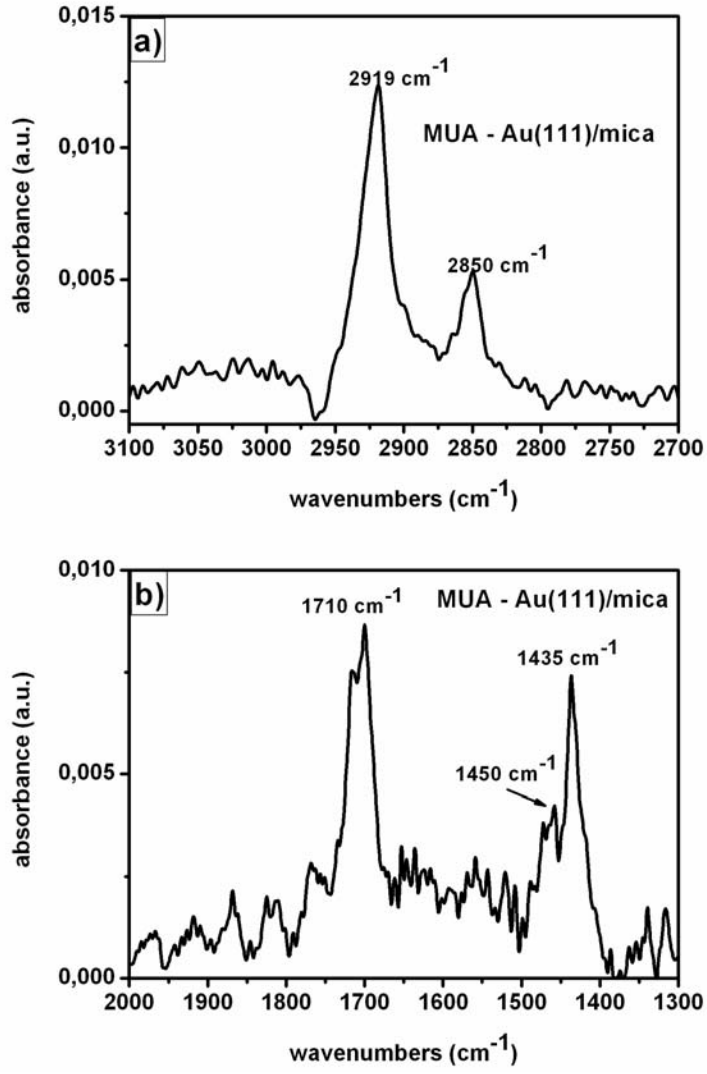

Figure 45. IRRAS - spectra of a MUA SAM on Au(111)/mica. The peaks at 2919 cm^{-1} and 2850 cm^{-1} are attributed to CH_2 stretch vibrations (a). The C=O stretch vibration is observed at 1710 cm^{-1}, indicating the existence of hydrogen bonds. The feature at 1435 cm^{-1} is referred to C-O-H deformations (b).

5.3.3 TDS of ex-situ prepared SAMs

In Figure 46a,b the TD spectrum of the ex-situ prepared UDT SAM on a sputtered and annealed gold foil is shown. The spectrum basically corresponds to that of an evaporated SAM after long waiting time, characterized by desorption of standing molecules at 400 K (α-peak), followed by the β-peak of the remaining lying molecules. The standing molecules again desorb as disulfides, indicated by desorption of mass 374.

The desorption spectrum of MUA following the same preparation procedure is depicted in Figure 47. Interestingly, in this case a third desorption peak at 710 K develops, besides the peaks of the standing (α-peak) and the lying (β-peak) molecules. It is designated as γ-peak. This peak is characterized by desorption of a significant amount of mass 197, in addition to other cracking products of MUA. Since m = 197 is the mass of gold, this is a strong indication that desorption of gold containing molecules takes place in this temperature range. This gives evidence that the acid end group strongly influences the SAM formation, showing a complex binding mechanism leading to gold etching at elevated temperature. In fact, there is some evidence in recent literature [100-102,104] that the bonding of the sulfur headgroup to the gold surface involves Au-adatoms. In the group of Yates [100,102], the existence of methylthiolate-Au-adatom complexes in the context of methylthiolate self assembling on Au(111) is suggested according to their high-resolution STM experiments. Also, residuals of Au-atoms in the ethanolic solution of alkanethiols after SAM formation were found by Edinger et al. [112], indicating the existence of such Au-organic molecule complexes. A scheme of an thiol-Au-adatom-thiol complex similar as proposed in ref. [102] for methylthiolate is shown in Figure 48. However, we could not detect desorption of these large complexes, as the mass range of the QMS was limited by 500 amu.

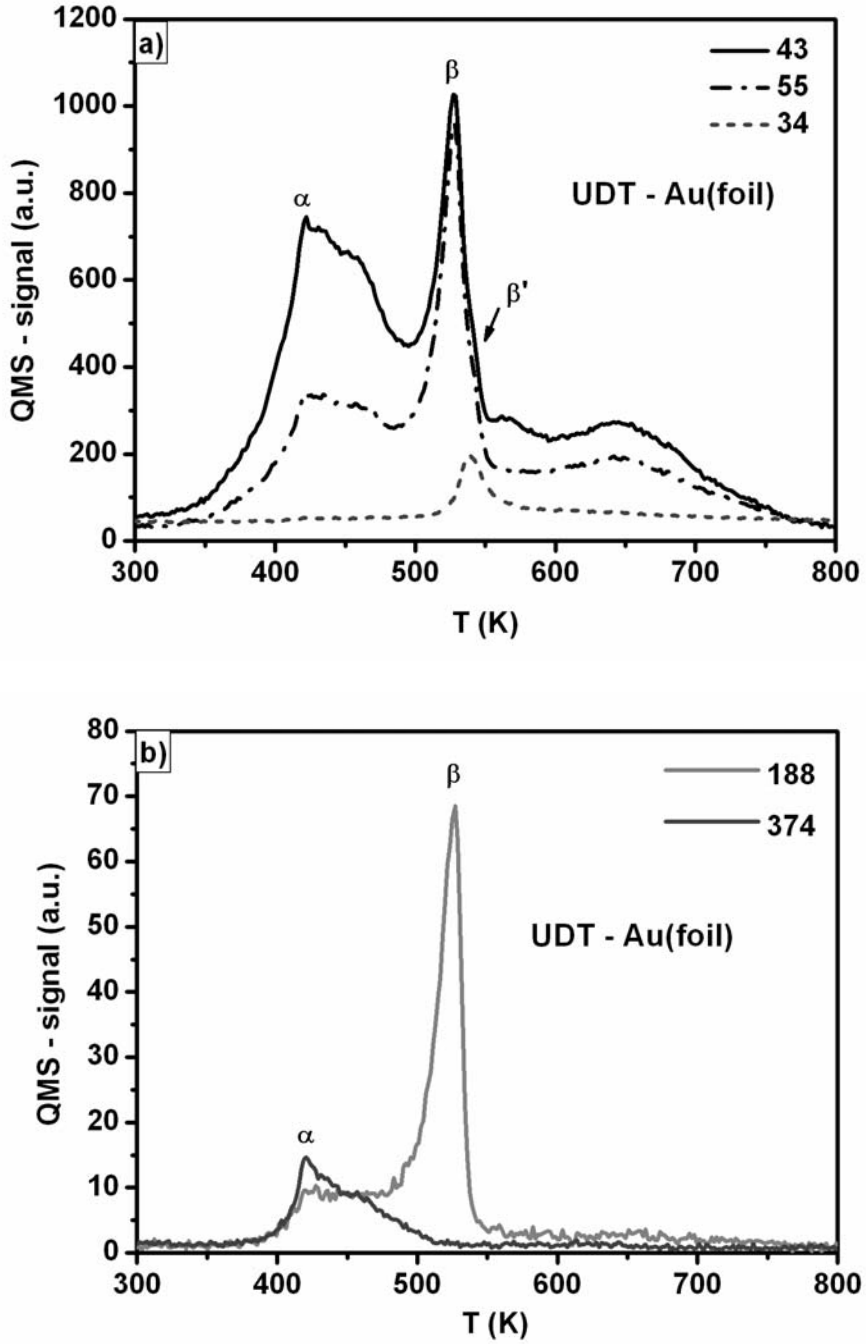

Figure 46. Desorption spectrum of an UDT SAM on a gold foil prepared ex-situ in ethanolic solution. The substrate was prior cleaned by Ar^+-sputtering and annealing at 900 K. The spectrum is similar to that of a SAM prepared by PVD, showing the α-peak of the standing molecules and the β-peak of the remaining lying molecules. A small H_2S peak can also be observed (β'-peak). (a). In addition, the mass 374 is shown, indicating desorption of disulfides around 400 K (α-peak) (b).

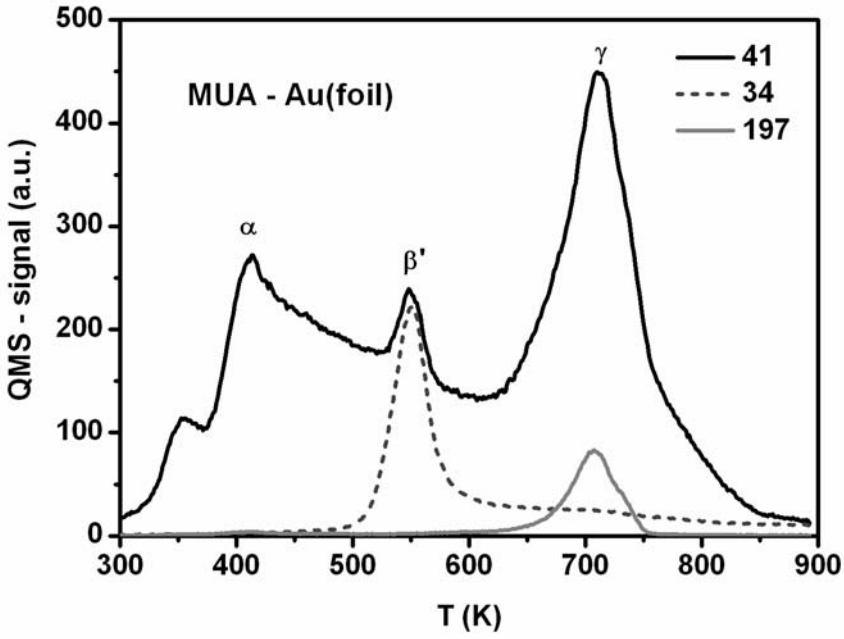

Figure 47. Multiplexed desorption spectrum of an in-situ prepared MUA SAM on a sputtered and annealed gold substrate. The α-peak of the standing molecules and the β'-peak of the lying molecules are followed by a third desorption feature (γ-peak). This feature can be attributed to desorption of gold containing molecules (m_{Au} = 197 amu).

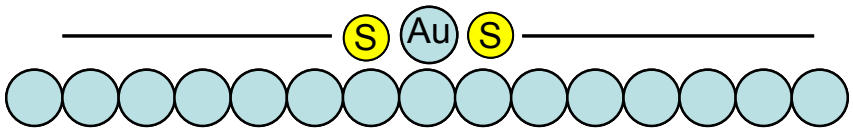

Figure 48. Scheme of Au-adatom-thiol complexes similar as suggested in ref. [102] for methylthiolate on gold.

5.3.4 Temperature-dependent XPS on ex-situ prepared SAMs

For further characterization of the γ-peak, XPS measurements were performed at different temperatures. Figure 49a-c displays the data for the S2p and Figure 49d-f for the C1s XPS signals, before heating (a,d), after heating to 650 K (b,e),

and after heating to 900 K (c,f), respectively. Several important features can be noticed. At first, the binding energy of the S2p photoelectrons decreases, indicating a weakening of the S-C bond strength and a strengthening of the S-Au bond. This is in good agreement with our assumption of the presence of gold-adatom-thiol complexes. In general, the binding energy of electrons decreases when the atom is bonded to a substrate. Similarly, the C1s spectrum also shifts towards lower binding energies and the shape of the carbon peak changes. The observed shifts of the C1s peak are in good agreement with the values reported in [162]. According to this, the C1s-binding energy of 284.6 eV is typical for aliphatic carbon and the slightly slower binding energy of C1s at 284.1 eV can be attributed to graphitic carbon. The rather low binding energy of 283.1 eV is typical for carbidic carbon, which is strongly bonded to a metal surface.

The feature arising from the carboxylic carbon as observed before heating to 650 K disappears after heating. We believe that the chemical configuration of the carboxylic carbon has changed so strongly that no or only little related emission can take place. But this also could indicate that the acid group is already separated from the molecule. In addition, the C1s peak becomes narrower, indicating less different chemical environments for the individual carbon atoms in the adsorbed species.

Furthermore, the sulfur signal increased after heating the SAM to 650 K, although a significant amount of molecules has desorbed as intact molecules or in form of H_2S. This is a strong indication that now the sulfur signal is not attenuated by the carbon chain anymore. In fact, this is not surprising, as we know that the standing molecules start desorbing already at a temperature of 400 K. After heating to 900 K still a considerable amount of carbon and some sulfur remain on the surface, which are now even more strongly bonded to the surface, as deduced from the further decrease of the XPS binding energies of the S2p and C1s peaks, respectively.

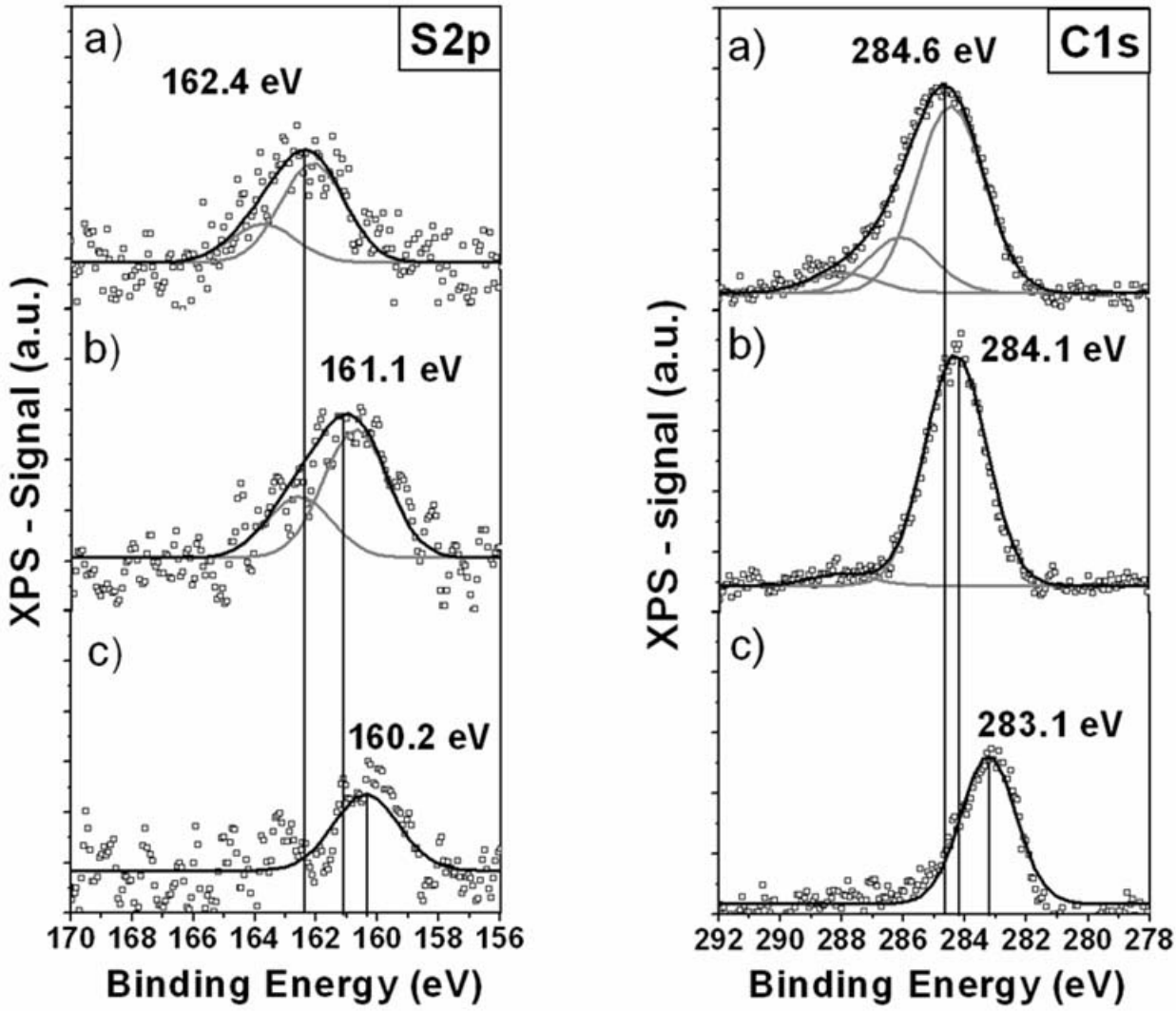

Figure 49. XPS measurements for MUA on the gold foil. The signal of the S2p peak is shown before heating (a), after heating at 650 K (b), and after heating at 900 K (c). One observes a shift of the signal towards lower binding energies. Furthermore, the signal of the C1s peak is shown before heating (d), showing the peak of the carboxylic carbon around 289 eV, after heating at 650 K (e), where no peak of the carboxylic carbon can be detected anymore and after heating at 900 K (f). One observes a shift of the aliphatic carbon binding energy towards lower values.

5.3.5 The influence of the substrate preparation on the ex-situ SAM formation

As mentioned already in the former section, the reproducibility of the results of the ex-situ prepared SAMs was worse than that of the in-situ prepared SAMs. Therefore it was difficult to find an unambiguous correlation between a parameter and an effect. However, the substrate preparation method was found to have a strong influence on the SAM formation. In order to investigate this issue, UDT SAMs were prepared on three differently prepared gold foils:

1) Sputtered and annealed gold foils, which have been shown to provide a clean and smooth surface.
2) Gold foils cleaned in Piranha solution. XPS measurements revealed that still carbon and sulfur contaminations are present on these substrates (Section 4.1.1). For simplicity, these substrate are designated 'ex-situ cleaned' gold foils.
3) Gold foils as received from Ögussa Inc., which have been shown to be heavily contaminated with carbon and chloride impurities (Section 4.1.1).

The TD spectrum of an ex-situ prepared UDT SAM on an ex-situ cleaned gold foil is shown in Figure 50a,b. For comparison, we refer to the desorption spectrum of UDT on a sputtered and annealed gold foil in Figure 46. A significant change of the layer is observed. The α-peak of the standing molecules is significantly smaller, while the β-peak remains unchanged. The interesting point is that one can observe again the γ-peak characterized by the mass 197, which has already been observed for the ex-situ prepared MUA SAM (Section 5.3.3). As the mass 197 is even higher than the mass of the whole UDT molecule, this affirms the assumption that it concerns gold desorption. Apparently, during the removal of carbon impurities in Piranha solution a rough gold surface is

generated, which leads to a strong gold adatom-thiol binding complex. As a result of this ill-defined surface also the SAM formation is less pronounced, as indicated by the small α-peak. An interesting detail is that the gold containing molecules have a different cracking pattern than the single UDT molecules showing a high desorption peak of mass 155 (the sulfur-free molecule). This is evidence that the sulfur-carbon-bond breaks easily when thiol-adatom complexes are formed.

Further characterization of the UDT SAM on the ex-situ cleaned gold foil was performed by AES. In Figure 50, the corresponding S- and C- Auger peaks are shown, the spectrum of the UDT SAM on the sputtered and annealed gold foil is added. Interestingly, the ratio between the C- and the S-peaks is different for both substrates: In the case of the UDT SAM on the sputtered gold foil, a rather small sulfur peak is observed which is explained by the fact that for standing molecules the sulfur signal is strongly attenuated by the carbon chain. In the case of the UDT SAM on the ex-situ cleaned gold foil, a significantly higher sulfur signal is observed. This high sulfur-signal is in good agreement with the corresponding TD spectrum showing that only a small fraction of molecules is standing upright.

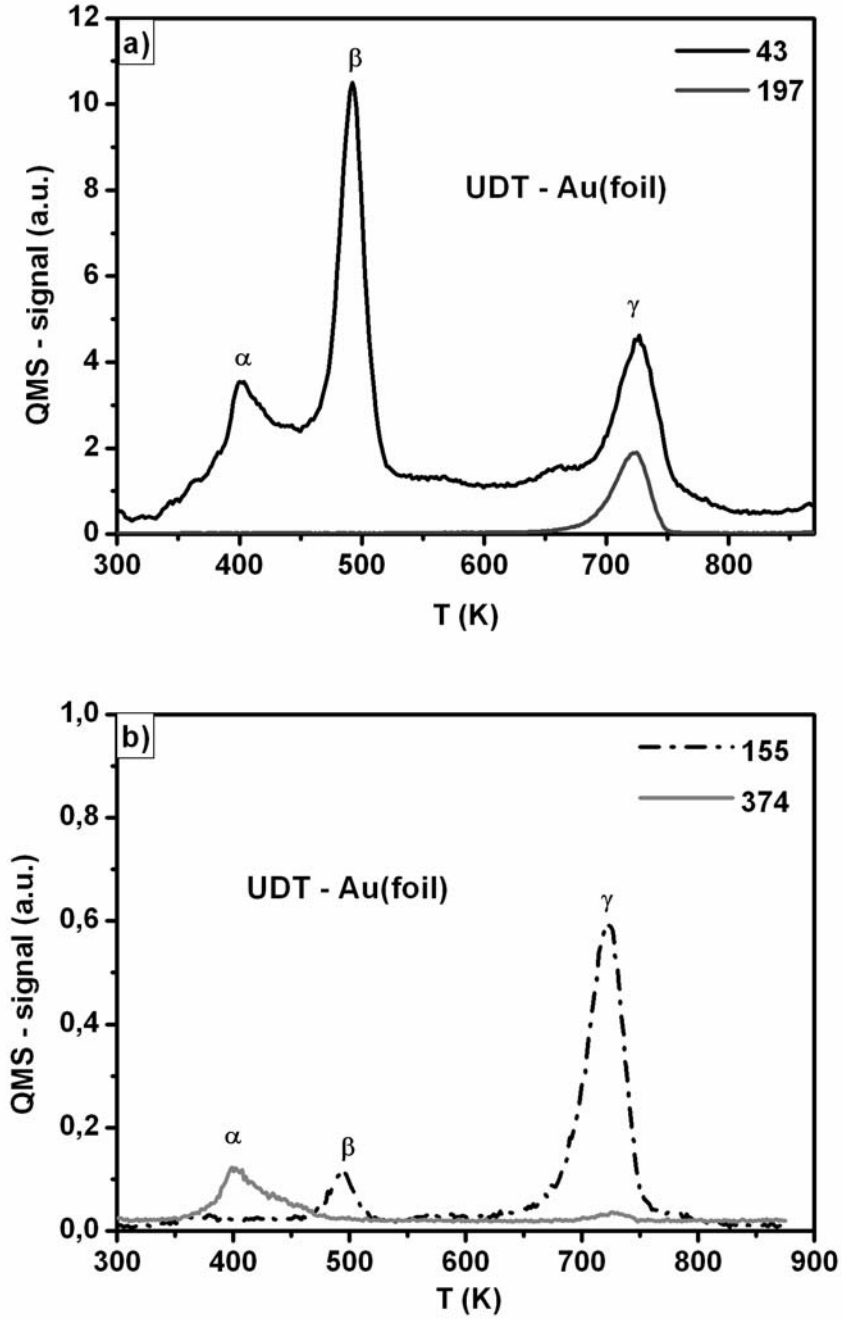

Figure 50. Multiplexed desorption spectrum of UDT on a gold foil, prepared ex-situ in ethanolic solution. The substrate was cleaned in Piranha solution. The small α-peak indicates that only a small amount of standing molecules is present, the high β-peak reveals a much higher amount of molecules lying on the surface. The γ-peak characterized by mass 197 again denotes desorption of gold containing molecules.

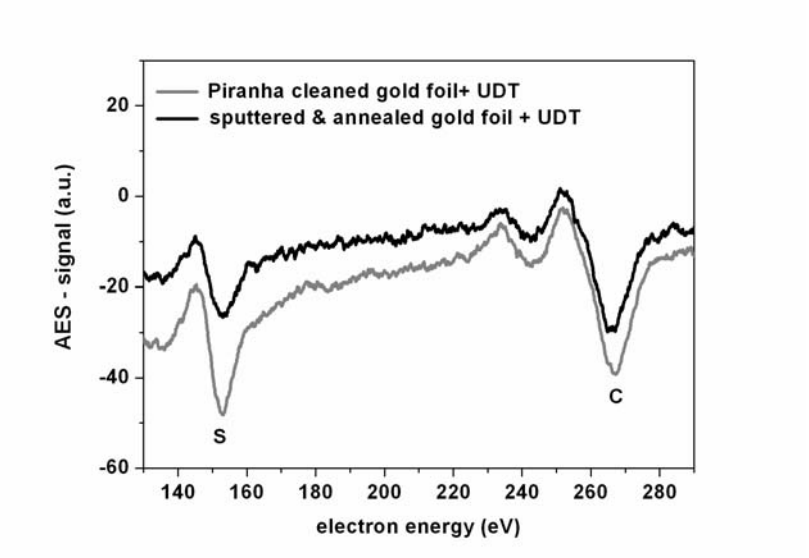

Figure 51. Auger spectrum of an ex-situ prepared UDT SAM on a Piranha cleaned gold foil, for comparison the Auger spectrum of a UDT SAM on a sputtered and annealed gold foil is added. The significantly higher sulfur signal in the case of the Piranha-cleaned substrate is attributed to a lower fraction of standing molecules.

Furthermore, the ex-situ UDT SAM formation on a gold foil 'as received' was investigated. In Section 5.2.5, it has been shown that no in-situ adsorption of molecules took place on these substrates. For comparison, the results for ex-situ UDT growth on an untreated gold foil is shown in Figure 52, even though it is poorly understood. There is only one desorption peak at 520 K, stemming from desorption of disulfides (see inset). An important observation is that there is no desorption of gold containing molecules in this case.

A possible explanation could be a flat lying configuration of molecules and an additional disulfide-formation. The presence of flat lying molecules can explain the rather high desorption temperature (in comparison to the α-peak), as in this case also interactions between the carbon chain and the substrate are present. The tendency to form disulfides can be explained by the assumption that the heavily contaminated gold surface does not allow for the evolution of sulfur-gold bonds. The latter assumption can also explain the fact that the impurities on the substrate inhibit the formation of strong sulfur – Au adatom complexes.

For further characterization, AES was performed on these samples. The corresponding spectrum is shown in Figure 53. For comparison, the spectrum of a UDT SAM on a sputtered and annealed gold-foil is added. One can observe a remarkably high sulfur peak, suggesting that the sulfur-signal is not attenuated by the carbon chain in this case. This corroborates our assumption of a flat-lying configuration of molecules. Furthermore, a small shift of the sulfur peak towards lower electron energies can be observed. As explained in Section 3.3, the interpretation of peak-shifts in an Auger spectrum is rather complicated. However, a shift of the sulfur peak towards higher electron energies was associated with the evolution of a strong sulfur-gold bond in Section 5.2.4. In analogy, the here observed peak shift towards lower electron energies could be attributed to a weaker bond to the substrate, which again is in good agreement with the above presented model. However, there is a lack of further experimental data and therefore these results, even though interesting, will not be discussed in more detail.

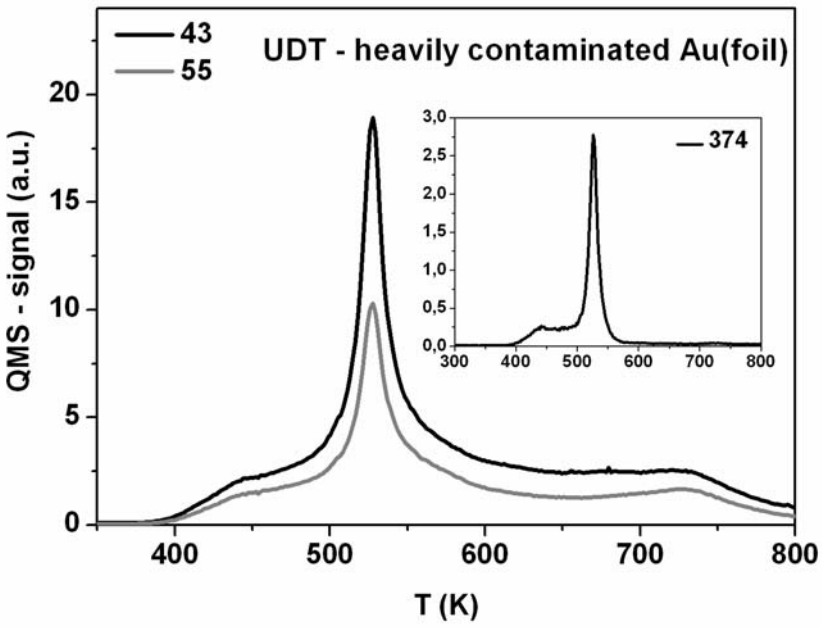

Figure 52. Multiplexed desorption spectrum of ex-situ prepared UDT on a heavily contaminated gold foil. The single desorption peak is attributed to desorption of disulfides.

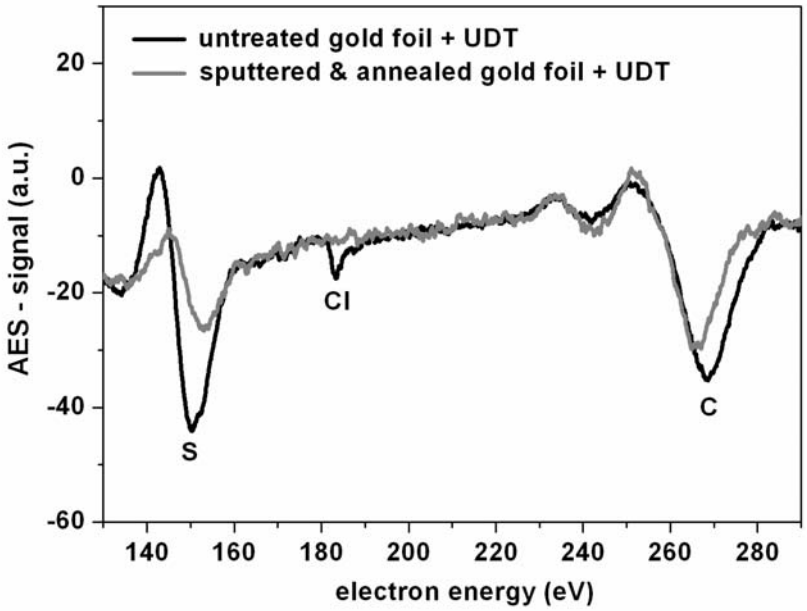

Figure 53. Auger spectrum of an ex-situ prepared UDT SAM on a heavily contaminated (‚untreated') gold foil. The remarkably high S-peak indicates that the sulfur signal is not attenuated by the carbon chain, in contrast to the case of upright standing molecules.

5.3.6 The influence of the immersion time in solution

The most astonishing result of this work was the detection of gold in the desorption spectrum of *ex situ* prepared MUA/UDT SAMs. In the last sections, it has been shown that the substrate cleaning procedure can have an impact on the appearance of the γ-peak. However, it turned out that also the residual time in solution influences this desorption feature.

In Figure 54, the desorption peak of mass 197 is shown for four ex-situ prepared MUA SAMs on Au(111)/mica. Differently long immersion times in solution were applied to these samples: 20 sec, 20 min, 2 days and 2 weeks, respectively. The γ-peak is observed already after 20 sec immersion in solution, and it increases steadily with the residual time in solution. This correlation of the desorption of gold-containing molecules to the immersion time is a remarkable

finding, as typically prolonged times in solution are assumed to improve the SAM quality [51]. Indeed, with respect to the formation of the α-peak of standing molecules, sufficiently long immersion times are necessary (as shown in Figure 55). But our results indicate that some kind of gold etching process can additionally happen in solution during time.

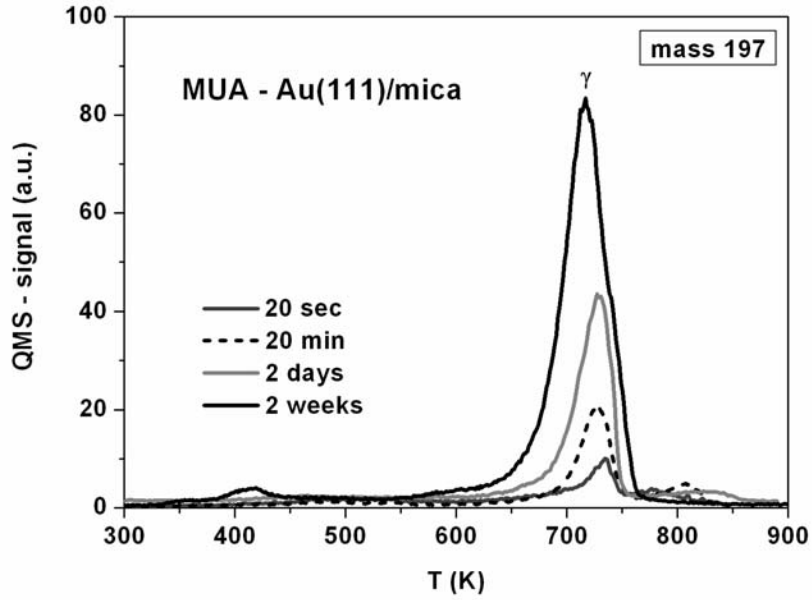

Figure 54. The γ-peak in dependence on the immersion time in solution of MUA. The longer a sample is stored in solution, the higher the corresponding gold desorption peak becomes.

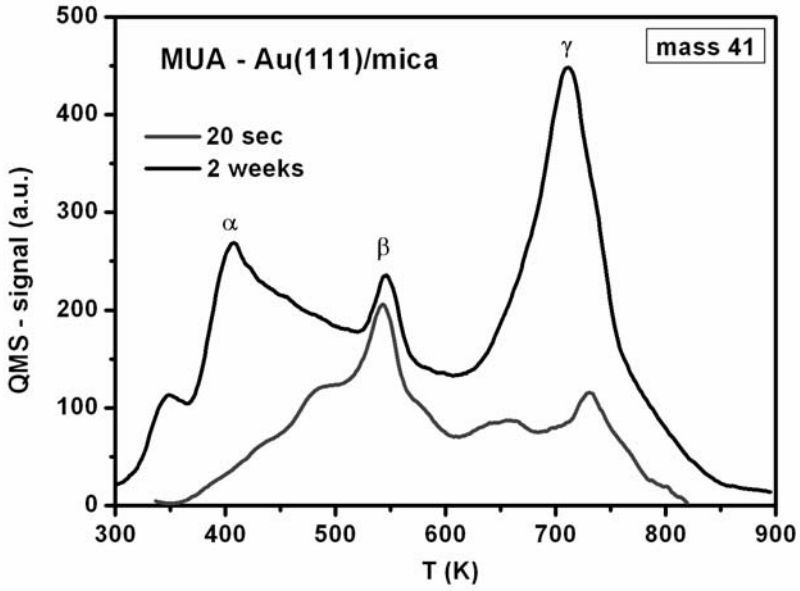

Figure 55. Desorption spectra of MUA on Au(111)/mica after an immersion time of 20 seconds and 2 weeks, respectively. The β-peak of the lying molecules is almost saturated after 20 seconds, while the γ- and the α-peak evolves within time.

5.3.7 Further modification of ex-situ prepared MUA SAMs

It is often stated in literature that acid-terminated molecules are favourable in view of further modifications [25]. Carboxylic acid-terminated surfaces can be activated by conversion to the anhydride [163,164], the acyl chloride/fluoride [165], or the active ester [166]. When treating an acid-terminated SAM with gaseous thionyl chloride ($SOCl_2$), the following reaction is assumed to take place [75]:

Reaction 1.

In order to probe this reaction, we treated an ex-situ prepared MUA SAM with $SOCl_2$ for 5 min and examined it with XPS. The corresponding C1s-signal is shown in Figure 56a, before and after the treatment with $SOCl_2$, respectively. A peak shift towards lower binding energies is observed, the peak position at 284.2 eV is typical for graphitic carbon. Furthermore, the feature of the carboxylic carbon is not detected anymore. The O1s-signal is shown in Figure 56b, before and after the treatment with $SOCl_2$, respectively. The crucial observation is that the O1s-peak becomes higher after the treatment with $SOCl_2$. According to Reaction 1, rather a decrease of the oxygen-signal would have been expected.

For further characterization, AES measurements were performed. Spectra of the following samples are shown in Figure 57:

a) an ex-situ prepared MUA SAM
b) an ex-situ prepared MUA SAM after 5 min treatment in $SOCl_2$
c) an ex-situ prepared MUA SAM after 30 min treatment in $SOCl_2$
d) a gold substrate without SAM which has been treated with $SOCl_2$

After the treatment of the MUA SAM with $SOCl_2$ for 5 min, a small chloride peak evolves. Furthermore, the sulfur peak decreases in comparison to the pristine MUA SAM. After a longer reaction time (30 min), a huge chloride peak and a significantly smaller sulfur peak is detected. Remarkably, this spectrum corresponds to the spectrum of the gold foil without a SAM which has been treated with $SOCl_2$. We therefore assume that the MUA SAM is destroyed or removed by the $SOCl_2$ within time rather than being activated. In fact, both the XPS- and the Auger-measurements suggest that Reaction 1 has not taken place.

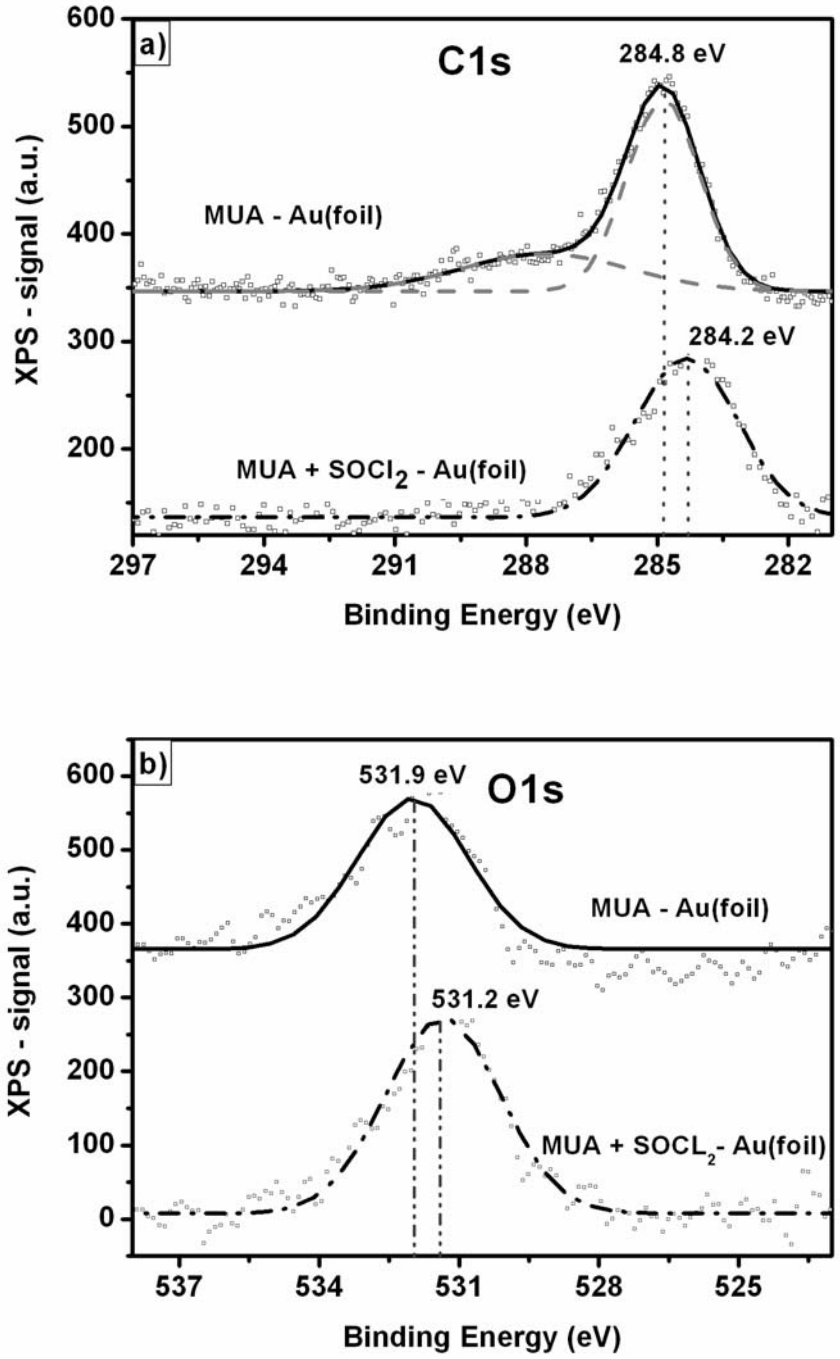

Figure 56. XPS carbon-peak (a) after 5 min treatment of a MUA SAM with thionylchloride. The broad shoulder due to the carboxylic acid has disappeared. The XPS oxygen-peak increases after the treatment with thionylchlorid (b). Both features suggest that Reaction 1 has not taken place.

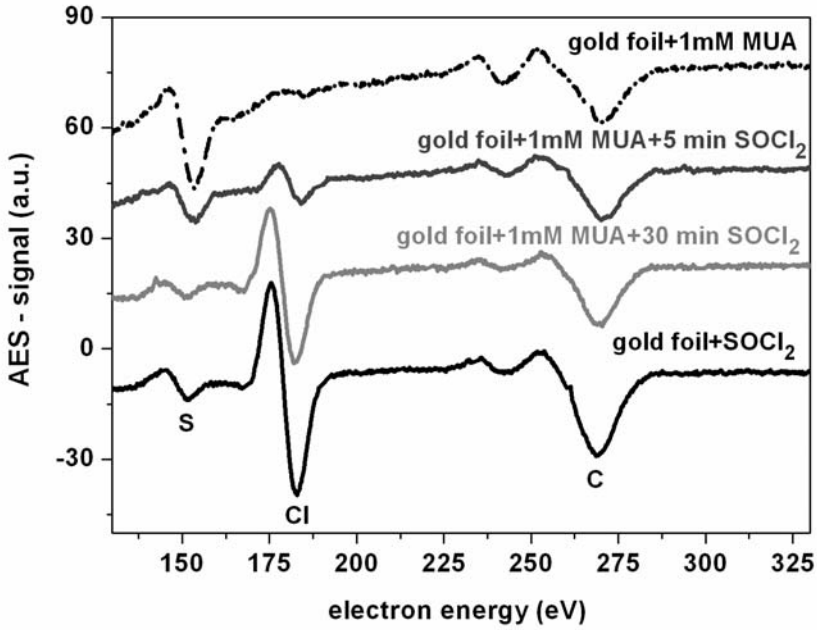

Figure 57. Auger-spectra showing the influence of $SOCl_2$-treatment on a MUA SAM. These spectra suggest that the MUA SAM is removed or destroyed by the $SOCl_2$ after 30 min.

6 Summary and Conclusion

This work deals with different aspects of alkanethiol SAM formation on gold. We investigated the molecules undecanethiol (UDT) and mercaptoundecanoic acid (MUA) by means of TDS, LEED, XPS, AES, IRRAS and AFM. The film preparation was performed in-situ by gas phase deposition in an UHV chamber as well as ex-situ in ethanolic solution of the corresponding molecules. The most important conclusions for in-situ and ex-situ film growth, respectively, are listed in the following.

In-situ SAM formation

- We found that UDT SAM formation is possible. LEED and TDS measurements indicate the presence of two different phases. The 'low-coverage-phase' is attributed to lying molecules exhibiting a (12 x √3) rect. structure with respect to the Au(111) surface. Lying molecules desorb at 510 K. This phase evolves in the early stage of SAM formation as well as after partial thermal desorption (heating at 400 K) of the (standing) SAM. Waiting overnight and repeated exposure to UDT results in the evolution of a second phase. The 'full-coverage' phase is attributed to standing molecules and an actual coverage of ~ 30%. This phase exhibits a (2√3 x 3) rect. structure with respect to the Au(111) surface, as deduced from the corresponding LEED pattern. Standing molecules desorb at 400 K. The detection of disulfides is a hint that recombinative desorption takes place.

- In contrast, only little SAM formation takes place in the case of MUA. Within two weeks only a small fraction of standing molecules evolved.

The presence of the low-coverage phase and a (12 x √3) structure has also been observed in this case. The uptake curve reveals a simple first-order Langmuir adsorption for this phase.

- AES could successfully be applied without any hint of destroying the SAM. A shift of the AES-sulfur-peak could be correlated with the evolution of a strong sulfur-gold-bond during SAM formation.

- An influence of the geometry and the chemical composition of the substrate surface on the SAM formation could be found. A smaller fraction of standing molecules is observed on a polycrystalline gold foil than on a Au(111) single crystal, which is referred to the higher packing density in the latter case. We found out that contaminations on the substrate surface reduces the sticking probability of the molecules.

Ex-situ SAM formation

- We found that ex-situ preparation of UDT on gold results in the formation of a well-ordered SAM exhibiting the same features as the in-situ prepared SAM.

- Characterization of the ex-situ prepared MUA SAM is complicated. XPS measurements indicate all the features which are expected for a well defined SAM. However, TDS indicates three different temperature regions in this case:
  - We found a small amount of standing molecules on the ex-situ prepared MUA SAM, which again desorb recombinatively at 400 K (α-peak).

- Lying molecules desorb at 510 K, similar as for the in-situ prepared SAMs (β-peak). However, some of these molecules desorb dissociatively (S-C cracking) at a slightly higher temperature (520 K).
- We found a third desorption feature at 710 K which was characterized by the appearance of mass 197 amu. This desorption peak (γ-peak) is attributed to the desorption of gold containing molecules.

- The γ-peak was also found in the desorption spectrum for an ex-situ prepared UDT SAM on a substrate which was cleaned in Piranha solution. This is a strong indication that mass 197 really concerns gold desorption, as this mass is even higher than the mass of the intact UDT molecule (188 amu). We assume that the Piranha solution leads to a roughening of the gold surface which results in the exposure of gold-adatoms on which the thiols strongly bond.

- We observed that the formation of gold-thiol moieties is correlated with the residual time in solution. Such moieties have been observed already after very short immersion times in the range of several minutes. We assume that some kind of gold-etching process takes place, leading to the formation of strongly bonded gold-adatom-thiol complexes.

In conclusion we can state that thermal desorption spectroscopy is a powerful method to characterize SAM formation on surfaces. Fingerprints in the spectra allow to differentiate between lying and standing molecules (SAMs). Furthermore, the thermal stability and possible reactions with the substrate can easily be determined.

I. List of publications and conference contributions

Publications in international scientific journals

Stettner, J.; Winkler, A. *Characterization of alkanethiols self-assembled monolayers on gold by thermal desorption spectroscopy*. Langmuir 2010, 26, 9659.

Stettner, J.; Frank, P.; Grießer, T.; Trimmel, G.; Schennach, R.; Gilli, E.; Winkler, A. *A study on the formation and thermal stability of 11-MUA SAMs on Au(111)/mica and on polycrystalline gold foils*. Langmuir 2009, 25, 1427.

Stettner, J.; Frank, P.; Grießer, T.; Trimmel, G.; Schennach, R.; Resel, R.; Winkler, A. *Characterisation of 11-MUA SAM formation on gold*. Springer proceedings in physics 2009, 129, 101.

Frank, P.; Nußbacher, F; Stettner, J.; Winkler, A. *SAMs of 11-MUA grown on polycrystalline Au foils by physical vapour deposition in UHV* 2009, Springer proceedings in physics 2009, 129, 107.

Jeanquartier, C.; Schider, G.; Feichtenhofer, S.; Schwab, H.; Schennach, R.; Stettner, J.; Winkler, A.; Gruber-Wölfler, H.; Schitter, G.; Eder, R.; Khinast, J. *A two-step method to covalently bind biomolecules to group IV semiconductors: Si(111)/1,2-Epoxi-9-decene/Esterase*. Langmuir 2008, 24, 13957.

Kratzer, M.; Stettner, J.; Winkler, A. *Angular distribution of permeating/desorbing deuterium from modified Pd(111) surfaces*. Surface science 2007, 601, 3456.

Demirci, E.; Stettner, J.; Kratzer, M.; Schennach, R.; Winkler, A. *Methanol adsorption on Cu(110) and the angular distribution of the reaction products*. The journal of chemical physics 2007, 126, 164710.

Kratzer, M.; Stettner, J.; Winkler, A. *Water formation on clean and vanadium oxide covered Pd(111) by permeating deuterium*. The journal of physical chemistry (Washington, DC) / C 2007, 111, 12723.

Conference contributions

Stettner, J.; Frank, P.; Grießer, T.; Trimmel G.; Winkler, A. *TDS as a tool to investigate SAMs*. Winterscool on organic electronics, Planneralm March 2010. (Talk)

Stettner, J.; Frank, P.; Grießer, T.; Trimmel, G.; Winkler, A. *Self assembled monolayers of alkanethiols on gold*. Materials Day, Graz October 2009. (Talk)

Stettner, J.; Frank, P.; Grießer, T.; Trimmel, G.; Winkler, A. *Self assembled monolayers of alkanethiols (MUA, UDT) on gold studied by TDS, AES and LEED*. Interafce controlled and functionalised organic films, Admont September 2009. (Talk Winkler)

Stettner, J.; Frank, P.; Grießer, T.; Trimmel, G.; Winkler, A. *Alkanethiols SAM formation on gold: growth from solution versus physical vapor deposition*, 59.

Jahrestagung der Österreichischen Physikalischen Gesellschaft, Innsbruck September 2009. (Talk)

Frank, P.; Stettner, J.; Nußbacher, F.; Winkler, A. *Thermal Desorption of SAMs of 11-MUA grown on polycrystalline gold foils by physical vapor deposition in UHV*. 58. Jahrestagung der Österreichischen Physikalischen Gesellschaft, Leoben September 2008. (Poster)

Stettner, J.; Frank, P.; Grießer, T.; Trimmel, G.; Schennach, R.; Resel, R.; Winkler, A. *The stability of 11-MUA SAMs on gold*. 58. Jahrestagung der Österreichischen Physikalischen Gesellschaft, Leoben September 2008. (Poster)

Frank, P.; Stettner, J.; Nußbacher, F.; Winkler, A. *Thermal desorption spectroscopy investigations of SAMs of 11-MUA on polycrystalline Au-foils by PVD in UHV*. The 8th international symposium in functional Pi-electron systems, Graz July 2008. (Poster)

Stettner, J.; Frank, P.; Grießer, T.; Trimmel, G.; Schennach, R.; Resel, R.; Winkler, A. *A study on 11-MUA SAM formation on gold.* The 8th international symposium in functional Pi-electron systems, Graz July 2008. (Poster)

Stettner, J.; Frank, P.; Grießer, T.; Trimmel, G.; Schennach, R.; Resel, R.; Winkler, A. *Characterisation of 11-MUA SAM formation on gold surfaces*. EMRS, Strasbourg May 2008. (Talk)

Frank, P.; Nussbacher, F.; Stettner, J.; Winkler, A. *SAMs of 11-MUA grown on polycrystalline Au-foils by physical vapor deposition in UHV*. EMRS, Strasbourg May 2008. (Poster)

Stettner, J.; Frank, P.; Grießer, T.; Trimmel, G.; Schennach, R.; Resel, R.; Winkler, A. *Self assembled monolayers: A study on 11-mercaproundecanoic acid on Au-surfaces*. Winterscool on organic electronics, Planneralm January 2008. (Poster)

Stettner, J.; Grießer, T.; Frank, P.; Track, A.; Trimmel, G.; Kern, W.; Winkler, A. *SAM formation of 11-mercaptoundecanoic acid on gold: The influence of substrate structure and composition*. Interface controlled and functionalised organic films, Eisenerz September 2007. (Talk)

Track, A.; Lex, A:; Grießer, T.; Koller, G.; Pacher, P.; Romaner, L.; Frank, P.; Stettner, J.; Winkler, A.; Schennach, R.; Trimmel, G.; Kern, W.; Zojer, E.; Ramsey, M. *Photoreactive thin layers for organic electronics*. Euromat, Nürnberg September 2007. (Poster)

Kratzer, M.; Stettner, J.; Winkler, A. *Water formation studies on vanadium oxide thin films covered Pd(111)*. DPG-Frühjahrstagung, Regensburg May 2007. (Talk)

Demirci, E.; Stettner, J.; Kratzer, M.; Schennach, R.; Winkler, A. *Methanol adsorption on Cu(110) and the angular distribution of the reaction products*. Bunsentagung, Graz May 2007. (Poster)

Kratzer, M.; Stettner, J.; Winkler, A. *Water formation studies on vanadium oxide thin films covered Pd(111)*. Bunsentagung, Graz May 2007. (Poster)

II. List of figures

III. Bibliography

[1] Schmidt, E.; Schurig, W.; Sellschopp, W. *Tech. Mech. Thermodyn.* **1993**, 1, 53.

[2] Nagle, W. M.; Drew, T. B. *Trans. Am. Inst. Chem. Eng*. **1933**, 30, 217.

[3] Emmons, H. *Trans. Am. Inst. Chem. Eng*. **1939**, 35, 109.

[4] Poirier, G. E. *Chem. Rev*. **1997**, 97, 1117.

[5] Kidoaki, S.; Matsuda, T. *Langmuir* **1999**, 15**,** 7639.

[6] Whitesides, G. M.; Laibinis, P. E. *Langmuir* **1990**, 6, 87.

[7] Miller, W. J.; Abbott, N. L. *Langmuir* **1997**, 13, 7106.

[8] Hautman, J.; Klein, M. L. *Phys. Rev. Lett*. **1991**, 67, 1763.

[9] Miura, Y. F.; Takenaga, M.; Koini, T.; Graupe, M.; Garg, N.; Graham R. L.; Lee, T. R. *Langmuir* **1998**, 14, 5821.

[10] Engquist, I.; Liedberg, B. *J. Phys. Chem*. **1996**, 100, 20089.

[11] Swalen, J. D.; Allara, D. L.; Andrade, J. D.; Chandross, E. A.; Garoff, S.; Israelachvili, J.; McCarthy, T. J.; Murray, R.; Pease, R. F.; Rabolt, J. F.; Wynne, K. J.; Yu, H. *Langmuir* **1987**, 3, 932.

[12] Ostuni, E.; Yan, L.; Whitesides, G. M. *Colloids Surf*. *B* **1999**, 15, 3.

[13] Diaz, D. J.; Hudson, J. E.; Storrier, G. D.; Abruna, H. D.; Sundararajan, N.; Ober, C. K. *Langmuir* **2001**, 17, 5932.

[14] Schierbaum, K. D.; Weiss, T.; Thoden van Velzen, E. U.; Engbersen, J. F. J.; Reinhoudt, D. N.; Gopel, W. *Science* **1994**, 265, 1413.

[15] Alain, C.; Geissler, M.; Schmid, H.; Michel, B.; Delamarche, E. *Langmuir* **2002**, 18, 2406.

[16] Maboudian, R. *Surf. Sci. Rep.* **1998**, 30, 207.

[17] Chidsey, C. E. D. *Science* **1991**, 251, 919.

[18] Deng, T.; Wu, H. K.; Brittain, S. T.; Whitesides, G. M*. Analytical Chemistry* **2000**, 72, 3176.

[19] Xia, Y. N. Whitesides, G. M. *Langmuir* **1997**, 13, 2059.

[20] Lahiri, J.; Ostuni, E.; Whitesides, G. M*. Langmuir* **1999,** 15, 2055.

[21] Wilbur, J. L.; Kumar, A.; Biebuyck, H. A.; Kim, E.; Whitesides, G. M. *Nanotechnology* **1996**, 7, 452.

[22] Xia, Y. N.; Qin, D.;.Whitesides, G. M*. Adv. Mater.* **1996**, 8, 1015.

[23] Kumar, A.; Biebuyck, H. A.; Whitesides, G. M*. Langmuir* **1994**, 10, 1498.

[24] Xia, Y. N.; Whitesides, G. M. *Adv. Mater*. **1995**, 7, 471.

[25] Li, X. - M.; Huskens, J.; Reinhoudt, D. N. *J. Mater. Chem*. **2004**, 14, 2954.

[26] Ehler, T. T.; Malmberg, N.; Noe, L. J. *J. Phys. Chem. B* **1997**, 101, 1268.

[27] Rieley, H.; Kendall, G. K. *Langmuir* **1999**, 15, 8867.

[28] Bucher, J. P.; Santesson, L.; Kern, K. *Langmuir* **1994**, 10, 979.

[29] Dhirani, A.; Hines, M. A.; Fisher, A. J.; Ismail, O.; Guyotsionnest, P. *Langmuir* **1995**, 11, 2609.

[30] Walczak, M. M.; Chinkap, C.; Stole, S. M.; Widrig C. A.; Porter, M. D. *J. Am. Chem. Soc.* **1991**, 113, 2370.

[31] Driver, S. M.; Woodruff, D. P. *Langmuir* **2000,** 16, 6693.

[32] Rieley, H.; Kendall, G. K.; Chan, A.; Jones, R. G.; Lüdecke, J.; Woodruff, D. P.; Cowie, B. C. C. *Surf. Sci* **1997**, 392, 143.

[33] Loepp, G.; Vollmer, S.; Witte, G.; Wöll, C. *Langmuir* **1999**, 15, 3767.

[34] Imanishi, A.; Isawa, K.; Matsui, F.; Tsuduki, T.; Yokoyama, T.; Kondoh, H.; Kitajima, Y.; Ohta, T. *Surf. Sci*. **1998**, 407, 282.

[35] Yan, C.; Gölzhäuser, A.; Grunze, M.; Wöll, C. *Langmuir* **1999**, 15, 2414.

[36] Love, J. C.; Estroff, L. A.; Kriebel, J. K.; Nuzzo, R. G.; Whitesides, G. M. *Chem. Rev.* **2005**, 105, 1103-1169.

[37] Schreiber, F. *Progress in Surface Science* **2000**, 56, 151.

[38] Kondoh, H.; Kondama, C.; Sumida, H.; Nozoye, H.; *J. Chem. Phys*. **1999,** 111, 1175.

[39] Masel, R. I. *Principles of adsorption and reaction on solid surfaces*, John Wiley & Sons, New York, Chichester, Brisbane, Toronto, Singapore, **1996**.

[40] Lennard-Jones, J. E. *Trans. Farady. Soc*. **1932**, 28, 333.

[41] Kolasinski, K. W. *Surface Science*, John Wiley & Sons, Chichester, **2008**.

[42] Dannenberger, O.; Buck, M.; Grunze, M. *J. Phys. Chem. B* **1999**, 103, 2202.

[43] Peterlinz, K. A.; Georgiadis, R. *Langmuir* **1996**, 12, 4731.

[44] Bain, C. D.; Troughton, E. B.; Tao, Y. T.; Evall, J.; Whitesides, G. M.; Nuzzo, R. G. *J. Am. Chem. Soc*. **1989**, 111, 321.

[45] Poirier, G. E.; Tarlov, M. J.; Rushmeier, H. E. *Langmuir* **1994**. 10, 3383.

[46] Bensebaa, F.; Voicu, R.; Huron, L.; Ellis, T. H.; Kruus, E. *Langmuir* **1997,** 13, 5335.

[47] Karpovich, D. S.; Blanchard, G. J. *Langmuir* **1994,** 10**,** 3315.

[48] Dannenberger, O.; Wolff, J. J.; Buck, M. *Langmuir* **1998**, 14, 4679.

[49] Buck, M.; Grunze, M.; Eisert, F.; Fischer, J.; Träger, F. *J. Vac. Sci. Technol. A* **1992**, 10, 926.

[50] DeBono, R. F.; Loucks, G. D.; Manna, D. D.; Krull, U. J.; *Can. J. Chem* **1996**, 74, 677.

[51] Terrill, R. H.; Tanzer, T. A.; Bohn, P. W. *Langmuir* **1998**, 4, 845.

[52] Himmelhaus, M.; Eisert, F.; Buck, M.; Grunze, M. J*. Phys. Chem. B* **2000**, 104, 576.

[53] Poirier, G. E.; Pylant, E. D. *Science* **1996**, 272, 1145.

[54] Poirier, G. E. *Langmuir* **1999**, 15, 1167.

[55] Dubois, L. H.; Zegarski, B. R.; Nuzzo, R. G.; *J. Phys. Chem.* **1993**, 98, 678.

[56] Camillone, N.; Leung, T. Y. B.; Schwartz, P.; Eisenberger, P.; Scoles, G. *Langmuir* **1996**, 12, 2737.

[57] Gerlach, R.; Polanski, G.; Rubahn, H. G. *Appl. Phys. A* **1997**, 65, 375.

[58] Schwartz, D. *Annu. Rev. Phys. Chem.* **2001**, 52, 107.

[59] Schreiber, F.; Eberhardt, A.; Leung T. Y. B.; Schwartz, P.; Wetterer, S. M.; Lavrich, D. J.; Berman, L.; Fenter, P.; Eisenberger, P.; Scoles, G. *Phys. Rev. B* **1998**, 57, 12476.

[60] Schreiber, F. *J. Phys. Condens. Matter* **2004**, 16, 881.

[61] Ulman, A. *Chem. Rev*. **1996**, 96, 1522.

[62] Nuzzo, R. G.; Dubois, L. H.; Allara, D. L. *J. Am. Chem. Soc*. **1990**, 112, 558.

[63] Bertilsson, L.; Liedberg, B. *Langmuir* **1993**, 9, 141.

[64] Himmel, H. - J.; Weiss, K.; Jäger, B.; Dannenberger, O.; Grunze, M.; Wöll, C. *Langmuir* **1997**, 13, 4943.

[65] Kang, J. F.; Ulman, A.; Jordan, R.; Kurth, D. G. *Langmuir* **1999**, 15, 5555.

[66] Fisher, G. L.; Hooper, A. E.; Opila, R. L.; Allara, D. L.; Winograd, N. *J. Phys. Chem. B* **2000**, 104, 3267.

[67] Kokkoli, E.; Zukoski, C. F*. J. of colloid and interface science* **2000**, 230, 176.

[68] Smith, D. A.; Wallwork, M. L.; Zhang, J.; Kirkham, J.; Robinson, C.; Marsh, A.; Wong, M. *J. Phys. Chem. B* **2000**, 104, 8862.

[69] Yang, H. C.; Dermody, D. L.; Xu, C. J.; Ricco, A. J.; Crooks, R. M*. Langmuir* **1996**, 12, 726.

[70] Sugihara, K.; Shimazu, K.; Uosaki, K. *Langmuir* **2000**, 16, 7101.

[71] Chapman, R. G.; Ostuni, E.; Yan, L.; Whitesides, G. M*. Langmuir* **2000**, 16, 6927.

[72] Lee, S. W.; Laibinis, P. E. *J. Chem*. **2000**, 40, 99.

[73] Xu, S.; Miller, S.; Laibinis, P. E.; Liu, G. Y. *Langmuir* **1999**, 15, 7244.

[74] Czanderna, A. W.; King, D.; Spaulding, D. *J. Vac. Sci. Technol. A* **1991,** 5, 2607.

[75] Duevel, R. V.; Corn, R. M. *Anal. Chem* **1992,** 64, 337.

[76] Frey, B. L.; Corn, R. M. *Anal. Chem.* **1996,** 68, 3187.

[77] Dannenberger, O.; Weiss, K.; Himmel, H. - J.; Jäger, B.; Buck, M.; Wöll, C. *Thin Solid Films* **1997**, 307, 183.

[78] Arnold, R.; Azzam, W.; Terfort, A.; Wöll, C. *Langmuir* **2002**, 18, 3980.

[79] Willey, T. M.; Vance, A. L., Van Buuren, T.; Bostedt, C.; Nelson, A. J.; Terminello, L. J.; Fadley, C. S. *Langmuir* **2004**, 20, 2746.

[80] Wang, H.; Chen, S.; Li, L.; Jiang, S. *Langmuir* **2005**, 21, 2633.

[81] Myrskog, A.; Anderson, H.; Aastrup, T.; Ingemarsson, B.; Liedberg, B. *Langmuir* **2010**, 26, 821.

[82] Mendoza, S. M.; Arfaoui, I.; Zanarini, S.; Paolucci, F.; Rudolf, P. *Langmuir* **2007**, 23, 582.

[83] Ito, E.; Konno, K.; Noh, J.; Kanai, K.; Ouchi, Y.; Seki, K.; Hara, M. *Appl. Surf. Sci*. **2005**, 244, 584.

[84] Gorman, C. B.; He, Y.; Carroll, R. L*. Langmuir* **2001**, 17, 5324.

[85] Wood, E. A. *J. Appl. Phy.* **1964**, 35, 1306.

[86] Park, R. L.; Madden, H. H. *Surf. Sci*. **1968**, 11, 188.

[87] Meyer, R.; Lemire, C.; Shaikhudinov, Sh. K.; Freund, H. - J. *Gold Bulletin* **2004**, 37/1-2, 72.

[88] Bergmann, L.; Schaefer, C. *Lehrbuch der Experimentalphysik, Band 6: Festkörper*, Walter de Gruyter, Berlin, New York, **2005**.

[89] Hallmark, V. M.; Chiang, S.; Rabolt, J. F.; Swalen J. D.; Wilson, R. J. *Phys. Rev. Lett*. **1987**, 59, 2879.

[90] Wöll, C.; Chiang, S.; Wilson, R. J.; Lippel, P. H. *Phys. Rev. B* **1989**, 39, 7988.

[91] Barth, J. V.; Brune, H.; Ertl, G.; Behm, R. J. *Phys. Rev. B* **1990**, 42, 9307.

[92] Der Brockhaus. *Naturwissenschaft und Technik, Band 2: GE-PG*, F.A. Brockhaus & Spektrum Akademischer Verlag, Mannheim, Heidelberg, **2003**.

[93] Gerlach, R.; Polanski, G.; Rubahn, H. –G: *Appl. Phys. A* **1997**, 65, 375.

[94] Camillone, N.; Eisenberger, P.; Leung, T. Y. B.; Schwartz, P.; Scoles, G.; Poirier, G. E.; Tarlov, M. J. *J. Chem. Phys*. **1994**, 101, 11031.

[95] Balzer, F.; Gerlach, R.; Polanski, G.; Rubahn, H.-G. *Chem. Phys. Lett.* **1997**, 274, 145.

[96] Woodruff, D. P. *Phys. Chem. Chem. Phys*. **2008**, 10, 7211.

[97] Fenter, P.; Eberhardt, A.; Eisenberger, P. *Science* **1994**, 266, 1216.

[98] Fenter, P.; Schreiber, F.; Berman, L. Scoles, G.; Eisenberger, P; Bedzyk, M. *J. Surf. Sci*. **1998**, 412, 213.

[99] Torrelles, X.; Barrena, E.; Munuera, C.; Rius, J.; Ferrer, S.; Ocal, C. *Langmuir* **2004**, 20, 9396.

[100] Maksymovych, P.; Sorescu, D. C.; Yates, J. T. *Phys. Rev. Lett.* **2006,** 97, 1461031.

[101] Kautz, N. A.; Kandel, S. A. *J. Am. Chem. Soc.* **2008**, 130, 6908.

[102] Voznyy, O.; Dubowski, J. J.; Yates, J. T.; Maksymovych, P. *J. Am. Chem. Soc.* **2009,** 131, 12989.

[103] Poirier, G. E. *Langmuir* **1997**, 13, 2019.

[104] Yu, M.; Bovet, N.; Satterley, C. J.; Bengio, S.; Lovelock, K. R. L.; Milligan, P. K.; Jones, R. G.; Woodruff, D. P.; Dhanak, V. *Phys. Rev. Lett*. **2006**, 97, 166102.

[105] Mazzarello, R.; Cossaro, A.; Verdini, A.; Rousseau, R.; Casalis, L.; Danisman, M. F.; Floreano, L.; Scandolo, S.; Morgante, A.; Scoles, G. *Phys. Rev. Lett*. **2007**, 98, 016102.

[106] Cossaro, A.; Mazzarello, R.; Rousseau, R.; Casalis, L.; Verdini, A.; Kohlmeyer, A.; Floreano, L.; Scandolo, S.; Morgante, A.; Klein, M. L.; Scoles, G. *Science* **2008**, 321, 943.

[107] Chaudhuri, A.; Odelius, M.; Jones, M.; Jones, R. G.; Lee, T. L.; Detlefs, B.; Woodruff, D. P. *J. Chem. Phys*. **2009**, 130, 124708.

[108] Gronbeck, H.; Hakkinen, H. *J. Phys. Chem. B* **2007**, 111, 3325.

[109] Nagoya, A.; Morikawa, Y. *J. Phys. Condens. Matter* **2007**, 19, 365245.

[110] Wang, J. G.; Selloni, A. *J. Phys. Chem. C* **2007**, 111, 12149.

[111] Torres, E.; Blumenau, A. T.; Biedermann, P. U. *Phys. Rev. B* **2009**, 79, 075440.

[112] Edinger, K.; Gölzhäuser, A. Demota, K.; Wöll, C.; Grunze, M. *Langmuir* **1993**, 9, 4.

[113] Bucher, J. - P.; Santesson, L.; Kern, K. *Langmuir* **1994**, 10, 979.

[114] Cavalleri, O.; Hirstein, A.; Kern, K. *Surf. Sci*. **1995**, 340, 960.

[115] Delamarche, E.; Michel, B.; Kang, H.; Gerber, C. *Langmuir* **1994**, 10, 4103.

[116] Poirier, G. E.; Tarlov, M. J. *J. Phys. Chem*. **1995**, 99, 10966.

[117] Oura, K.; Lifshits, V. G.; Saranin, A. A.; Zotov, A. V.; Katayama, M. *Surface Science*, Springer, Berlin, Heidelberg, New York, Hong Kong, London, Milan, Paris, Tokyo, **2003**.

[118] King, D.A. *Surf. Sci.* **1975**, 47, 384.

[119] Redhead, P. A.; *Vacuum* **1962**, 12, 203.

[120] Winkler, A. *Interface controlled organic thin films*; Rubahn, H. G., Sitter, H., Horowitz, G., Al-Shamery, K. (Editors), Springer Verlag, Berlin, Heidelberg, **2009**.

[121] Paserba, K. R.; Gellman, A. J. *Phys. Rev. Lett.* **2001**, 86, 4338.

[122] Müllegger, S.; Winkler, A. *Surf. Sci.* **2006**, 600, 1290.

[123] Tait, S. L.; Dohnalek, Z.; Campbell, C. T.; Kay, B. D. *J. Chem. Phys.* **2005**, 122, 164708.

[124] Zhdanov, V. P. *Surf. Sci. Rep*. **1991**,12, 183.

[125] Davisson C. J.; Germer L. H. *Phys. Rev.* **1927**, 29, 908.

[126] Jepsen, D. W.; Marcus, P. M.; Jona, F. *Phys.Rev. B* **1972**, 5, 3933.

[127] Ibach, H. *Surf. Sci. Rep*. **1999**, 35, 71.

[128] Ertl, G.; Küppers, J. *Low Energy Electrons and Surface Chemistry*, Vol. 4 of *Monographs in Modern Chemistry*, Verlag Chemie, Weinheim, **1974**.

[129] Vickerman, J. C.; Gilmore, I. S. (Editors) *Surface Analysis: The Principal Techniques*, John Wiley & Sons, Singapore, **2009**.

[130] Woodruff, D. P.; Delchar, T. A. *Modern Techniques of Surface Science*, Cambridge University Press, Cambridge, **1986**.

[131] Briggs, D.; Seah, M. P. (Editors) *Practical Surface Analysis by Auger and X-ray Photoelectron Spectroscopy*, John Wiley & Sons, Chichester, New York, Brisbane, Toronto, Singapore, **1983**.

[132] Bubert, H.; Jenett, H. (Editors) *Surface and Thin Film Analysis: Principles, Instrumentation, Applications*, Wiley-VCH, Weinheim, **2002**.

[133] O'Connor, D. J.; Sexton, B. A.; Smart, R. St. C. (Editors) *Surface Analysis Methods in Materials Science*, Springer Verlag, Berlin, Heidelberg, New York, Hong Kong, London, Milan, Paris, Tokyo, **2003**.

[134] Tolstoy, V. P.; Chernyshova, I. V.; Skryshevsky, V. A. *Handbook of Infrared Spectroscopy of Ultrathin Films*, John Wiley & Sons, New Jersey, **2003**.

[135] Kuzmany, H. *Festkörperspektroskopie*, Springer Verlag, Berlin, Heidelberg, New York, **1990**.

[136] Wilson jr., E. B.; Decius, J. C.; Cross, P. C. *Molecular Vibrations*, Dover Publications Inc., New York, **1980**.

[137] Bergmann, L; Schaefer, C. *Lehrbuch der Experimentalphysik, Band 3: Optik*, Walter de Gruyter, Berlin, New York, **1993**.

[138] Elving, P. J.; Winefordner, J. D. (Editors) *Fourier Transform Infrared Spectroscopy*, John Wiley & Sons, Chichester, New York, Brisbane, Toronto, Singapor, **1986**.

[139] Günzler, H.; Heise, H. M. *IR-Spektroskopie,* VCH, Weinheim, **1996**.

[140] Steward, J. E. *Infrared Spectroscopy. Experimental Methods and Techniques,* Marcel Dekker, New York, **1970**.

[141] Magonov, S. N.; Whangbo, M. - H. *Surface Analysis with STM and AFM*, VCH, Weinheim, New York, Basel, Cambridge, Tokyo, **1996**.

[142] http://www.georg-albert-pvd.de/

[143] http://www.oegussa.at/

[144] http://www.mateck.de/

[145] Lüssem, B.; Karthäuser, S.; Haselier, H.; Waser, R. *App. Surf. Sci.* **2005**, 249, 197

[146] Hove, M. A.; Koestner, R. J.; Stair, P. C:; Biberian, J. P.; Kesmodel, L. L.; Bartos, I.; Somorjai, G. A. *Surf. Sci*. **1981**, 103, 189.

[147] Wöll, C.; Chiang, S.; Wilson, R. J.; Lippel, P. H. *Phy. Rev. B* **1989**, 39(11), 7988.

[148] DeRose, J. A.; Thundat, T.; Nagahara, L. A:; Lindsay, S. M. *Surf. Sci*. **1991**, 265, 102.

[149] Shimoni, N.; Biham, O.; Millo, O. *Surf. Sci*. **1998**, 414, 925-931.

[150] Mülleger, S.; Mitsche, S.; Pölt, P; Hänel, K.; Birkner, A.; Wöll, C.; Winkler, A. *Thin Solid Films* **2005**, 484, 408.

[151] Käfer, D.; Witte, G.; Cyganik, P.; Terfort, A.; Wöll, C. *J. Am. Chem. Soc.* **2006**, 128, 1723.

[152] Kondoh, H.; Kodama, C.; Sumida, H.; Nozoye, H. *J. Chem. Phys.* **1999,** 3, 1175.

[153] Hayashi, T.; Wakamatsu, K.; Ito, E.; Hara, M. *J. Phys. Chem.* **2009,** 113, 18795.

[154] Stettner, J.; Frank, P.; Griesser, T.; Trimmel, G.; Schennach, R.; Gilli, E.; Winkler, A. *Langmuir* **2009,** 25, 1427.

[155] Voets, J.; Gerritsen, J. W.; Grimbergen, R. F.; van Kempen, H. *Surface Science* **1998,** 399, 316.

[156] Lavrich, D. J.; Wetterer, S. M.; Bernasek, S. L.; Scoles, G. *J. Phys. Chem. B* **1998**, 102, 3456.

[157] Hobara, D.; Sasaki, T.; Imabayashi, S.; Kakiuchi, T. *Langmuir* **1999,** 15, 5073

[158] Cecchet, F.; Rudolf, P.; Rapino, S.; Margotti, M.; Paolucci, F.; Baggerman, J.; Brouwer, A. M.; Kay, E. R.; Wong, J. K. Y.; Leigh, D. A. *J. Phys. Chem. B* **2004**, 108, 15192.

[159] Jiang, P.; Liu, Z. F.; Cai, S. M. *Langmuir* **2002**, 18, 4495.

[160] Porter, M. D.; Bright, T. B.; Allara, D. L.; Chidsey, C. E. D. *J. Am. Chem. Soc.* **1987**, 109, 3559.

[161] Nuzzo, R. G.; Dubois, L. H.; Allara, D. L. *J. Am. Chem. Soc.* **1984**, 112, 558.

[162] Wagner, C. D.; Riggs, W. M.; Davis, L. E.; Moulder, J. F.; Muilenberg, G. E. (Editor) *Handbook of X-ray photoelectron spectroscopy*, Perkin-Elmer Corporation, Minnesota, **1978**.

[163] Yan, L.; Zhao, X.-M.; Whitesides, G. M. *J. Am. Chem. Soc.* **1998**, 120, 6179.

[164] Chapman, R. G.; Ostuni, E.; Yan, L.; Whitesides, G. M. *Langmuir* **2000**, 16, 6927.

[165] Galow, T. H.; Rodrigo, J.; Cleary, K.; Cooke, G.; Rotello, V. M. *J. Org. Chem.* **1999**, 15, 1208.

[166] Patel, N.; Davies, M. C.; Hartshorne, M.; Heaton, R. J.; Roberts, C. J.; Tendler, S. J. B.; Williams, P. M. *Langmuir* **1997**, 13, 6485.